SCTLD resistance research consortium (RRC) *Orbicella faveolata* bioinformatics and data analyses synthesis
Final Summary Report

Florida Department of Environmental Protection
Coral Protection and Restoration Program

SCTLD resistance research consortium (RRC) *Orbicella faveolata* bioinformatics and data analyses synthesis Final Summary Report

Prepared By:
Brian K. Walker[1], Greta S. Aeby, Andrew C. Baker[2], Neha Garg[3], Jeff Maynard[8], Julie L. Meyer[4], Karen Neely[1], Valerie J. Paul[5], Nikki Traylor-Knowles[2], Josh D. Voss[6], David R. Whitall[7], Gareth J. Williams[8], Cheryl M. Woodley[9], Natalia Andrade[2], Cynthia C. Becker[4], Samantha Buckley[1], Allison R. Cauvin[4], Caroline E. Dennison[2], Jay Houk[5], Hannah Mazurek[1], Hunter Noren[1], Alex Parry[5], Janet Saunders[9], and Reagan Sharkey[1]

[1]Nova Southeastern University, Halmos College of Arts and Sciences; [2] University of Miami, Rosenstiel School of Marine, Atmospheric, and Earth Science; [3] Georgia Tech University; [4]University of Florida; [5]Smithsonian Marine Station at Fort Pierce; [6]Florida Atlantic University's Harbor Branch Oceanographic Institute; [7]NOAA NOS NCCOS; [8]SymbioSeas; [9]NOAA NOS NCCOS, Coral Health and Disease Program Manager

April 30, 2025

Completed in Partial Fulfillment of PO C2205D for

Florida Department of Environmental Protection
Coral Protection and Restoration Program
1277 N.E. 79th Street Causeway
Miami, FL 33138

This report should be cited as follows:
Walker BK, Aeby GS, Baker AC, Buckley S, Garg N, Maynard J, Meyer J, Neely K, Paul VJ, Traylor-Knowles N, Voss J, Whitall DR, Williams GJ, Woodley CM, Andrade N, Becker CC, Buckley S, Cauvin AR, Dennison CE, Houk J, Mazurek H, Noren H, Parry A, Saunders J, and Sharkey R. 2025. SCTLD resistance research consortium (RRC) *Orbicella faveolata* bioinformatics and data analyses synthesis. Final Summary Report. Florida DEP. Miami, FL, 124p.

This report was prepared for the Florida Department of Environmental Protection, Coral Protection and Restoration Program by Nova Southeastern University. Funding was provided by the Florida Department of Environmental Protection Award No. C2205D. The views, statements, findings, conclusions, and recommendations expressed herein are those of the authors and do not necessarily reflect the views of the State of Florida or any of its sub-agencies.

Table of Contents

List of Figures

List of Tables

List of Acronyms

FAU	Florida Atlantic University Harbor Branch Oceanographic Institute
DEP	Florida Department of Environmental Protection
ORCP	Office of Resilience and Coastal Protection
FWC	Florida Fish and Wildlife Conservation Commission
NSU	Nova Southeastern University
KJCAP	Kristin Jacobs Coral Aquatic Preserve (formerly Coral ECA)
FCR	Florida's Coral Reef
SCTLD	stony coral tissue loss disease
SE FL	Southeast Florida
NOAA	National Oceanic and Atmospheric Administration
NCRMP	National Coral Reef Monitoring Program
CIMAS	Cooperative Institute for Marine and Atmospheric Studies
GIS	Geographic Information System
MDS	Multidimensional Scaling
AVLP	Anisometric viral like particle

Acknowledgements

Thank you to the Florida Department of Environmental Protection's Coral Protection and Restoration Program (DEP CPR), NOAA CRCP, and US EPA for supporting these efforts. We thank the Florida Coral Disease Advisory Committee for the large number of volunteers assisting in the meeting and planning of coral disease efforts. We thank Lisa Gregg and Joanne Delaney for assisting with permitting. Thanks to the DEP CPR staff including Nick Parr, Kristi Kerrigan, and Kylie Morgan for contract and report-review coordination. Thank you to the many employees and graduate students involved in the collection, processing, and analyses.

Management Summary (300 words or less)

The Stony Coral Tissue Loss Disease Resistance Research Consortium's (SCTLD RRC) integrated approach to understanding the underpinnings for SCTLD resistance and susceptibility among Florida *O. faveolata* populations has been a success. The synchronized core sampling across time of year, regions, and disease resistance classes of a statistically robust number of corals has given many insights into the genetic, biochemical, and physiological underpinnings in the holobiont of individuals. However, there is much work remaining to uncover the many statistical associations and pathways across the various components. The analyses of the various components in this investigation, genomics, transcriptomics, metabolomics, proteomics, lipidomics, histopathology, microbiomes, endosymbionts, tissue regeneration, and fecundity, have elicited many future research leads to gain a wholistic understanding of the coral's condition.

Executive Summary

Coral diseases continue to cause enormous impacts to Florida's Coral Reef. Regular monitoring and treatments have reduced the loss of live tissue area and provided valuable information on the temporal and spatial variations of colonies with lesions. SCTLD persisted throughout 2023 and 2024 cycling with seasons in SEFL and showing a general decline with time at Sand and Looe Key. SCTLD prevalence on RRC colonies remained higher in the Keys than in southeast Florida until summer of 2023 where it shut off during peak heat stress but picked up again upon recovery from bleaching. Eleven of the thirty (36.7%) high resistant corals showed lesions for the first time between May 2022 and December 2024 (3 in 2022, 6 in 2023, and 2 in 2024) indicating that historically SCTLD resistant corals continue to succumb to disease.

The resistance categories generated from these data were supported by histopathology. Disease was evident in all coral samples at varying levels. Histopathology scoring showed increased lytic necrosis and degenerative Symbiodiniaceae in the low resistance colonies, but only over certain times of year. Differences between coral that never had lesions (unaffected) versus those that did (affected) proved significant in the wintertime samples in antibiotic activity, metabolomics, transcriptomics, and proteomics.

Several analyses suggest that SCTLD may not originate from the host, but rather their symbiodiniaceae. 1) 2bRAD sequencing results suggest that there are neither uniquely SCTLD-susceptible nor SCTLD-resistant genetic lineages. Rather, across the sampled populations, each genetic lineage identified included both SCTLD-affected and SCTLD-unaffected colonies. Even within clonal groups we observe both SCTLD-affected and unaffected colonies. 2) Considering damaged tissue might be more susceptible to disease in an endemic area on colonies with many previous SCTLD lesions, only 7 cores (0.44% of total cores taken) on two colonies had disease emanate from the core site. This low amount of disease from coring wounds may indicate that SCTLD is not directly infecting host tissues. 3) SCTLD disappeared with the onset of significantly reduced symbiont

densities (bleaching) but persisted in areas without bleaching and returned upon bleaching recovery.

Colony variability results showed a dominant association with the Symbiodiniaceae genus *Breviolum* across all corals, except for one dominantly associated with *Durusdinium*. Symbiont to host cell ratios significantly varied between colonies and sampling timepoints. A significant decrease in the symbiont to host ratio (S:H) was observed during the 2023 bleaching event when comparing all corals, even though only one coral visibly bleached. The two colonies without active SCTLD lesions throughout the sampling timeframe were dominated with *Durusdinium* and *Cladocopium*. These results align with Dennison et al., 2021 which suggests *Breviolum* has the highest level of susceptibility to SCTLD compared to *Cladocopium* and *Durusdinium* which showed lower but relatively equal susceptibility. Various Lyso-lipids were detected in higher abundance in *Breviolum* dominated samples when compared to *Durusdinium* dominated samples, suggesting a link between dominant algal symbiont and the biochemical pathways these lipids are involved in. Additionally, the vitamin E analogue α-tocomonoenol was detected in higher abundance in *Durusdinium* dominant samples compared to *Breviolum* in February 2023 suggesting frontloading of this compound during cooler months that could potentially provide enhanced antioxidant protection in corals dominated by *Durusdinium*.

Metabolite, lipid, and protein data all provided evidence that a coral's state is dynamic over time and varied by region. Differences in resistance were found only in specific regions at specific times of the year. In the Lower Keys, resistance classes differed by metabolite species in June and September, by lipid species in June and March, and by protein species in June. In the KJCAP, no significant differences were found in all metabolite, lipid, or protein species between resistance classes. Seasonal and regional differences were prominent throughout the analyses, but somewhat contradictory to the general idea that Keys corals would be healthier. Core healing was higher in the KJCAP than the lower Keys, indicating a generally healthier state in northern colonies. Fecundity was also higher in the KJCAP colonies than the lower Keys where higher mean temperatures the previous summer significantly reduced fecundity.

Orbicella favelota colonies that have been visually affected by SCTLD had a distinct transcriptomic signature during winter compared to colonies that had never been visually affected by the disease. Most genes were down-regulated in SCTLD unaffected colonies during winter in both regions: 33 genes differentially expressed between SCTLD affected and unaffected colonies from the Lower Keys during winter and 169 genes differentially expressed between SCTLD affected and unaffected colonies from the KJCAP. A network analysis used to find the correlation between gene expression and symbiont density collected per symbiont genus showed that *Breviolum* and *Cladocopium* were significantly correlated with some gene modules, and one module was significantly correlated with SCTLD susceptibilities and the symbiont density. Lyctic necrosis and antibiotic inhibition also significantly correlated with the module that showed correlation with SCTLD susceptibility state.

Statistical analyses revealed an evident environmental and temporal effect on the metabolome, which resulted in grouping the corals based on their sample period and reef location prior to subsequent analysis. The metabolites that drove differences in statistically significant SCTLD-based comparison groups were largely predicted as fatty acids. Annotations of these metabolite features included acylcarnitines, betaine lipids, phosphocholines, and peptidic-like natural products. Preliminary lipidome analysis revealed the detection of several monogalactosyldiacylglycerol and digalactosyldiacylglycerol lipids. These lipids are a major component of the symbiont thylakoid membrane and higher unsaturation of the fatty acyl tails is indicative of higher thermal tolerance. Additional analysis is needed to determine statistical significance of these metabolite features across group categories.

Thirty-five proteins were altered in abundance between colonies with active disease and those that never had lesions. These proteins were primarily involved in membrane trafficking, exosomes, chaperones and other folding catalysts, cytoskeletal proteins, and enzymes. Likewise, they played roles in signaling pathways related to protein processing in the endoplasmic reticulum, endocytosis, and cytoskeleton. This suggests that during active SCTLD, protein processing in the coral host is disrupted, likely contributing to lesion formation due to cytoskeletal protein dysregulation.

Microbial communities vary through time, space, and lineage. Shifts in the corals' microbiomes may serve as early indicators of disease susceptibility or resilience in *O. faveolata*. Bacterial functions varied by region, Symbiodiniaceae composition, and by disease history. Corals with active disease had more variable bacterial functions, indicating a disruption of the function of the microbiome in the whole colony as disease lesions were not sampled. In the Lower Keys where SCTLD was more active, unaffected colonies harbored bacteria with more abundant genes for the production of antibiotics, which may play a protective role for the coral. These results suggest that while SCTLD disrupts bacterial functions in apparently healthy tissue on actively diseased colonies, this effect is temporary and is outweighed by the influence of the Symbiodiniaceae composition or local environmental conditions.

Environmental conditions (seawater temperature, inlet outflow, rainfall, wind) varied significantly during the three sampling periods. Sample period 1 occurred during moderate inlet outflow in the KJCAP, high rainfall, and moderate winds. Sample period 2 saw peak seawater temperatures, moderate rainfall, and low wind speeds. Sample period 3 experienced the lowest inlet outflow, lowest temperatures, minimal rainfall, and stronger seaward winds. Not surprisingly, all metrics of local human impacts were higher in the KJCAP than the Keys. Within the KJCAP, high intensity land use and population density appeared slightly higher in the North and Middle KJCAP than the South at the broadest scale, while septic tanks were slightly more abundant in the Middle KJCAP. These patterns highlight the spatial and temporal complexity of environmental stressors, such as seawater temperature, that influence coral health.

Although highly informative and successful, this incredibly valuable and unique project requires more time for data analyses and meetings to spin off additional research to gain

the most understanding possible about the health and dynamics of one of Florida's Coral Reef's historically prominent reef-builders.

1. BACKGROUND

Florida's Coral Reef is currently experiencing a multi-year disease-related mortality event, that has resulted in massive die-offs in multiple coral species. Approximately 21 species of coral, including both Endangered Species Act-listed and the primary reef-building species, have displayed tissue loss lesions which often result in whole colony mortality. First observed near Virginia Key in late 2014, the disease has since spread to the northernmost extent of Florida's Coral Reef, and southwest past the Marquesas and into the Dry Tortugas as well as throughout much of the Caribbean.

Coral diseases have devastated many coral populations globally over the past few decades and are becoming more frequent and virulent. Some are associated with coral stress events like bleaching and nutrient enrichment, however others are not, which obfuscates our understanding of disease sources and pathogen identification. After decades of research using the one pathogen one disease framework with little success, more complex paradigms investigating the members of the holobiont separately and collectively are being employed to uncover the interactions between host, agent and environment of a given coral disease.

Understanding intraspecific coral disease susceptibility is critical to disentangling causation. Comparisons in holobiont biological data (e.g. omics, symbionts, microbiomes) between highly susceptible and highly resistant conspecifics can identify reasons for the variation and possible disease markers. For example, on the Great Barrier Reef, immunity level directly relates to bleaching and disease susceptibility. Furthermore, these data could be tied to environmental conditions occurring during lesion outbreaks and cessation.

Stony Coral Tissue Loss Disease (SCTLD) has devastated the coral populations along Florida's Coral Reef over the last eight years. Its unique trait of affecting many species at varying infection and virulence rates remains perplexing. Identifying the cause of the disease and how to mitigate it is a top management priority. Populations of mountainous star coral (*Orbicella faveolata*) in Florida waters have been prioritized for intensive disease intervention efforts to stop SCTLD. These successful disease intervention treatments throughout Florida's Coral Reef have kept diseased reef-building corals alive, providing a unique opportunity to test intraspecific differences between groups of corals with differing infection patterns. Some corals get infected once, some are reinfected numerous times, and some not at all. Viewing this collection of *O. faveolata* as patients or individual cases that are grouped as at risk (no infection) or differentially affected (i.e., degrees of infection rates) by SCTLD, it is important to have a basic 'patient history' or anamnesis as a foundation to interpret and contextualize more probative or diagnostic analyses.

Therefore, in 2021 a consortium of experts, the SCTLD Resistance Research Consortium (RRC), was formed to undertake an integrated approach to understanding the underpinnings for SCTLD resistance and susceptibility among Florida *Orbicella faveolata* populations. This team was assembled to target many various components in disease

investigation: genomics, transcriptomics, metabolomics, proteomics, lipidomics, histopathology (tissue and subcellular structure), microbiomes, endosymbionts, tissue regeneration, and fecundity. Synchronized core samples were collected to obtain a sample for each methodology at the same location on the same coral at the same time providing the optimum chance to correlate results across the many investigated aspects and gain a wholistic understanding of the coral's condition. The RRC's goal is to understand the genetic, biochemical, and physiological underpinnings in the holobiont of individuals between infection categories to characterize risk factors that are driving differences in SCTLD infection rates and determine SCTLD resistance and susceptibility factors in corals. All of the sample data have been processed and sequenced. Therefore in 2023, the RRC is focusing on bioinformatics and statistical analyses of these data to understand the connections between components and conceptualize biological pathways associated with corals with lesions and those without.

2. PROJECT DESCRIPTION

Sampling was conducted for two purposes: 1) a unified sample across all colonies for each sample period (Unified Sample) and 2) to collect many samples across a few colonies for each sample period to investigate within-colony variability (Colony Variability Sample). The unified sampling occurred on the 90 corals in both regions and the colony variability sampling occurred on seven colonies in the KJCAP. The colony variability samples are reported separately.

Forty-five *Orbicella faveolata* colonies were selected in each region based on previous regional disease intervention monitoring data, equaling ninety total colonies (Figure 1). Fifteen corals with a high number of lesions and frequency of disease when visited (low resistance), fifteen corals with a single or few lesion and low frequency of disease (some resistance), and fifteen apparently healthy corals (no previous lesions) (high resistance) were sampled in each of two regions, Kristen Jacob's Coral Aquatic Preserve (KJCAP) (Figure 2) and the Lower Florida Keys (Keys) (Figures 3 and 4).

The unified samples were collected during three sample periods to coincide with different times of the year: late-May – mid-June (mid-gametogenesis, rainy season onset, low heat stress), mid-August – mid-September (pre spawning in KJCAP, post spawning in Keys, end of heat stress and rainy season), and late-February – early March (early gametogenesis, dry season, low heat stress). Tables 1 and 2 show the samples collected and dates of collections for each coral by sample period.

During each sampling period, unified core samples were collected on visually healthy-looking tissue on the horizontal upper surface of the colony (where possible) away from any present or previously diseased margins. Cores were taken as shallow as possible to limit stress on the colony. Within a 10 cm x 10 cm general sampling location, eight tissue cores were collected in sample period one, five in sample period two, and six in sample period three using various-size punch cores (Figure 5). A 10 mm core was used to collect tissue for genotyping (Voss), microbiome analyses (Voss/Meyer); microbial metagenomes (Meyer); proteomics (Woodley); transcriptomics and symbionts (Traylor-Knowles/Baker)

and an archive sample. A 14 mm core was used to collect tissue for chemical defenses (Paul), metabolomics (Garg), and lipidomics (Paul/Garg). A 20 mm core was used to collect tissue for histology (Hawthorne). Seven colonies had a one-time 10 mm tissue core of an active disease margin and a location far away from any disease on the same colony for TEM analysis (Work). Core collections occurred at least 1 cm away from each other to allow remaining tissue to heal the wounds.

During sample period 1, the holes from the cores were left unfilled. Subsequent visits revealed varying levels of fish predation on the hole edges, therefore the sample period 1 holes and all subsequent cores were immediately filled with a Roma Plastilina #2 artist clay as recommended by NOAA to eliminate predation and facilitate tissue regeneration.

During collections all cores were placed in individually labeled WhirlPaks underwater (Figure 6). Once all cores for a single coral were collected, they were immediately transferred to the boat for processing. Once a collection of cores was received on the boat, the cores were transferred to newly labeled containers and preserved. All cores were processed in less than 15 minutes from the time of initial collection.

Core samples were preserved in a variety of ways. The histology cores were transferred to a Flacon tube, preserved in Z-fix, and kept on ice. The TEM cores were placed in Tina's fixative on ice. The genotyping and microbiome cores were placed in small vials in Zymo DNA shield and placed on dry ice. The microbial metagenome, proteomics, transcriptomics/symbionts, chemical defense/metabolomics/lipidomics, and archive samples were placed in new WhirlPaks, submerged in liquid nitrogen, and stored in a liquid nitrogen dry shipper. Once back at the lab they were transferred to a -80 freezer, where they remained until shipping. Samples were shipped to individual labs for additional processing. See Appendix 1 for additional processing details for each sample.

Each sampled area was photographed before and after the sampling using a digital camera on a sample PVC frame with a ruler for scale. Sampled areas, core sites, were revisited and photographed regularly to monitor wound healing; monthly in the KJCAP and every other month in the Keys. Healing was assessed in the imagery using standard scaled photographic comparison techniques (Image J, NCRI CPCe) to quantify healing rates and amounts.

At each visit, all sampled corals were photographed and visually assessed by a diver estimating the percentage of live tissue, diseased tissue, bleached tissue, recent mortality, and old mortality. If SCTLD was found, the lesion was treated with antibiotic paste. No treatments occurred before sample collections on the same day. All margins were treated with the Ocean Alchemists antibiotic ointment CoreRx B2B with amoxicillin (1:8 ratio by weight). Photographs were taken of all areas before treatment at both the 0.5 m standard distance and wider scenes. Lesion treatments were determined to be failures if the active disease continued progressing past the treatment line.

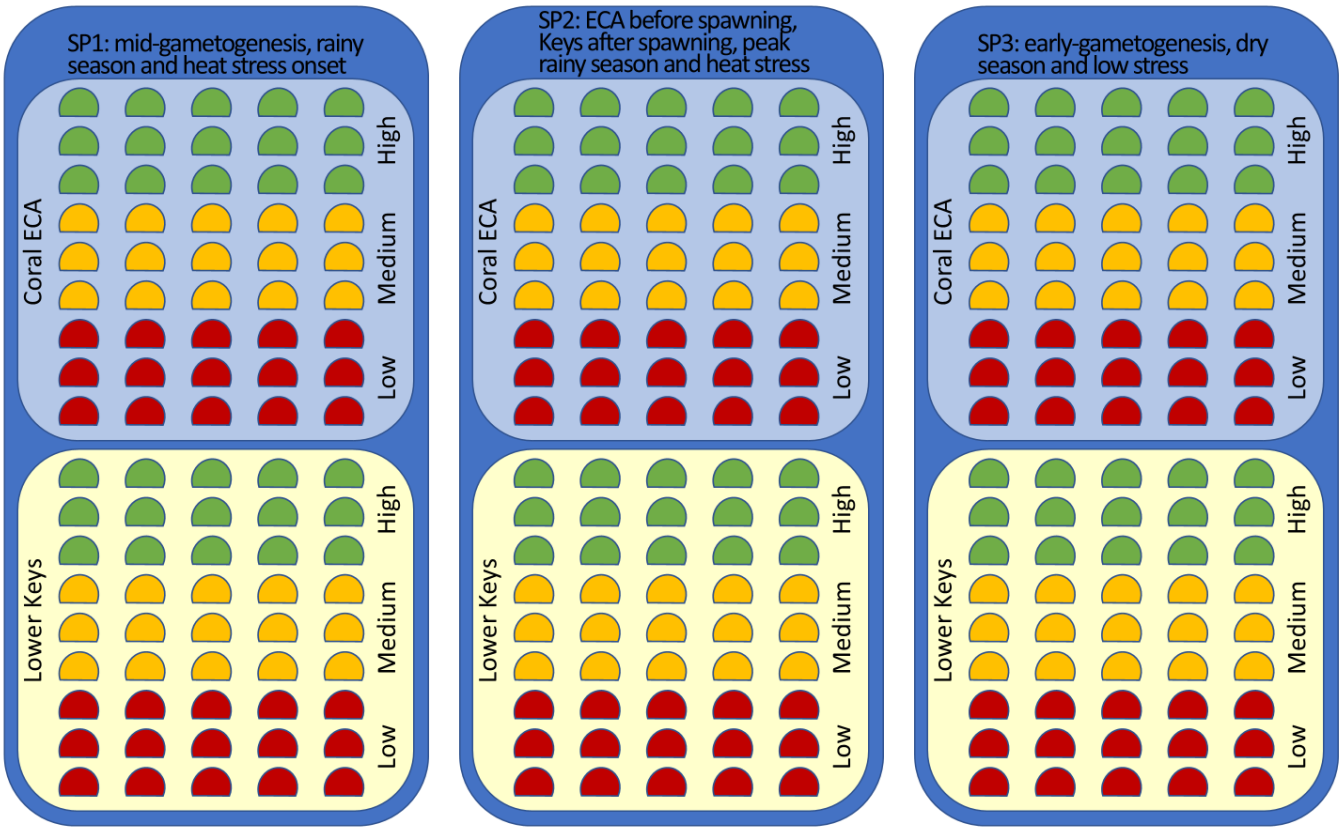

Figure 1. Illustration of sample design. Each colored semi-circle is a sampled coral colored by its disease resistance classification. Forty-five corals were sampled in each region at 3 separate times throughout the year.

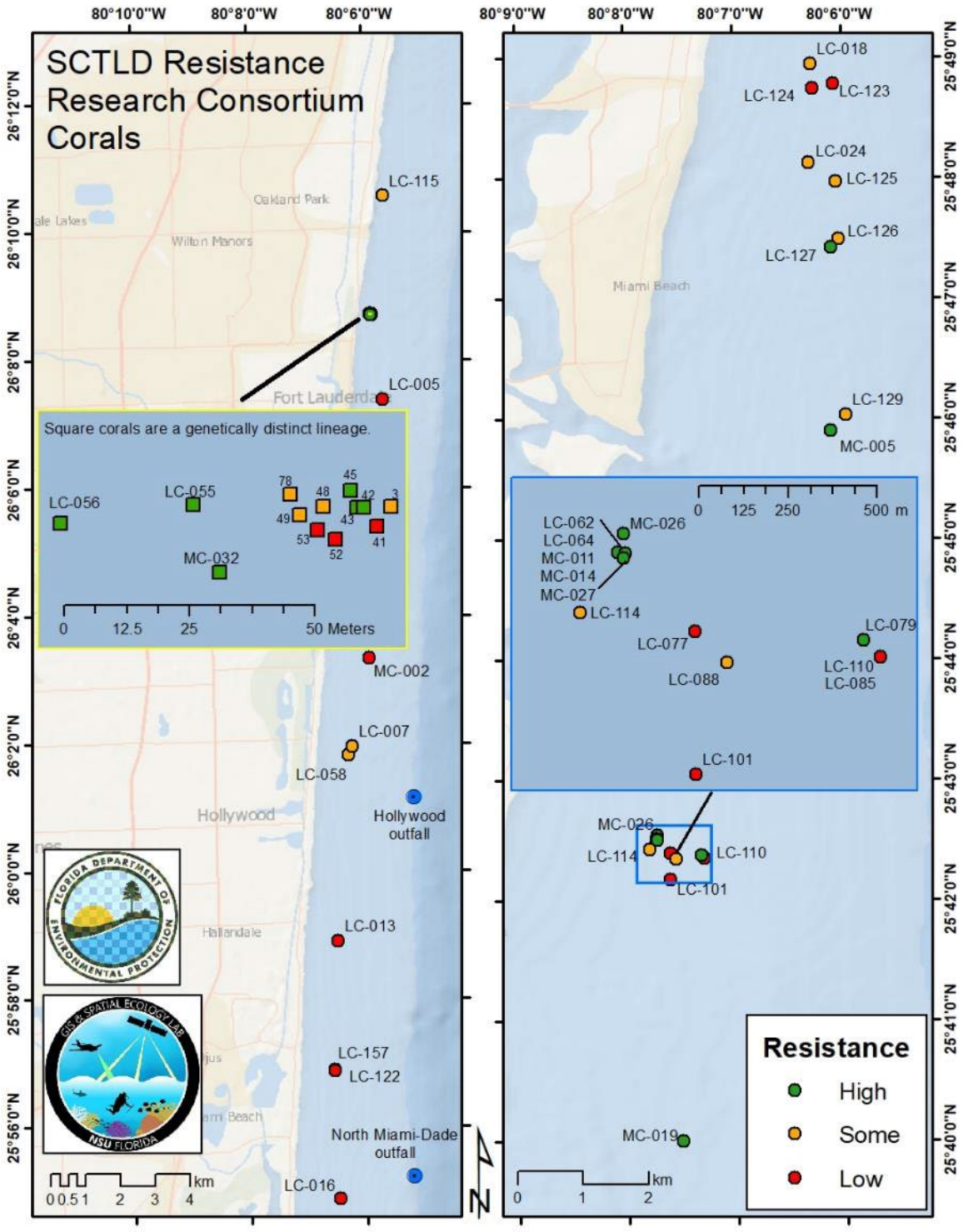

Figure 2. Map showing the location and category of the forty-five *O. faveolata* colonies sampled in the Kristen Jacob's Coral *Aquatic Preserve*.

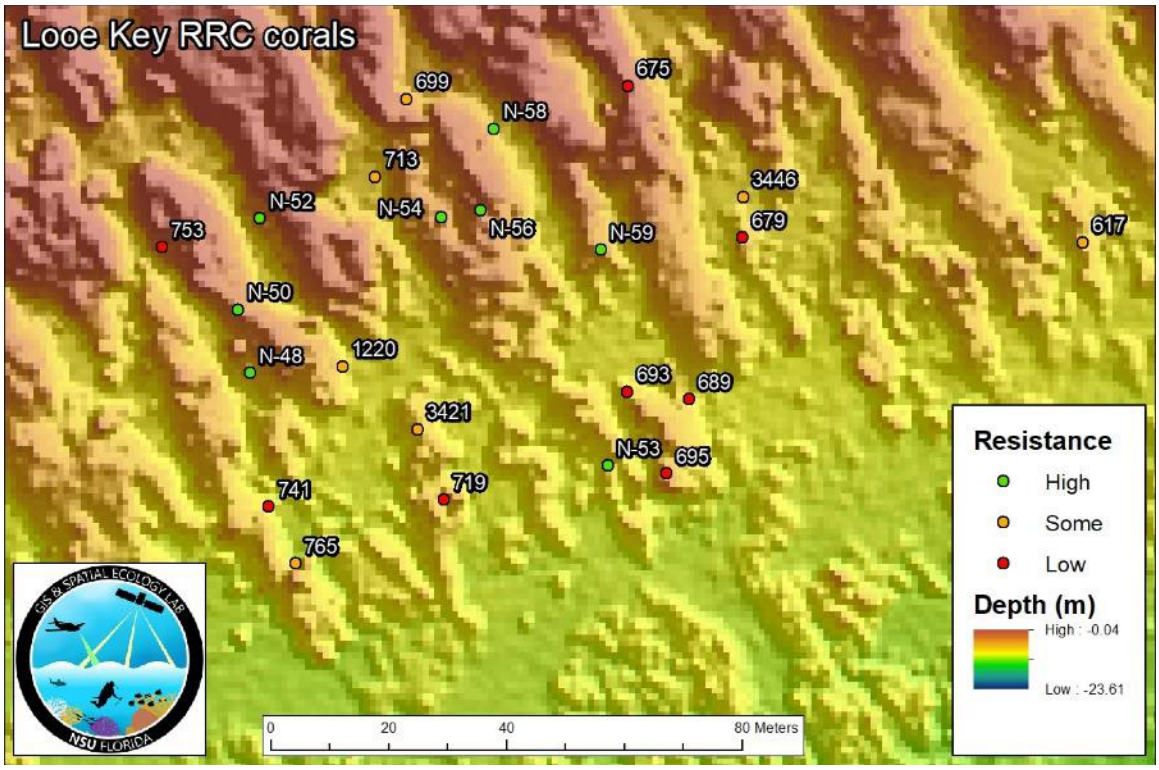

Figure 3. A map of the *O. faveolata* corals sampled at Looe Key.

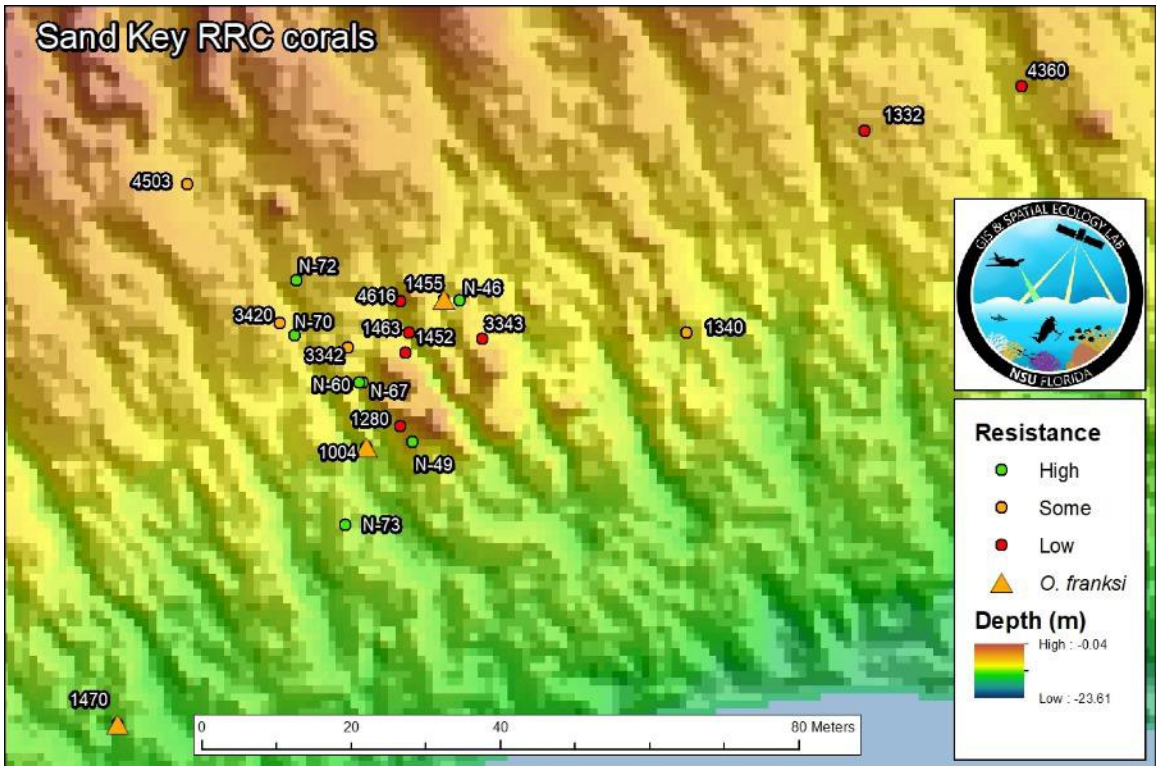

Figure 4. A map of the *O. faveolata* and inadvertently *O. franksi* corals sampled at Sand Key.

Table 1. Sample collection tables documenting the number, size, and date of each sample collected on each colony in the KJCAP by sample period. Colored rows indicate the SCTLD resistance categories: Green = High resistance, light coral = Medium resistance, and coral = Low resistance.

			Sample Period 1 - May/June 2021										Sample Period 2 - August 2021							Sample Period 3 - March 2022						
		Task:	Tasks 6,7,8,9,10, 11, Genotyping, Microbiome, Histo, TEM, Proteomics										Tasks 6,7,8,9,10, Microbiome, Histo							Tasks 6,7,8,9,10, Microbiome, Histo, Proteomics							
		Fixative:	Zymo & Liquid Nitrogen (10mm)		Liquid Nitrogen (4 - 10mm, 1 - 14mm)					Z fix (20mm)	Tina's fix (10mm)		Liquid Nitrogen (4 - 10mm, 1 - 14mm)				Z fix (14mm)	Tina's fix (10mm)		Liquid Nitrogen (3 - 10mm, 1 - 14mm)					Z fix (14mm)	
Coral ID	Location	Resistance Category	Genotyping (Voss)	Bacterial metagenome (Meyer)	Microbiome (Voss/Meyer)	Metabolomics (Garg/Paul)	Proteomics (Woodley)	Transcriptome, Symbionts (Baker/Traylor-Knowles)	Cryomill backup/archive	Histology (Hawthorn)	TEM (Work)	P1 Sample Date	Microbiome (Voss/Meyer)	Metabolomics (Garg/Paul)	Transcriptome, Symbionts (Baker/Traylor-Knowles)	Cryomill backup/archive	Histology (Hawthorn)	TEM (Work)	P2 Sample Date	Microbiome (Voss/Meyer)	Metabolomics (Garg/Paul)	Proteomics (Woodley)	Transcriptome, Symbionts (Baker/Traylor-Knowles)	Cryomill backup/archive	Histology (Hawthorn)	P3 Sample Date
LC-042	North	High	10	10	10	14	10	10	10	20		5/28/2021	10	14	10	10	20		8/19/2021	10	14	10	10	10	20	3/19/2022
LC-043	North	High	10	10	10	14	10	10	10	20		5/28/2021	10	14	10	10	20		8/19/2021	10	14	10	10	10	20	3/19/2022
LC-045	North	High	10	10	10	14	10	10	10	20		5/28/2021	10	14	10	10	20		8/19/2021	10	14	10	10	10	20	3/19/2022
LC-055	North	High	10	10	10	14	10	10	10	20		5/28/2021	10	14	10	10	20		8/19/2021	10	14	10	10	10	20	3/19/2022
LC-056	North	High	10	10	10	14	10	10	10	20		5/28/2021	10	14	10	10	20		8/19/2021	10	14	10	10	10	20	3/19/2022
LC-064	South	High	10	10	10	14	10	10	10	20		6/21/2021	10	14	10	10	20		8/21/2021	10	14	10	10	10	20	3/18/2022
LC-079	South	High	10	10	10	14	10	10	10	20		6/21/2021	10	14	10	10	20		8/21/2021	10	14	10	10	10	20	3/18/2022
LC-127	Middle	High	10	10	10	14	10	10	10	20		6/17/2021	10	14	10	10	20		8/20/2021	10	14	10	10	10	20	3/17/2022
MC-005	Middle	High	10	10	10	14	10	10	10	20		6/17/2021	10	14	10	10	20		8/20/2021	10	14	10	10	10	20	3/17/2022
MC-011	South	High	10	10	10	14	10	10	10	20		6/21/2021	10	14	10	10	20		8/21/2021	10	14	10	10	10	20	3/18/2022
MC-014	South	High	10	10	10	14	10	10	10	20		6/21/2021	10	14	10	10	20		8/21/2021	10	14	10	10	10	20	3/18/2022
MC-019	South	High	10	10	10	14	10	10	10	20		6/21/2021	10	14	10	10	20		8/21/2021	10	14	10	10	10	20	3/18/2022
MC-026	South	High	10	10	10	14	10	10	10	20		6/21/2021	10	14	10	10	20		8/21/2021	10	14	10	10	10	20	3/18/2022
MC-027	South	High	10	10	10	14	10	10	10	20		6/21/2021	10	14	10	10	20		8/21/2021	10	14	10	10	10	20	3/18/2022
MC-032	North	High	10	10	10	14	10	10	10	20		5/28/2021	10	14	10	10	20		8/19/2021	10	14	10	10	10	20	3/19/2022
LC-003	North	Some	10	10	10	14	10	10	10	20		5/28/2021	10	14	10	10	20		8/19/2021	10	14	10	10	10	20	3/19/2022
LC-007	Middle	Some	10	10	10	14	10	10	10	20		6/17/2021	10	14	10	10	20		8/20/2021	10	14	10	10	10	20	3/17/2022
LC-018	Middle	Some	10	10	10	14	10	10	10	20		6/17/2021	10	14	10	10	20		8/20/2021	10	14	10	10	10	20	3/17/2022
LC-024	Middle	Some	10	10	10	14	10	10	10	20		6/17/2021	10	14	10	10	20		8/20/2021	10	14	10	10	10	20	3/17/2022
LC-048	North	Some	10	10	10	14	10	10	10	20		5/28/2021	10	14	10	10	20		8/19/2021	10	14	10	10	10	20	3/19/2022
LC-049	North	Some	10	10	10	14	10	10	10	20		5/28/2021	10	14	10	10	20		8/19/2021	10	14	10	10	10	20	3/19/2022
LC-058	Middle	Some	10	10	10	14	10	10	10	20		6/17/2021	10	14	10	10	20		8/20/2021	10	14	10	10	10	20	3/17/2022
LC-062	South	Some	10	10	10	14	10	10	10	20		6/21/2021	10	14	10	10	20		8/21/2021	10	14	10	10	10	20	3/18/2022
LC-078	North	Some	10	10	10	14	10	10	10	20		5/28/2021	10	14	10	10	20		8/19/2021	10	14	10	10	10	20	3/19/2022
LC-088	South	Some	10	10	10	14	10	10	10	20		6/21/2021	10	14	10	10	20		8/21/2021	10	14	10	10	10	20	3/18/2022
LC-114	South	Some	10	10	10	14	10	10	10	20		6/21/2021	10	14	10	10	20		8/21/2021	10	14	10	10	10	20	3/18/2022
LC-115	North	Some	10	10	10	14	10	10	10	20		5/28/2021	10	14	10	10	20		8/19/2021	10	14	10	10	10	20	3/19/2022
LC-125	Middle	Some	10	10	10	14	10	10	10	20		6/17/2021	10	14	10	10	20		8/20/2021	10	14	10	10	10	20	3/17/2022
LC-126	Middle	Some	10	10	10	14	10	10	10	20		6/17/2021	10	14	10	10	20		8/20/2021	10	14	10	10	10	20	3/17/2022
LC-129	Middle	Some	10	10	10	14	10	10	10	20		6/17/2021	10	14	10	10	20		8/20/2021	10	14	10	10	10	20	3/17/2022
LC-005	North	Low	10	10	10	14	10	10	10	20		5/28/2021	10	14	10	10	20		8/19/2021	10	14	10	10	10	20	3/19/2022
LC-013	Middle	Low	10	10	10	14	10	10	10	20		6/17/2021	10	14	10	10	20		8/20/2021	10	14	10	10	10	20	3/17/2022
LC-016	Middle	Low	10	10	10	14	10	10	10	20		6/17/2021	10	14	10	10	20		8/20/2021	10	14	10	10	10	20	3/17/2022
LC-041	North	Low	10	10	10	14	10	10	10	20		5/28/2021	10	14	10	10	20		8/19/2021	10	14	10	10	10	20	3/19/2022
LC-052	North	Low	10	10	10	14	10	10	10	20		5/28/2021	10	14	10	10	20		8/19/2021	10	14	10	10	10	20	3/19/2022
LC-053	North	Low	10	10	10	14	10	10	10	20		5/28/2021	10	14	10	10	20		8/19/2021	10	14	10	10	10	20	3/19/2022
LC-077	South	Low	10	10	10	14	10	10	10	20		6/21/2021	10	14	10	10	20		8/21/2021	10	14	10	10	10	20	3/18/2022
LC-085	South	Low	10	10	10	14	10	10	10	20		6/21/2021	10	14	10	10	20		8/21/2021	10	14	10	10	10	20	3/18/2022
LC-101	South	Low	10	10	10	14	10	10	10	20		6/21/2021	10	14	10	10	20		8/21/2021	10	14	10	10	10	20	3/18/2022
LC-110	South	Low	10	10	10	14	10	10	10	20		6/21/2021	10	14	10	10	20		8/21/2021	10	14	10	10	10	20	3/18/2022
LC-122	Middle	Low	10	10	10	14	10	10	10	20		6/17/2021	10	14	10	10	20	10	8/20/2021	10	14	10	10	10	20	3/17/2022
LC-123	Middle	Low	10	10	10	14	10	10	10	20		6/17/2021	10	14	10	10	20		8/20/2021	10	14	10	10	10	20	3/17/2022
LC-124	Middle	Low	10	10	10	14	10	10	10	20		6/17/2021	10	14	10	10	20		8/20/2021	10	14	10	10	10	20	3/17/2022
LC-157	Middle	Low	10	10	10	14	10	10	10	20		6/17/2021	10	14	10	10	20	10	8/20/2021	10	14	10	10	10	20	3/17/2022
MC-002	Middle	Low	10	10	10	14	10	10	10	20		6/17/2021	10	14	10	10	20		8/20/2021	10	14	10	10	10	20	3/17/2022

Table 2. Sample collection tables documenting the number, size, and date of each sample collected on each colony in the lower Keys by sample period. Colored rows indicate the SCTLD resistance categories: Green = High resistance, light coral = Medium resistance, and coral = Low resistance.

			Sample Period 1 - June 2021										Sample Period 2 - September 2021							Sample Period 3 - February/March 2022						
Period:																										
Task:			Tasks 6,7,8,9,10, 11, Genotyping, Microbiome, Histo, TEM, Proteomics										Tasks 6,7,8,9,10, Microbiome, Histo, Proteomics							Tasks 6,7,8,9,10, Microbiome, Histo, Proteomics						
Fixative:			Zymo & Liquid Nitrogen (10mm)		Liquid Nitrogen (4 - 10mm, 1 - 14mm)					Z fix (20mm)	Tina's fix (10mm)		Liquid Nitrogen (4 - 10mm, 1 - 14mm)				Z fix (20mm)	Tina's fix (10mm)		Liquid Nitrogen (3 - 10mm, 1 - 14mm)					Z fix (14mm)	
Coral ID	Location	Resistance Catergory	Genotyping (Voss)	Bacterial metagenome (Meyer)	Microbiome (Voss/Meyer)	Metabolomics (Garg/Paul)	Proteomics (Woodley)	Transcriptome, Symbionts (Baker/Traylor-Knowles)	Cryomill backup/archive	Histology (Hawthorn)	TEM (Work)	P1 Sample Date	Microbiome (Voss/Meyer)	Metabolomics (Garg/Paul)	Transcriptome, Symbionts (Baker/Traylor-Knowles)	Cryomill backup/archive	Histology (Hawthorn)	TEM (Work)	P2 Sample Date	Microbiome (Voss/Meyer)	Metabolomics (Garg/Paul)	Proteomics (Woodley)	Transcriptome, Symbionts (Baker/Traylor-Knowles)	Cryomill backup/archive	Histology (Hawthorn)	P3 Sample Date
N-48	Looe	High	10	10	10	14	10	10	10	20		6/12/2021	10	14	10	10	20		9/15/2021	10	14	10	10	10	20	3/1/2022
N-50	Looe	High	10	10	10	14	10	10	10	20		6/12/2021	10	14	10	10	20		9/15/2021	10	14	10	10	10	20	3/1/2022
N-52	Looe	High	10	10	10	14	10	10	10	20		6/12/2021	10	14	10	10	20		9/15/2021	10	14	10	10	10	20	3/1/2022
N-53	Looe	High	10	10	10	14	10	10	10	20		6/12/2021	10	14	10	10	20		9/15/2021	10	14	10	10	10	20	3/1/2022
N-54	Looe	High	10	10	10	14	10	10	10	20		6/12/2021	10	14	10	10	20		9/15/2021	10	14	10	10	10	20	3/1/2022
N-56	Looe	High	10	10	10	14	10	10	10	20		6/12/2021	10	14	10	10	20		9/15/2021	10	14	10	10	10	20	3/1/2022
N-58	Looe	High	10	10	10	14	10	10	10	20		6/12/2021	10	14	10	10	20		9/15/2021	10	14	10	10	10	20	3/1/2022
N-59	Looe	High	10	10	10	14	10	10	10	20		6/12/2021	10	14	10	10	20		9/15/2021	10	14	10	10	10	20	3/1/2022
N-46	Sand	High	10	10	10	14	10	10	10	20		6/13/2021	10	14	10	10	20		9/14/2021	10	14	10	10	10	20	2/28/2022
N-49	Sand	High	10	10	10	14	10	10	10	20		6/13/2021	10	14	10	10	20		9/14/2021	10	14	10	10	10	20	2/28/2022
N-60	Sand	High	10	10	10	14	10	10	10	20		6/13/2021	10	14	10	10	20		9/14/2021	10	14	10	10	10	20	2/28/2022
N-67	Sand	High	10	10	10	14	10	10	10	20		6/13/2021	10	14	10	10	20		9/14/2021	10	14	10	10	10	20	2/28/2022
N-70	Sand	High	10	10	10	14	10	10	10	20		6/13/2021	10	14	10	10	20		9/14/2021	10	14	10	10	10	20	2/28/2022
N-72	Sand	High	10	10	10	14	10	10	10	20		6/13/2021	10	14	10	10	20		9/14/2021	10	14	10	10	10	20	2/28/2022
N-73	Sand	High	10	10	10	14	10	10	10	20		6/13/2021	10	14	10	10	20		9/14/2021	10	14	10	10	10	20	2/28/2022
617	Looe	Some	10	10	10	14	10	10	10	20		6/12/2021	10	14	10	10	20		9/15/2021	10	14	10	10	10	20	3/1/2022
663	Looe	Some	10	10	10	14	10	10	10	20		6/12/2021	10	14	10	10	20		9/15/2021	10	14	10	10	10	20	3/1/2022
699	Looe	Some	10	10	10	14	10	10	10	20		6/12/2021	10	14	10	10	20		9/15/2021	10	14	10	10	10	20	3/1/2022
713	Looe	Some	10	10	10	14	10	10	10	20		6/12/2021	10	14	10	10	20		9/15/2021	10	14	10	10	10	20	3/1/2022
765	Looe	Some	10	10	10	14	10	10	10	20		6/12/2021	10	14	10	10	20		9/15/2021	10	14	10	10	10	20	3/1/2022
1220	Looe	Some	10	10	10	14	10	10	10	20		6/12/2021	10	14	10	10	20		9/15/2021	10	14	10	10	10	20	3/1/2022
3421	Looe	Some	10	10	10	14	10	10	10	20	10	6/12/2021	10	14	10	10	20		9/15/2021	10	14	10	10	10	20	3/1/2022
3446	Looe	Some	10	10	10	14	10	10	10	20		6/12/2021	10	14	10	10	20		9/15/2021	10	14	10	10	10	20	3/1/2022
1004	Sand	Some	10	10	10	14	10	10	10	20		6/13/2021	10	14	10	10	20		9/14/2021	10	14	10	10	10	20	2/28/2022
1340	Sand	Some	10	10	10	14	10	10	10	20		6/13/2021	10	14	10	10	20		9/14/2021	10	14	10	10	10	20	2/28/2022
1455	Sand	Some	10	10	10	14	10	10	10	20		6/13/2021	10	14	10	10	20		9/14/2021	10	14	10	10	10	20	2/28/2022
1470	Sand	Some	10	10	10	14	10	10	10	20		6/13/2021	10	14	10	10	20		9/14/2021	10	14	10	10	10	20	2/28/2022
3342	Sand	Some	10	10	10	14	10	10	10	20		6/13/2021	10	14	10	10	20		9/14/2021	10	14	10	10	10	20	2/28/2022
3420	Sand	Some	10	10	10	14	10	10	10	20		6/13/2021	10	14	10	10	20		9/14/2021	10	14	10	10	10	20	2/28/2022
4503	Sand	Some	10	10	10	14	10	10	10	20		6/13/2021	10	14	10	10	20		9/14/2021	10	14	10	10	10	20	2/28/2022
675	Looe	Low	10	10	10	14	10	10	10	20		6/12/2021	10	14	10	10	20		9/15/2021	10	14	10	10	10	20	3/1/2022
679	Looe	Low	10	10	10	14	10	10	10	20		6/12/2021	10	14	10	10	20		9/15/2021	10	14	10	10	10	20	3/1/2022
689	Looe	Low	10	10	10	14	10	10	10	20		6/12/2021	10	14	10	10	20		9/15/2021	10	14	10	10	10	20	3/1/2022
693	Looe	Low	10	10	10	14	10	10	10	20		6/12/2021	10	14	10	10	20		9/15/2021	10	14	10	10	10	20	3/1/2022
695	Looe	Low	10	10	10	14	10	10	10	20		6/12/2021	10	14	10	10	20		9/15/2021	10	14	10	10	10	20	3/1/2022
719	Looe	Low	10	10	10	14	10	10	10	20	10	6/12/2021	10	14	10	10	20		9/15/2021	10	14	10	10	10	20	3/1/2022
741	Looe	Low	10	10	10	14	10	10	10	20	10	6/12/2021	10	14	10	10	20		9/15/2021	10	14	10	10	10	20	3/1/2022
753	Looe	Low	10	10	10	14	10	10	10	20		6/12/2021	10	14	10	10	20		9/15/2021	10	14	10	10	10	20	3/1/2022
1280	Sand	Low	10	10	10	14	10	10	10	20		6/13/2021	10	14	10	10	20		9/14/2021	10	14	10	10	10	20	2/28/2022
1332	Sand	Low	10	10	10	14	10	10	10	20		6/13/2021	10	14	10	10	20		9/14/2021	10	14	10	10	10	20	2/28/2022
1452	Sand	Low	10	10	10	14	10	10	10	20		6/13/2021	10	14	10	10	20	10	9/14/2021	10	14	10	10	10	20	2/28/2022
1463	Sand	Low	10	10	10	14	10	10	10	20		6/13/2021	10	14	10	10	20		9/14/2021	10	14	10	10	10	20	2/28/2022
3343	Sand	Low	10	10	10	14	10	10	10	20		6/13/2021	10	14	10	10	20		9/14/2021	10	14	10	10	10	20	2/28/2022
4360	Sand	Low	10	10	10	14	10	10	10	20		6/13/2021	10	14	10	10	20		9/14/2021	10	14	10	10	10	20	2/28/2022
4616	Sand	Low	10	10	10	14	10	10	10	20		6/13/2021	10	14	10	10	20	10	9/14/2021	10	14	10	10	10	20	2/28/2022

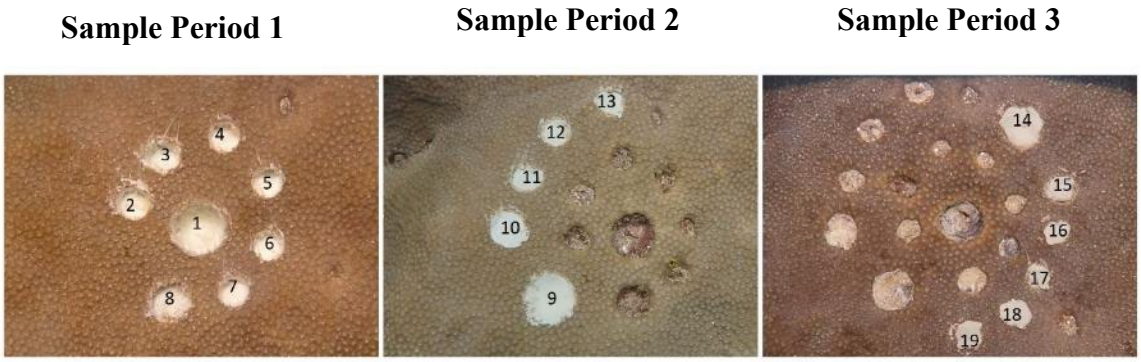

Figure 5. Example of the ideal sample core site arrangement. Core sample arrangements varied depending on colony morphology and available tissue. The example is from LC-005.

Figure 6. Photographs depicting the sample collection workflow from top left to bottom right. Photos by Karen Neely.

3. RESULTS AND DISCUSSION

3.1. Task 2: Colony and core site monitoring (Walker, Neely, Sharkey, and Kozachuk)

Goal: Continue revisiting the RRC corals semi-monthly to monitor for and treat new infections and collect core site photos until June 30, 2024.

Significant findings: SCTLD persisted throughout 2023 and 2024 cycling with seasons in SEFL and showing a general decline with time at Sand and Looe Key. SCTLD prevalence on RRC colonies remained higher in the Keys than in southeast Florida until summer of 2023 where it shut off during peak heat stress but picked up again upon recovery from bleaching. Eleven of the thirty (36.7%) high resistant corals showed lesions for the first time between May 2022 and December 2024 (3 in 2022, 6 in 2023, and 2 in 2024) indicating that historically SCTLD resistant corals continue to succumb to disease.

Results: Data and photographs from monitoring visits were added to the colony history database to document the number of treatments (Figure 7) and mortality (Figure 8) through time.

Discussion: The disease history data elucidates differences between regions and over time. The Lower Keys corals required significantly more treatments and were more frequently diseased when visited than the KJCAP. Funding for RRC monitoring in the Keys stopped in 2023 and is conducted opportunistically when possible. Disease interventions have not been allowed in the Keys since June 2024. The restriction of disease interventions threatens the corals' existence and inhibits our ability to monitor these colonies into the future because although we can note if corals have disease at a given point, we cannot be certain that subsequent observations are new lesions. We also expect these corals to continue to lose significant amounts of live tissue due to the lack of treatment. Long-term health histories, including presumed resistant corals that later developed lesions as well as corals that were historically sick but then became resilient can provide opportunities for researchers to identify disease markers or environmental correlates (See Section 3.18 for more on this). Disease interventions and monitoring must continue on these corals in order for us to capture SCTLD dynamics into the future.

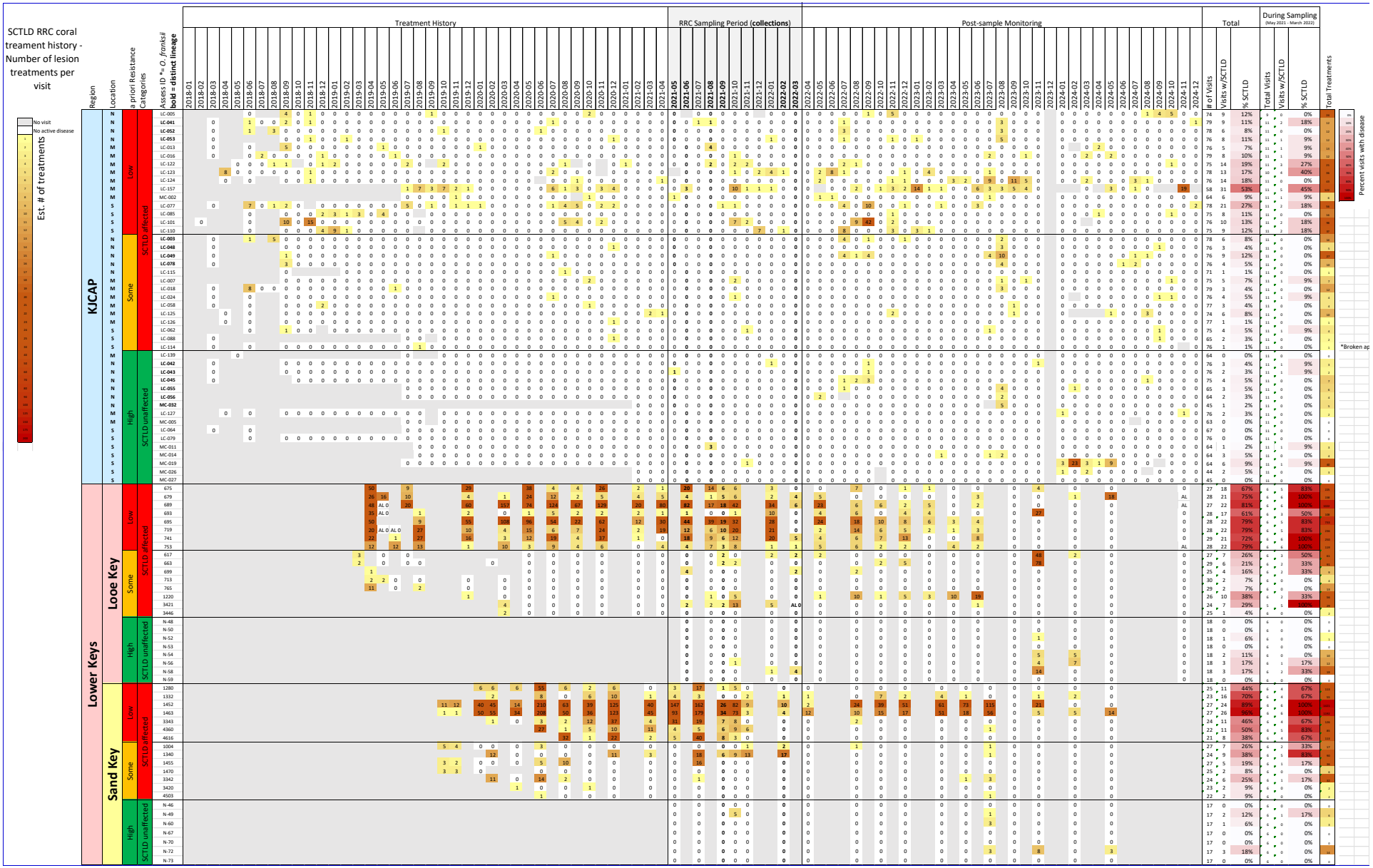

Figure 7. RRC colony disease treatment history.

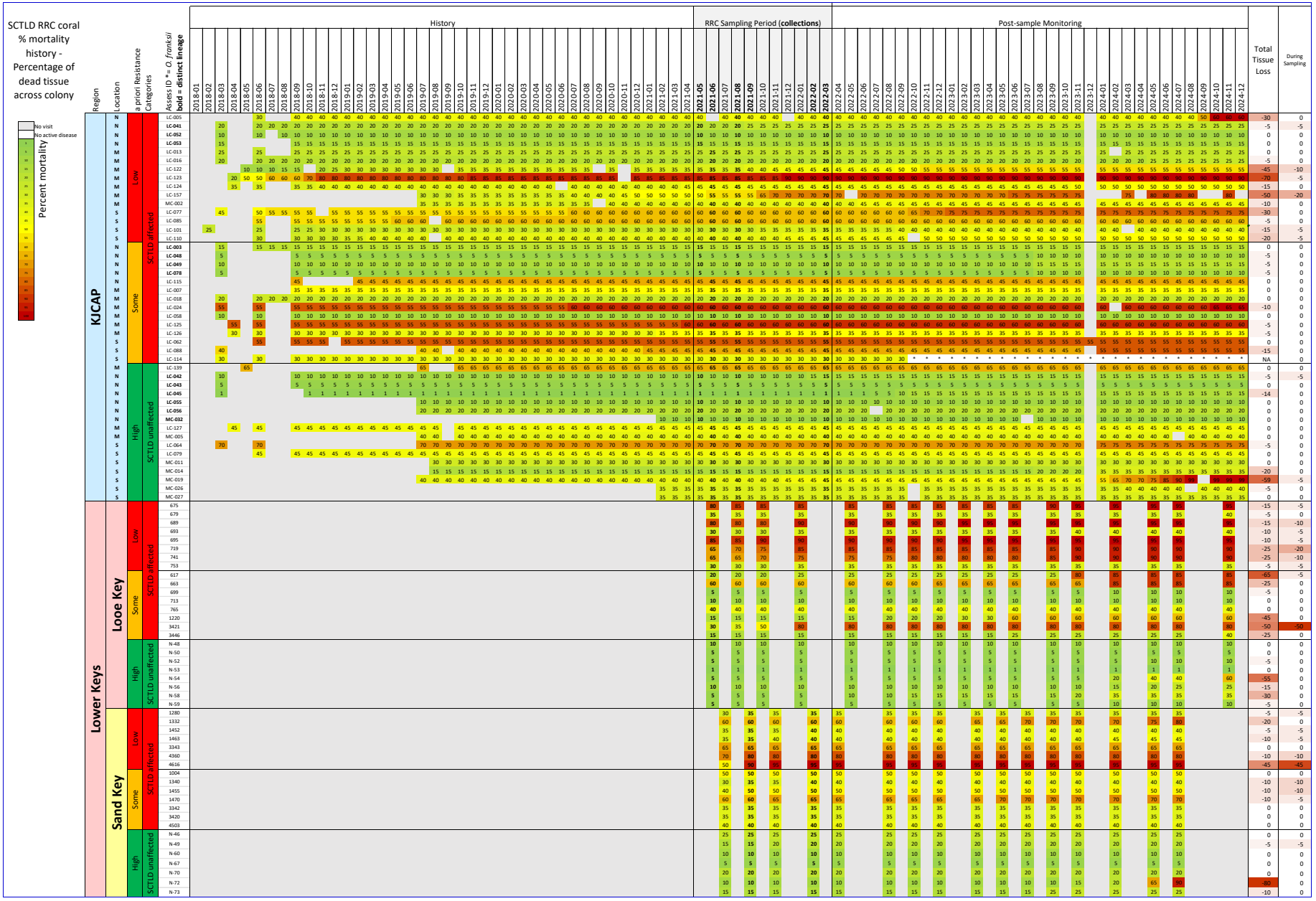

Figure 8. RRC colony percent mortality history.

3.2. **Task 3: Tissue regeneration and wound healing (Walker, Wheeler, Williams, Woodley)**

Goals: 1) Assess the tissue regenerative rates of all core lesions on the reef-building species *O. faveolata* and 2) quantify the amount of missing tissue associated with coring

Significant findings: Predation on core sites was comparable to similar studies and was reduced with the filling of cores with ablative clay. Disease emanating from core sites was very low even though SCLTD prevalence persisted throughout the period. 25% of biopsied tissue regrew by the end of the study. Regrowth was higher in the KJCAP than the lower Keys, indicating a generally healthier state in northern colonies. Low rates of disease and predation combined with considerable healing may ease the concerns of managers considering the cost benefit of coring *O. faveolata* colonies in this region.

Main results:

Daily Regeneration Rate Analysis

A Generalized Linear Mixed Model (GLMM) was used to analyze the relationship between the daily regeneration rate and several intrinsic and extrinsic variables (Table 3). An initial Wilcoxon rank sum test found significance ($W = 2581$, p-value < 0.05) in the lineage and region (KJCAP vs. Keys) factors and a Kruskal-Wallis rank sum test found significance (chi-squared = 18.408, p-value = 0.05) with region sublevels. Colony ID was included as a random factor. These three factors were then used in the model selection for the GLMM test (Table 4). The model of best fit found region and the random colony variable predicted the most variation in the DRR (Conditional R^2: 0.51, Marginal R^2: 0.13, AIC = 65.603).

The model showed a significantly higher DRR in the KJCAP versus the Keys (SE = 0.112, $p < 0.05$) (Figure 9), with KJCAP colonies growing an average of 0.615 mm^2/day and the Keys growing at an average rate of 0.455 mm^2/day. In a separate model with a slightly worse fit (AIC = 68.4) the subregions found significantly elevated regeneration rate between the North and Middle sections of the KJCAP and Sand Key ($p < 0.08$). There was also a large difference in conditional and marginal R^2 values, indicating the random variable was responsible for 37.8% of variation in the DRR. This suggests that large amounts of variation in our model were explained by our random variable (Figure 10).

Table 3. Variables tested against the daily regeneration rate in the GLMM model. Variable category, variable name, variable type, and details are included.

Variable Category	Variable	Type	Details
Region	KJCAP vs. Keys	Cat.	KJCAP vs. Keys
	All subregions	Cat.	North vs. Middle vs. South vs. Looe vs. Sand
Disease	Treats/SP	Cont.	Count of treatments w/ in first year of growth
	% Visits Diseased	Cont.	% of visits where the colony was diseased
	Disease History	Cont.	Count of all treatments prior to sampling
Lineage	Lineage	Cat.	Within and outside genetic lineage
Predation	Predation	Binary	Present / absent during study period
Sample Period	Sample Period	Cat.	SP1 vs. SP2 vs. SP3
Colony	Assess ID	Cat.	Colony effect (random)

Table 4. Model selection between three terms found to be initially significant: Region, Subregion, and Lineage. Model, AIC, conditional and marginal R^2 values are shown. Model of best fit shown in bold.

Candidate Model	AIC	Cond. R^2	Marg. R^2
DRR ~ Lineage * Region * Subregion + (1|AssessID)	66.61		
DRR ~ Lineage * Region + Subregion + (1|AssessID)	69.89		
DRR ~ Lineage * Region + (1|AssessID)	67.28		
DRR ~ Lineage * Subregion + (1|AssessID)	69.89		
DRR ~ Region + (1|AssessID)	**65.60**	**0.506**	**0.127**

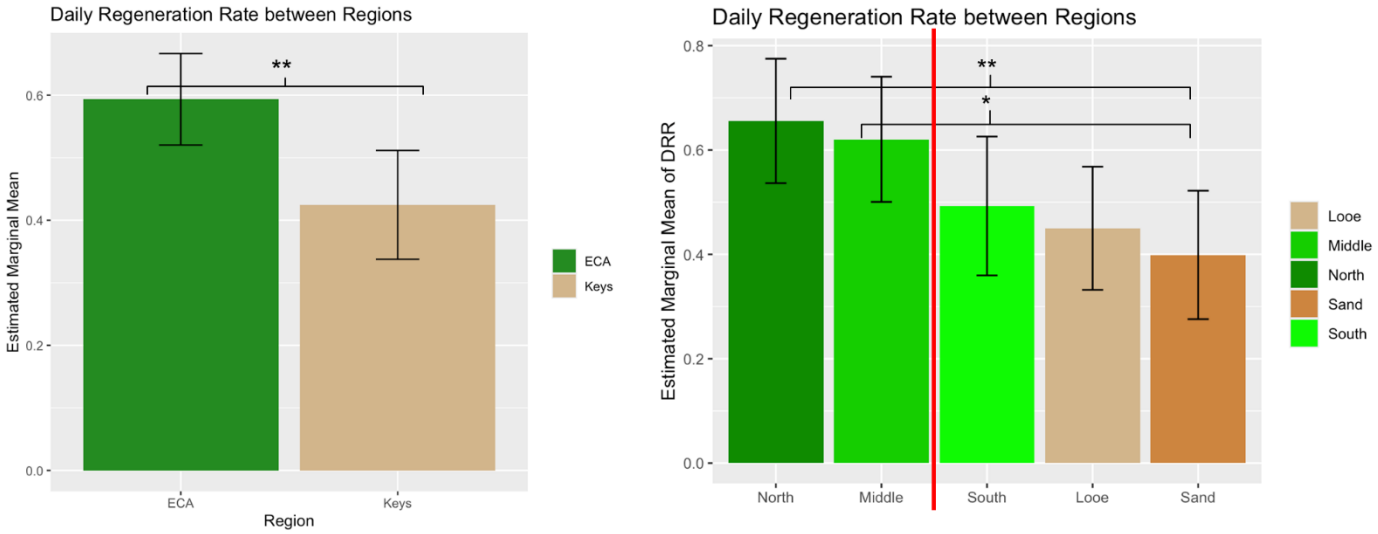

Figure 9. Chart comparing region against the estimated marginal means of the daily regeneration rate. Significant variation observed between regions. Standard error bars show margin of error.

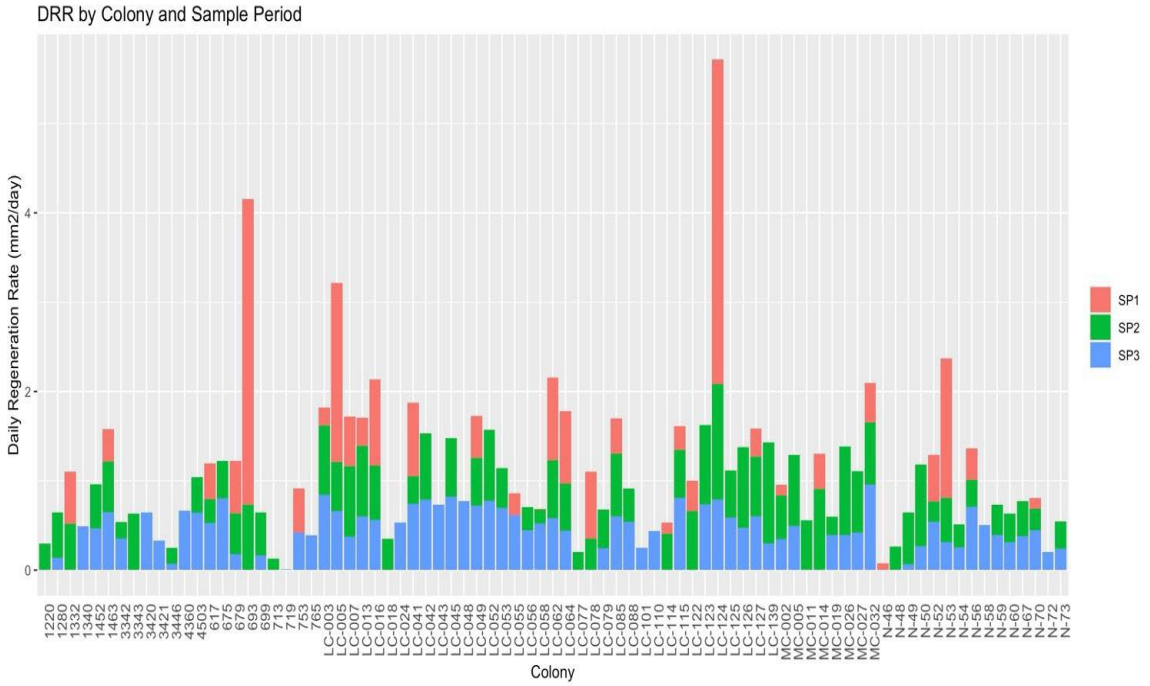

Figure 10. Stacked bar chart showing daily regeneration rate between colonies and sample period. X axis shows the colony and the y axis shows DRR. Color represents sample period. Some colonies had entire sample periods excluded from this analysis due to predation, disease, and/or fusion outcomes. High variation was observed between colonies.

Colony Impacts

In total, 1,609 cores were taken on 87 *O. faveolata* throughout the duration of the study (706 of days) totaling 436.17 cm^2 of biopsied tissue. By the end, 138.95 cm^2 of tissue regenerated passed the 0.001 mm^2 threshold by May 2023. In other words, 31.9% of the impacted tissue recovered over the 2-year monitoring period. No coral colonies had all of their cores fully heal but many experienced partial healing. Sixty-nine cores fully healed out of the 1,609 taken (4.10% of total) and 37 corals had at least one core fully heal (42.53% of total). Two colonies (2.3% of total) had disease emanate from the core site constituting only 7 cores between both colonies (0.44% of total). A total of 61 cores (3.7% of total) on 34 corals (39.1% of total) had cores with predation.

A 2-sample test for equality of proportions with continuity correction showed SP1 was responsible for the significant majority of all new predation instances throughout the study (X-squared = 86.7, p-value < 2.2e-16). Of the 34 colonies to experience predation throughout the study, SP1 contained 93.3% of all predation instances observed, with SP2 experiencing 6.6% and SP3 experiencing none.

A model showing predation as a function of region and filling before/after was the most significant. A Fisher's Exact Test of predation incidences showed the effect of filling as significant in suppressing predation across all regions in SP1 cores (p = 1.189e-06) (Figure 11), with a significant increase in predation observed before filling and a significant decrease observed after. A Tukey post-hoc test revealed significant differences before and after filling in both the KJCAP (SE = 1.055, $p < 0.05$) and Looe Key (SE = 1.091, $p <$

0.05). Sand Key experienced no predation before filling and only 2 instances afterwards, thus no significance of filling was observed in that region ($p > 0.05$) (Figure 12).

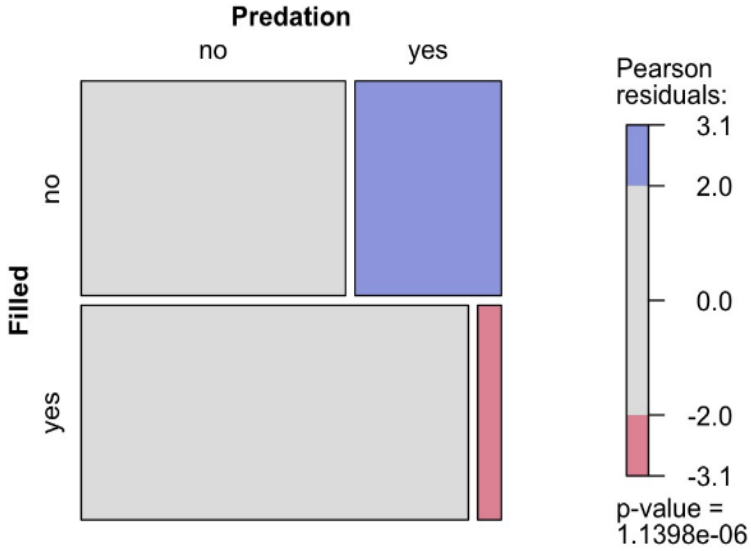

Figure 11. Mosaic plot showing count of predation status against count of predation instance throughout project (Spring 2021 - Spring 2023). Color signifies significance, with blue indicating significant increase and red indicating significant decrease in observation probability.

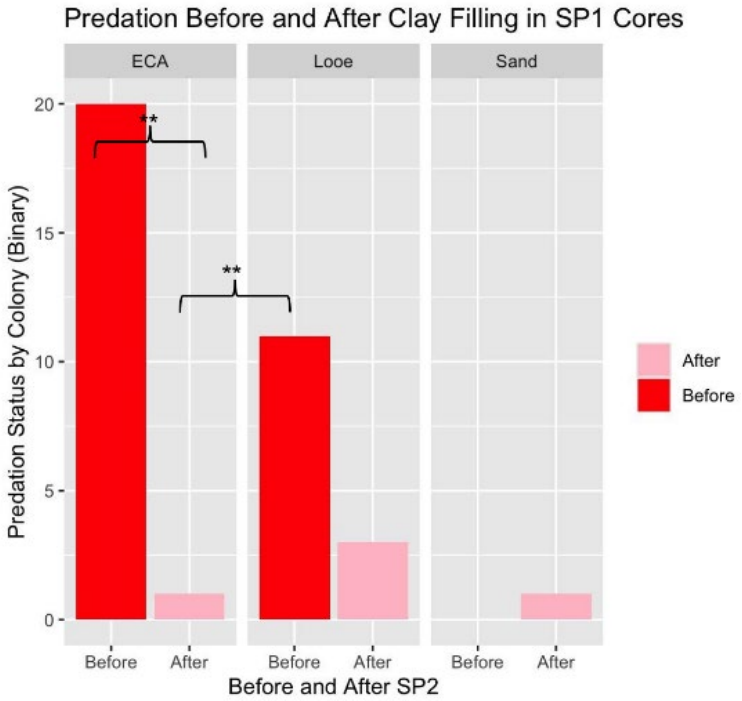

Figure 12. Predation status in SP1 cores measured before and after filling (SP2) considered by region. Red bars show "before", and pink bars show "after". Brackets show significance in the post-hoc test. Significant decrease in predation observed after filling and in interacting terms before and after in Looe Key and the KJCAP.

Discussion:

Patterns in the Daily Regeneration Rate

The analyses found that the regeneration rate varied most across the two largest subdivisions of our region variables, the KJCAP and Keys sites, and found high variation between colonies. A significant increase in regeneration rate was observed in the KJCAP when compared to both Keys reefs, with the KJCAP regenerating on average of 0.615 mm^2/day and the Keys growing at an average rate of 0.455 mm^2/day. A similar model comparing the DRR between subregions within the KJCAP and Keys also found a significant increase in growth rates between both the North and Middle sections when compared to Sand Key Reef ($p < 0.08$).

Spatially determined factors, such as temperature, may be limiting metabolic resources away from regrowth as well as oogenesis. The spatial pattern of growth observed between the Middle and South subregions align with other research on these same colonies. For example, oogenesis in the North and Middle sections of the KJCAP was found to be significantly elevated in comparison to the other three southern subregions (south KJCAP, Sand, & Looe Key) (Sharkey 2024) ($p < 0.05$). Denis et al. (2011) found higher regrowth rates from experimental wounds in *Porites lutea* in cooler months compared to warmer ones due to suppression of endosymbiont photosynthetic efficiency, limiting resources available for regeneration. However, elevated temperature can also be positively correlated with tissue regrowth, as demonstrated by Kramarsky-Winter & Loya (2000), who found increased growth in warmer ex-situ treatments of *Fungia granulosa* due to increase in coral host metabolism. Since the KJCAP sites experienced lower average sea surface temperatures than both Florida Keys sites (*NOAA Coral Reef Watch Daily 5km Regional Virtual Stations*, n.d.) our results indicate lower temperatures favor faster growth in this species.

The elevated DDR seen in the KJCAP cores versus those in the Keys may also align with proteomic and lipidomic results of these colonies. Variation in stress-related proteins were observed between the KJCAP and the Keys in low SCTLD-resistance colonies, with only 11 differentially abundant proteins expressing themselves in the KJCAP versus 80 observed in the Keys. Region also significantly predicted variation in the lipidome of these colonies by disease-susceptibility within the lower Keys, but not in the KJCAP. In combination, these results indicate a more stable state at the northerly region where corals are regenerating faster and maintain a more stable biological state in response to stress events (Walker et al., 2023).

There was no significant relationship of the regeneration rate to colony disease history. This result was unexpected as disease has been shown to affect many aspects of a coral's biology, including growth and regrowth potential in fan corals (Henry & Hart, 2005; Ruiz-Diaz et al., 2016). It is possible, given the unknown nature of the current SCTLD outbreak affecting the greater Caribbean, that differences in disease exposure are not sufficient to differentially affect the growth rates of large colonies if SCLTD is water-born as some have suggested (Rosenau et al., 2021). Still, disease resistance has been observed within certain populations of *O. faveolata* in SE Florida and further research is needed to key out the full implication of these infections.

Lastly, colony effect was included in our model as a random factor and represented almost 38% of the variation (AIC = 315.8, conditional $R^2 = 0.51$, marginal $R^2 = 0.18$). This result has been observed in recent scleractinian coring studies in both *O. faveolata* (Rodríguez-Martínez et al., 2016) and *M.* cavernosa (Horricks, 2017), both of which concluded intrinsic biological variables, like local environmental impacts or differences in protein expression, within the individual colonies were impacting regeneration more than any shared regenerative capacity within their respective species. This result ran contrary to other coring studies which have seen large interspecies variation and relative homogeny within members of the same species (Rodríguez-Martínez et al., 2016), however these studies were spatiotemporally limited. Most previous studies were either conducted on a smaller number of colonies or tested colonies clustered in a relatively small area. A larger sample size and spatial spread of colonies could increase variation. Given that genetic identity wasn't significant in our model, it's unlikely variation in growth rate between colonies was an effect of genetic distance and may vary by other colony factors not tested in this study, like colony size or core proximity or size.

Colony Impacts

Predation outcomes over the course of the study were widely dispersed, affecting approximately a third of all colonies, but rarely affecting all cores within that colony. While many corals were predated, the vast majority occurred within SP1 (93.3%) likely as a result of the cores being left unfilled. After SP1, a significant drop in predation was observed in subsequent sampling periods, with SP2 experiencing only 6.6% of total predation and SP3 cores experiencing no recorded predation throughout the entire study. The vast majority of predation occurred before core filling at the September 2021 SP2 initial time point than after, providing strong evidence that filling cores deterred fish predation within the initial month. Studies have shown decreases in fish predation within the initial two to four weeks post-outplant in *O. faveolata* and *M. cavernosa* (Koval et al., 2020; Page et al., 2018; Rivas et al., 2021). The use of ablative clay that can last long enough to prevent predation during this heavily trafficked window is recommended when taking core samples. However, this result would have been bolstered by the inclusion of other sample periods to account for time of year, but since rainbow parrotfish (a predominant local corallivorous species) show no evidence of ontogenetic migration (Paddack et al., 2009), its possible predation would be relatively constant throughout the year. Little research has been done on the predation of experimentally inflicted wounds on scleractinian corals, but if we consider the rate of predation on SP1's unfilled cores, we may surmise a relatively high amount in South Florida.

Healing outcomes across the study were comparable to those from similar wounding studies. Rodríguez-Martínez et al. (2016) conducted a long-term coring experiment on *O. faveolata* colonies in Puerto Morelos reef, Mexico across a four-year sample period. Over the course of their study, they reported 4% of lesions having fully healed and 52% underwent partial healing. Our study produced similar results, with 4.1% of our cores healing completely and 46.6% undergoing healing of some kind only ours took half the time (2 years). It should be noted that our small healing threshold may be deflating our results and it is likely many of these cores have, in the years since, continued and/or

completed their healing trajectory. Subsequent analyses hope to address this question. Like, Rodríguez-Martínez et al. (2016), our results lead us to recommend considering the potential impacts when taking experimental cores on slow-growing species like *O. faveolata*, although filling the cores may mitigate some of this effect.

Failure of wounds to heal has been shown on both diseased tissue and adjacent healthy tissue (Rodríguez-Martínez et al., 2016). Considering damaged tissue is more susceptible to disease (Aeby & Santavy, 2006; Page & Willis, 2006) and our study was conducted in a high-impact reef on colonies with many previous SCTLD lesions (Walker et al., 2023), the low disease instances observed in our study suggest coring of this magnitude is not sufficient to increase SCTLD prevalence on the sample colonies. Disease prevalence was low throughout the study, with only 2 colonies experiencing disease directly associated with coring, constituting only 7 cores in total. One colony's cores quickly died from a Type 2 fusion while the other, over the course of several months, was able to halt its lesion and start regenerating tissue again. However, other studies have reported similarly low disease instances associated with coring (Horricks, 2017; Rodríguez-Martínez et al., 2016). Regardless, this result may ease the concerns of reef managers considering the association with experimental coring and the further spread of SCTLD.

3.3. Task 4a: RRC Unified core ITS2, method comparison, and statistics (Dennison, Baker, and Voss)

Goals: Compare the relative abundance of detected Symbiodiniaceae genera across three sequencing methods – 2bRAD, qPCR, and ITS2 – of varying sensitivity to provide recommendations of future sampling techniques and algal symbiont identification and quantification approaches

Significant findings: Algal symbiont composition varied across the different identification and quantification methods compared here despite using the same samples across the methods. The detection of *Symbiodinium* and *Cladocopium* was higher when samples were analyzed using high-resolution 2bRAD single nucleotide polymorphism approach (2bRAD) in comparison to more sensitive approaches like qPCR and ITS2 sequencing. It is believed that the detection of *Symbiodinium* and inflated presence of *Cladocopium* using 2bRAD sequencing is likely an artifact of the approach and qPCR and ITS2 sequencing are more accurate means of estimating Symbiodiniaceae genera.

Results:
Across the samples and algal symbiont identification and quantification methodologies *Symbiodinium, Breviolum*, *Cladocopium*, *Durusdinium*, and *Gerakladium* were detected (Figure 13). Primer/probed based qPCR assays and ITS2 did not detect any amount of *Symbiodinium* in any of the samples, while 2bRAD sequencing detected background amounts of *Symbiodinium* (<20%) in all the samples. Additionally, ITS2 sequencing detected <2% *Gerakladium* in one sample. There were significant differences in the abundance of Symbiodiniaceae across the various methodologies (Figure 14). 2bRAD sequencing yielded a higher abundance of both *Symbiodinium* and *Cladocopium* relative to that detected in qPCR assays and ITS2 sequencing. However, the detection of *Breviolum* using 2bRAD was less than that of qPCR and ITS2. Finally, the abundance of *Durusdinium* detected using 2bRAD was significantly more than that detected using qPCR assays but not statistically different than that detected using ITS2. It is believed that the detection of *Symbiodinium* and inflated presence of *Cladocopium* using 2bRAD sequencing is likely an artifact of the approach and qPCR and ITS2 sequencing are more accurate means of estimating Symbiodiniaceae genera. To test this, comparative analyses of known combinations of algal symbiont assemblages would be ideal, e.g. 100% cultures of each, equally mixed with 25% each. Even starting with known assemblages, gene copy number variance among and within algal endosymbiont genera may influence the resultant data.

Given the method comparison results, additional ITS2 sequencing was conducted of the RRC unified core samples. SP1 samples were extracted, amplified, and sequenced using ITS2 primers to better understand the specific algal symbiont species present within the 90 corals selected. Generally, across the corals selected for this study we identified 14 unique *Breviolum* type profiles, six *Cladocopium* type profiles, and eight *Durusdinium* type profiles, with a couple samples having ITS2 profile reads mapping to the genus *Gerakladium* (likely an artifact of low read numbers associated with a couple samples). Patterns between SCTLD affected and unaffected colonies remain elusive (Figure 15), but there are interesting patterns associated with region and dominant contributing water inlet

(Figure 16) that may be inhibiting detection of SCTLD effects. Noteably, corals located north of Port Everglades inlet do not contain any detectable amounts of *Cladocopium* and/or *Durusdinium*.

The second plate of ITS2 sequencing has been sent to our sequencing facility and we are awaiting our results. This plate includes the remaining samples for the RRC unified corals for sample periods 2 and 3, as well as the 90 samples selected to compare 2bRAD, qPCR, and ITS2 algal symbiont identification.

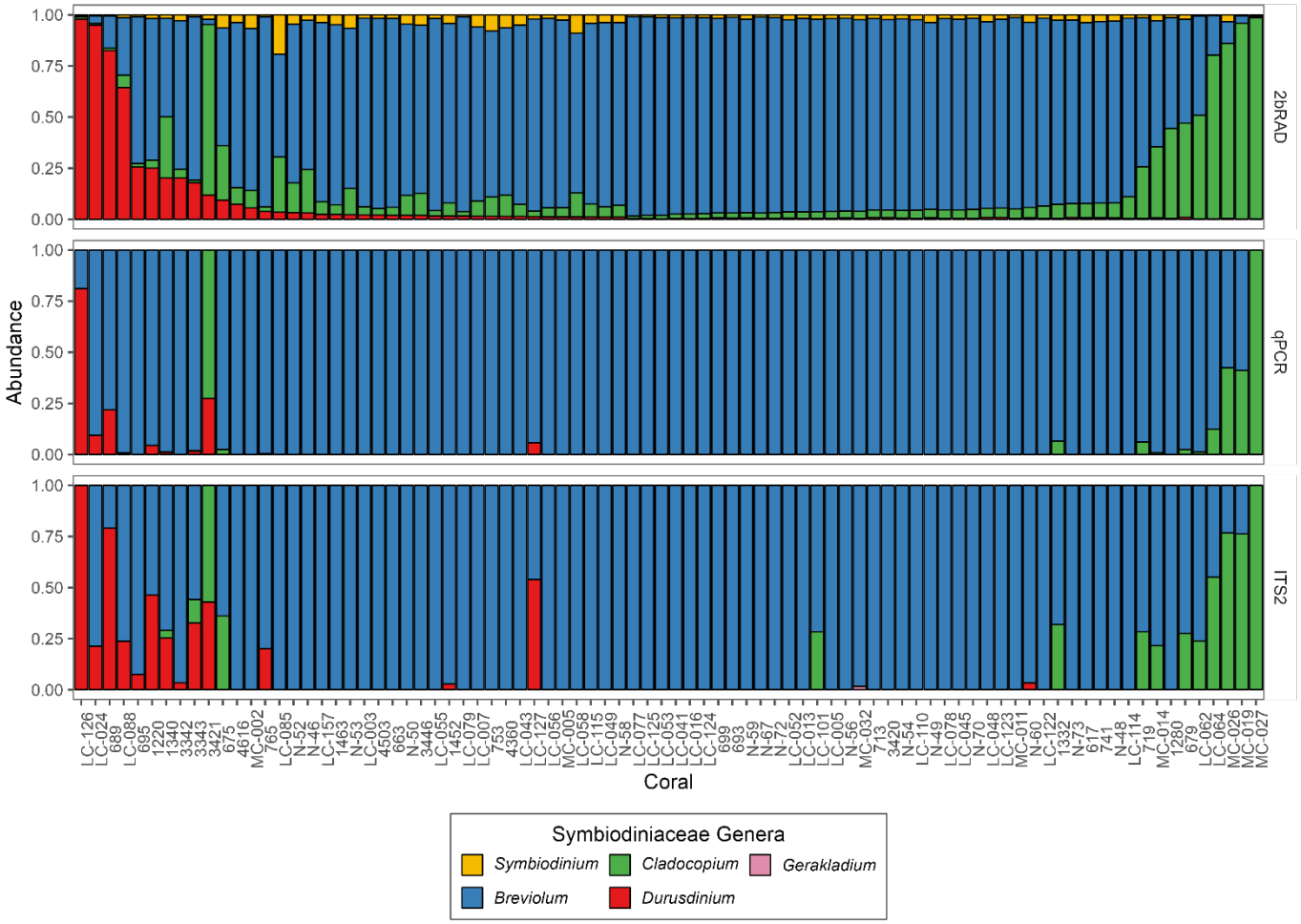

Figure 13. Relative abundance of Symbiodiniaceae genera detected across the same samples using different identification and quantification approaches.

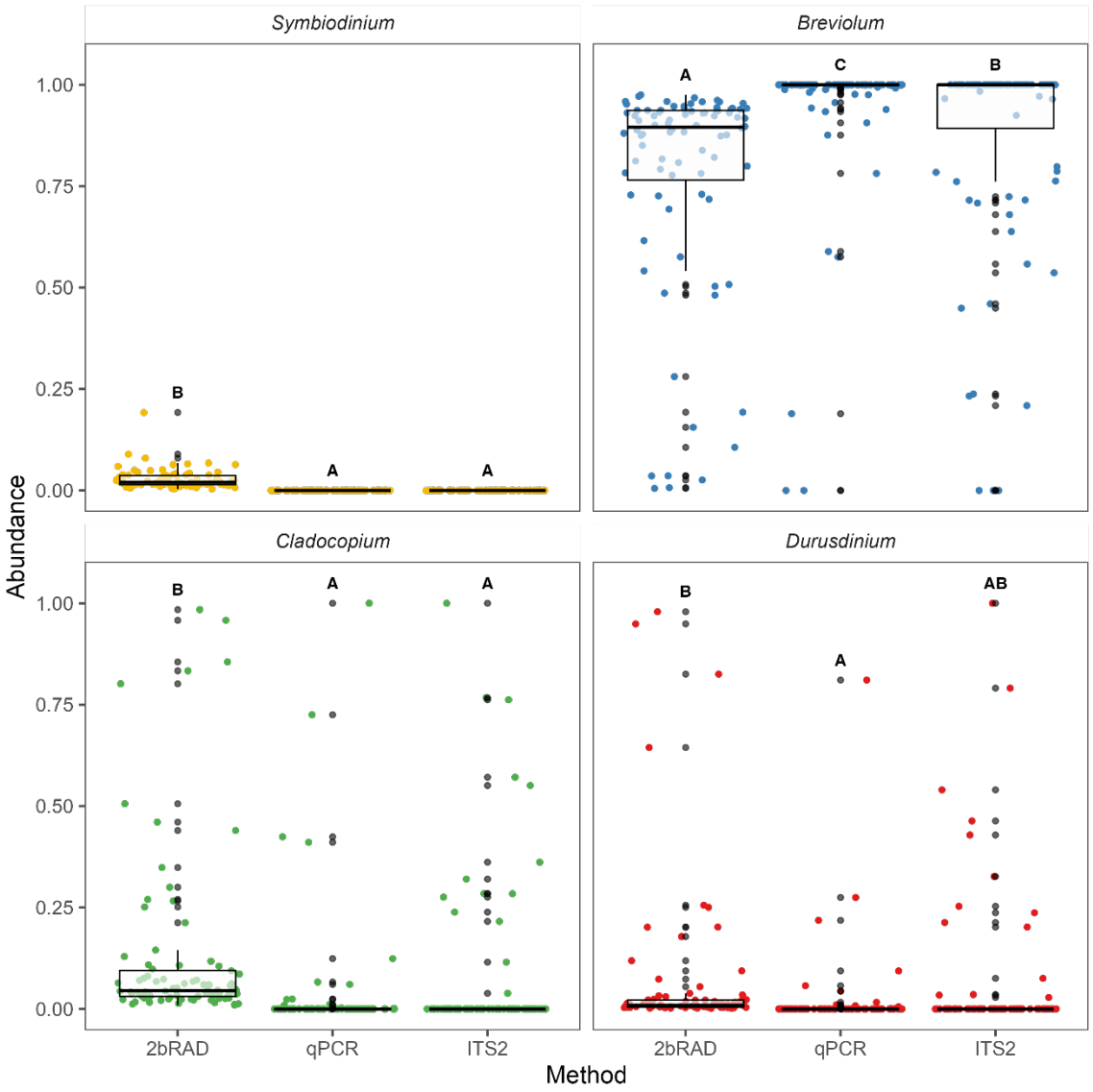

Figure 14. Comparison of Symbiodiniaceae abundance across different methods for *Symbiodinium*, *Breviolum*, *Cladocopium*, and *Durusdinium*. Raw data points (individual samples) are shown in color based on the Symbiodiniaceae genera, where yellow corresponds with *Symbiodinium*, blue corresponds with *Breviolum*, green corresponds with *Cladocopium*, and red corresponds with *Durusdinium*. *Gerakladium* was omitted from this analysis as it was found in very background amounts in a single sample across all the methodologies and therefore the sample size was small. Boxplots show the median and interquartile range of datapoints. Letters above the boxplots show statistical significance between methods based on pairwise comparisons using Bonferroni-adjusted p-values from a linear mixed effects model (Abundance ~ Method + (1|CoralID), alpha=0.01).

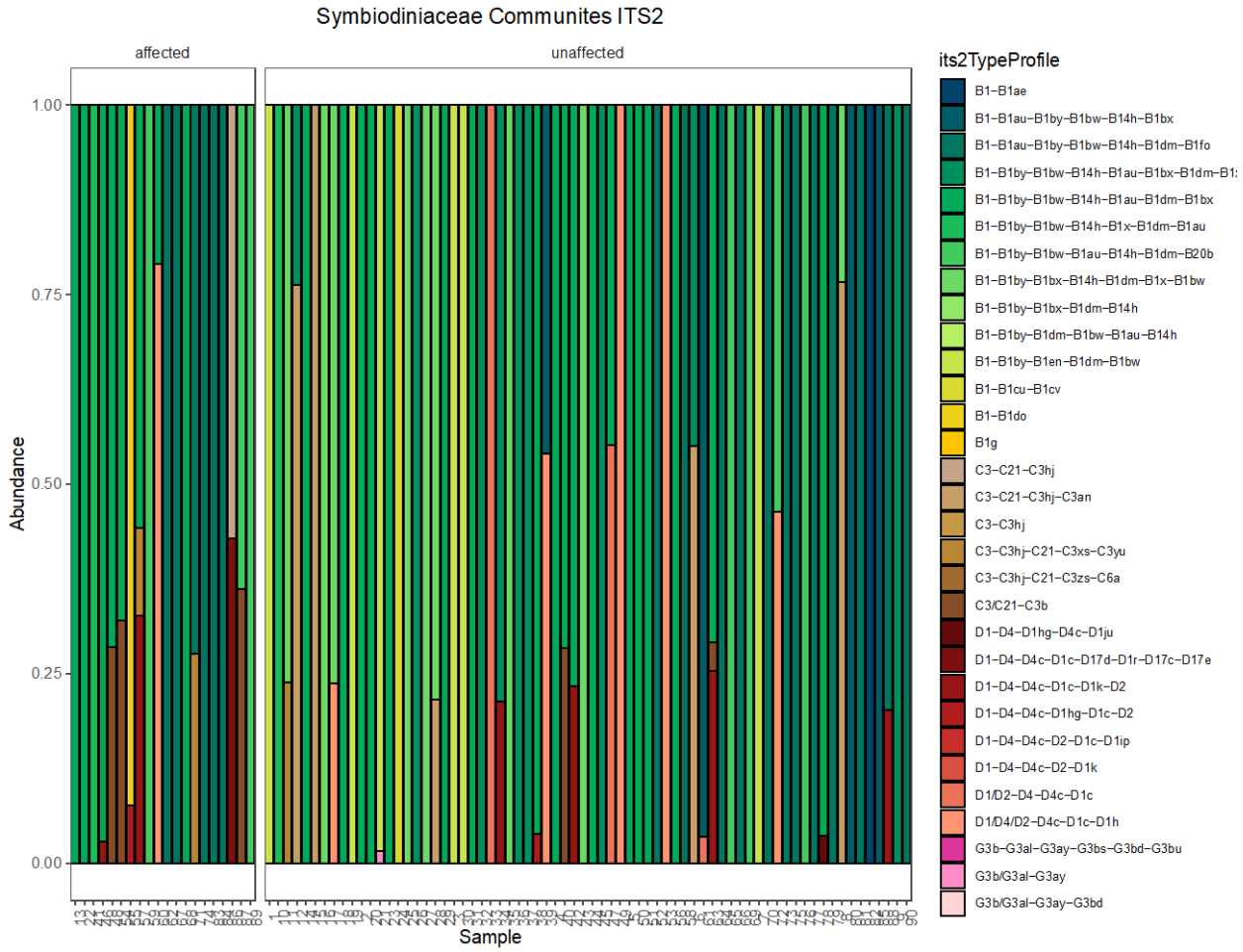

Figure 15. ITS2 algal symbiont profiles for the RRC unified coral colonies comparing SCTLD-affected and SCTLD-unaffected coral colonies.

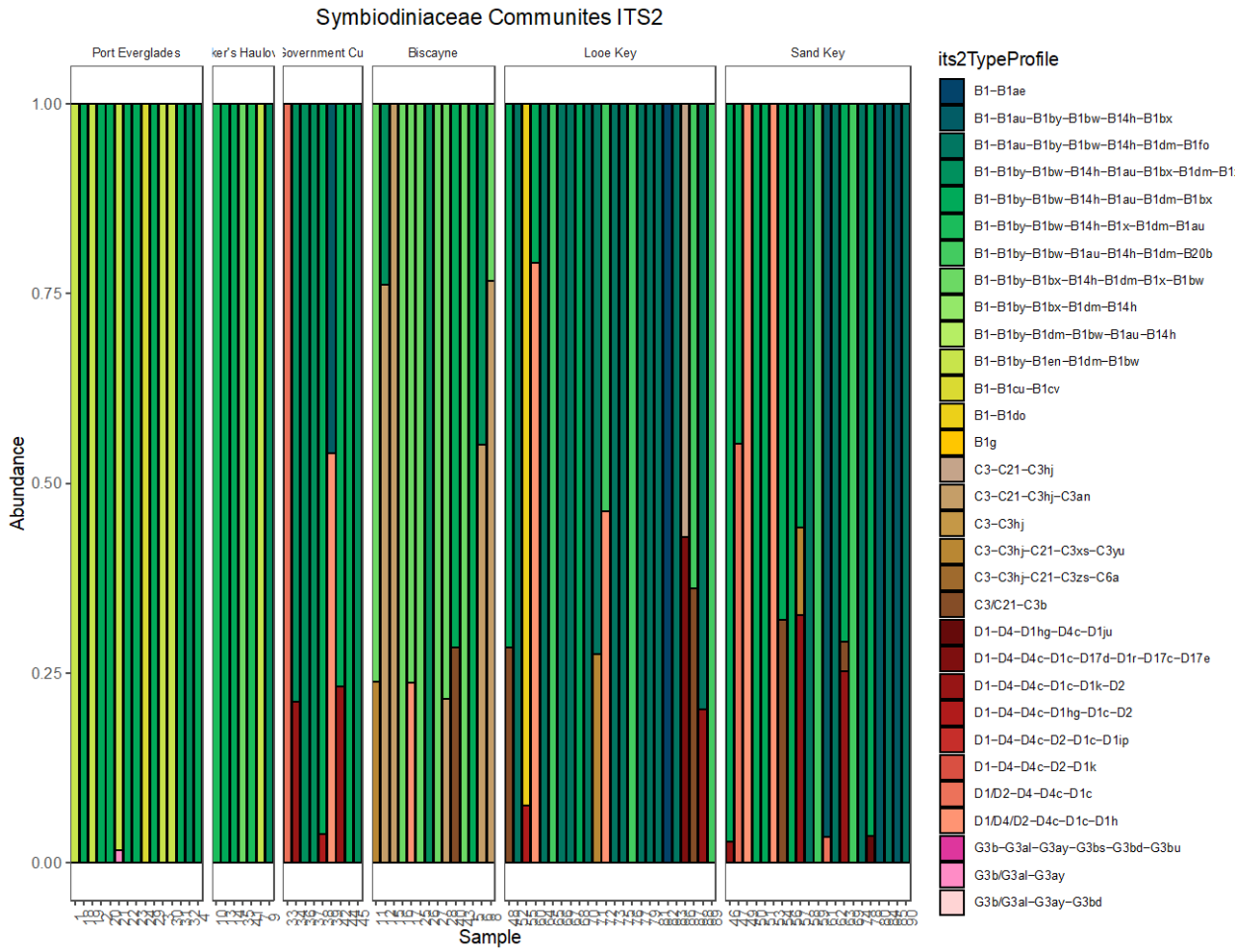

Figure 16. ITS2 algal symbiont profiles for the RRC unified coral colonies comparing the algal symbiont communities across the regions and their attributing water inlets.

3.4. Task 4b: Symbiodiniaceae and metabolomics variability (Buckley, Doty, Dennison, Baker, Garg, and Walker)

Goal: Continue spatiotemporal mapping and statistical analyses of all data to investigate associations of disease sites with Symbiodiniaceae and metabolomics.

Significant findings:
Symbiont mapping – Colony variability results show a dominant association with the Symbiodiniaceae genus *Breviolum* across all corals, except for one dominantly associated with *Durusdinium*. Symbiont to host (S:H) cell ratios significantly varied between colonies and sampling timepoints. A significant decrease in S:H was observed during the 2023 bleaching event when comparing all corals, even though only one coral visibly bleached. Spatial distributions of Symbiodiniaceae genera proportions in LC-101 show seasonal variability between the wet and dry seasons.

Metabolomics – Various Lyso-lipids were detected in higher abundance in *Breviolum* dominated samples when compared to *Durusdinium* dominated samples, suggesting a link between dominant algal symbiont and the biochemical pathways these lipids are involved in. Additionally, the vitamin E analogue α-tocomonoenol was detected in higher abundance in *Durusdinium* dominant samples compared to *Breviolum* in February 2023 suggesting frontloading of this compound during cooler months that could potentially provide enhanced antioxidant protection in corals dominated by *Durusdinium*.

Results and Discussion:
Symbiont mapping – Actin-based qPCR assays showed dominant association with the Symbiodiniaceae genus *Breviolum* while one colony predominantly associated with *Durusdinium* (LC-126). Two colonies, LC- 101 and LC-114, were found to have background amounts of *Cladocopium* and *Durusdinium* in their tissues across all sample points (Figure 17). The 2023 bleaching event was captured in timepoints T5 and T6 and LC-101 was the only coral sampled to visibly bleach. In the final two timepoints (T6 and T7) there was an increased proportion of *Durusdinium* in some samples compared to the previous timepoints.

Symbiont to host (S:H) cell ratios significantly varied between colonies and sampling timepoints (Figure 18). A significant decrease in S:H was observed during the 2023 bleaching event (T5 and T6) when comparing all corals, even though only one coral (LC-101) visibly bleached. A significant increase in S:H is seen in the final timepoint (Feb. 2024) during the bleaching recovery period. Generally, corals associated with *Breviolum* and *Cladocopium* had more symbionts per host cell, followed by corals exclusively associating with *Breviolum* and those with mixed *Durusdinium* and *Cladocopium* communities. LC-126 consistently shows the lowest S:H compared to the other colonies, but also predominantly associates with Durusdinium.

The southernmost coral, LC-101, showed significant spatial distributions of Symbiodiniaceae genera across the surface of the colony that varied by season (Figure 19).

In all sampling timepoints there were significant cold spots of the proportion of the dominant Symbiodiniaceae genus (*Breviolum*), which represents clustering of higher proportions of the background genera (*Cladocopium* and *Durusdinium*). In the first two dry season timepoints (April 2022 and Feb. 2023) this clustering was present on the eastern side of the colony, while in the four wet season timepoints (Aug and Sept 2022 and Aug and Oct. 2023) this clustering was present in the northwestern area of the colony. However, this seasonal pattern was disrupted in the following dry season timepoint (Feb. 2024), during the bleaching recovery period.

Low diversity of Symbiodiniaceae associations and a dominant association with *Breviolum* of corals in Southeast Florida align with previous studies (Kemp et al., 2015). Additionally, distributions of Symbiodiniaceae genera across colony surfaces, when diversity was present, followed similar patterns to previous studies showing *Breviolum* toward the tops, or more light-exposed, areas of a colony and *Cladocopium* toward the sides, or more shaded regions, of the colony (Kemp et al., 2015; Rowan et al., 1997). However, considering our sampling methods, some specific microenvironments across the surface of colonies may not have been fully accounted for, including areas directly shaded by overhanging leaves of the colony.

The four northern colonies had dominant associations with *Breviolum* while the southern colonies, off the coast of Key Biscayne, contained more background *Cladocopium*. These distributions could be influenced by environmental factors (i.e. water quality) which should be investigated further. Studies have shown that environmental factors like water quality (i.e. turbidity and nutrient load) can influence Symbiodiniaceae associations and distributions (Rubin et al., 2021) which tend to favor *Durusdinium* in more stressful environments. There are ongoing studies looking at the effects of water coming out of Government Cut (Port of Miami), where there is a very distinct difference in symbiont distributions in this study.

Symbiodiniaceae to coral host cell ratios (S:H) show significant differences both across time and between colonies. S:H showed the greatest declines in August and October 2023 which corresponded with the regional bleaching event recorded in Florida. The only colony to visibly bleach during sampling was LC-101 so the overall decrease in S:H seen looking at all the colonies suggests some of the colonies still experienced the stress of the higher temps without visibly bleaching. The only evidence of symbiont shuffling post-bleaching event was seen in LC-101 which showed some higher proportions of *Durusdinium* in Oct. 2023 and Feb. 2024 (Kemp et al., 2014).

The only two colonies to not experience any active SCTLD lesions throughout the sampling timeframe were LC-126 and LC-114 (Figure 20). LC-126 had a dominant association with *Durusdinium* and LC-114 had the highest background levels of *Cladocopium*. These results align with Dennison et al., 2021 which suggests *Breviolum* has the highest level of susceptibility to SCTLD compared to *Cladocopium* and *Durusdinium* which showed lower but relatively equal susceptibility.

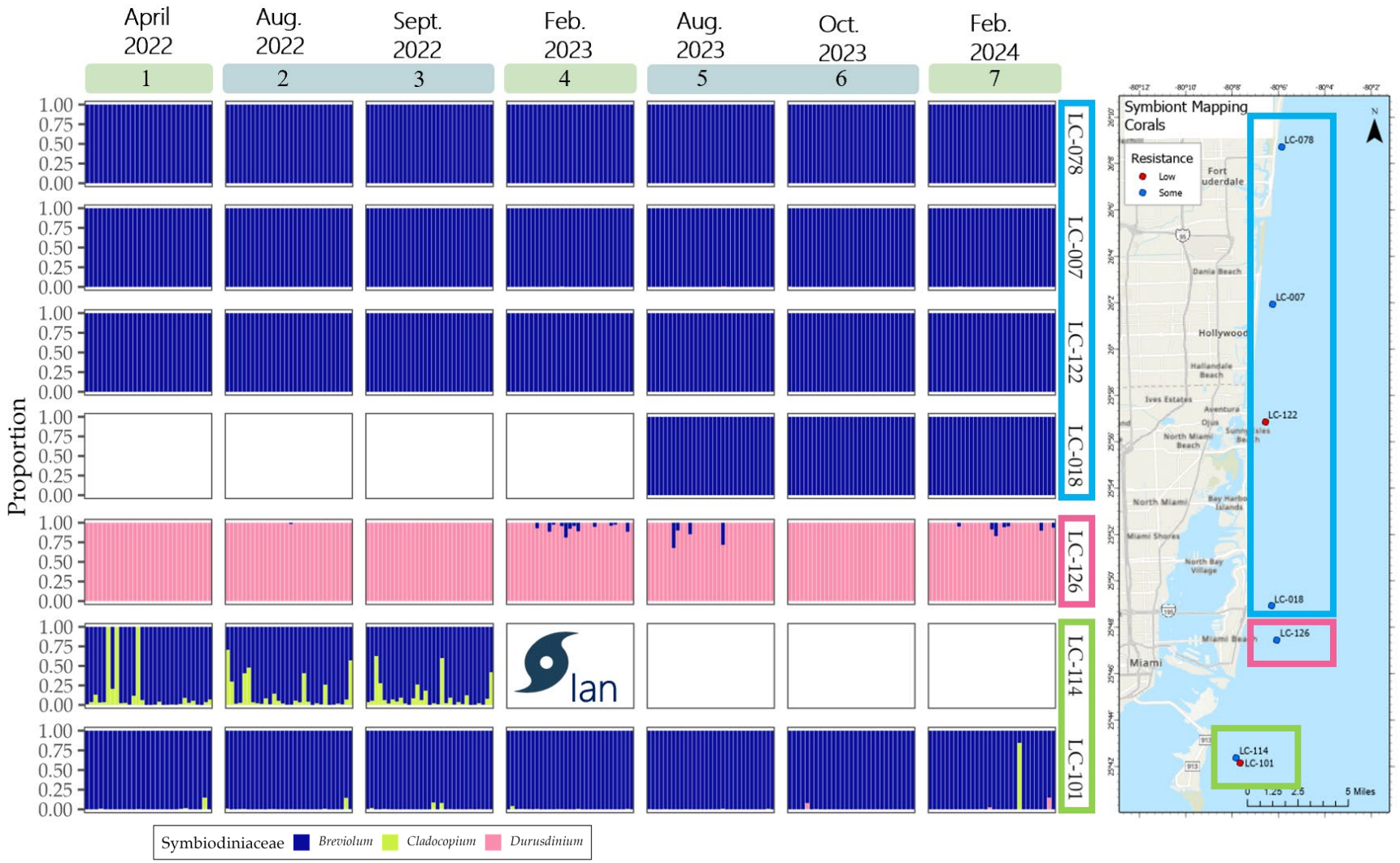

Figure 17. Symbiodiniaceae community composition of the seven coral variability colonies. Each horizontal line represents a coral's community structure over seven timepoints. Most corals predominantly associated with *Breviolum* while one coral predominantly associated with *Durusdinium*. LC-114 was broken into pieces from Hurricane Ian after T3 and was replaced by LC-018 on T5.

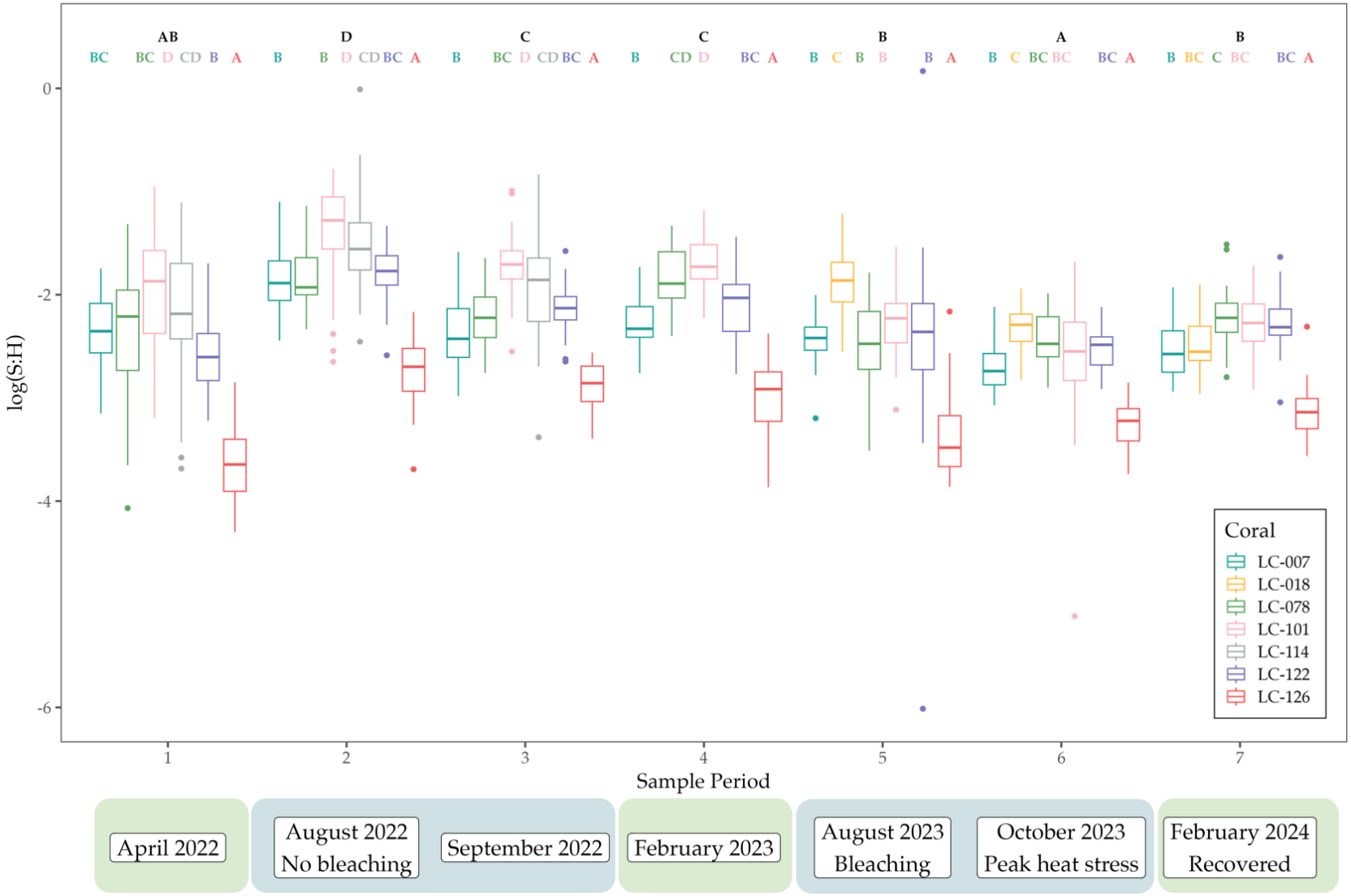

Figure 18. Average symbiont to host (S:H) cell ratios for the seven within-colony Symbiodiniaceae surveys for each sample period. Host colony and sample period had strong effects on S:H within a coral's tissues.

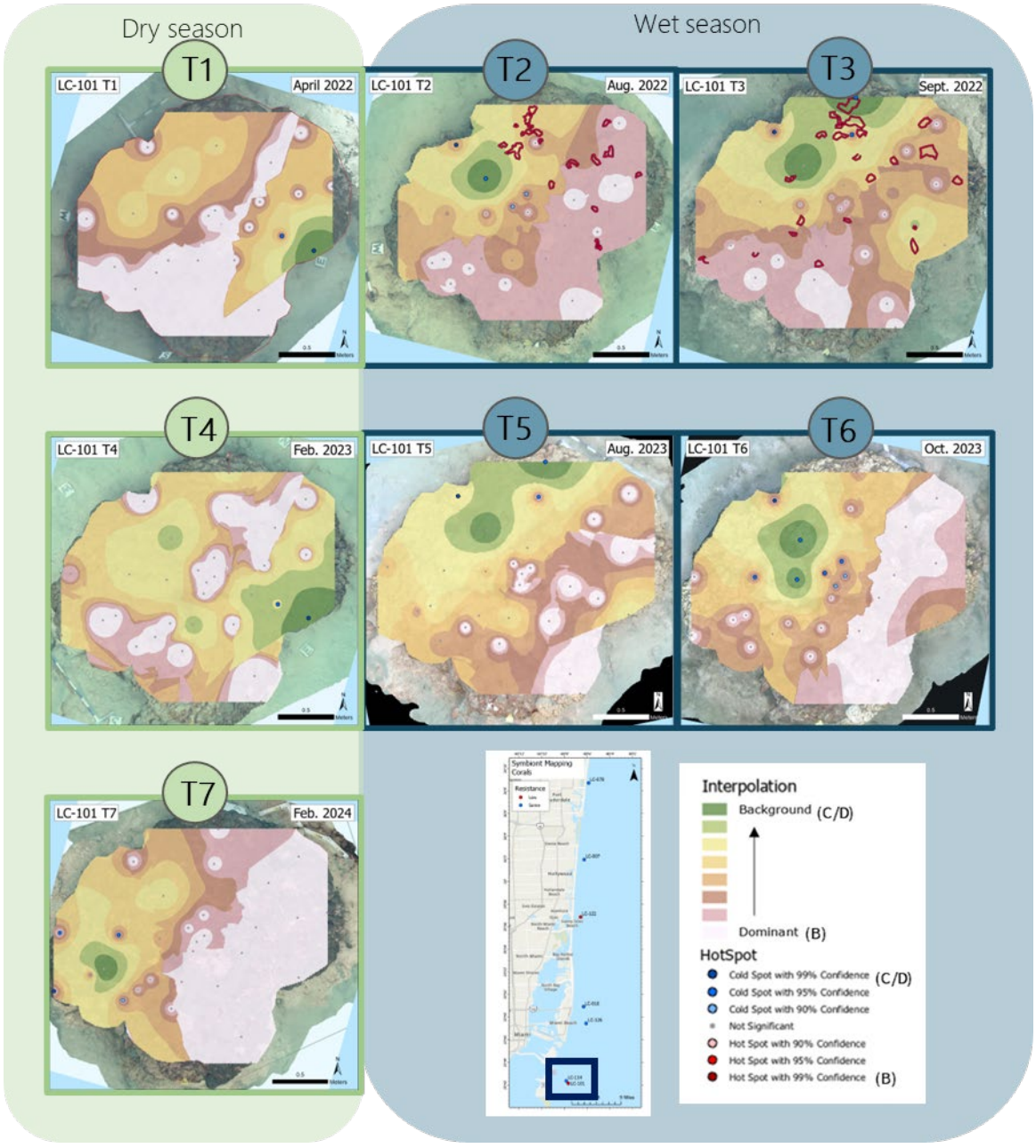

Figure 19. Spatial analysis of Symbiodiniaceae genera distributions of LC-101. Inverse distance weighted (IDW) interpolation and Hot Spot Analysis (Getis-Ord Gi*) were performed using the proportion of the dominant genera (*Breviolum*). Interpolation results represent high proportions of *Breviolum* in pink and low proportions (higher background genera presence) in green. Hot Spot Analysis shows significant clustering of high *Breviolum* proportions in red and significant clustering of low *Breviolum* proportions in blue. Time points 1, 4, and 7 were in Florida's dry season (November-May) and time points 2, 3, 5, and 6 were in the wet season (June-October).

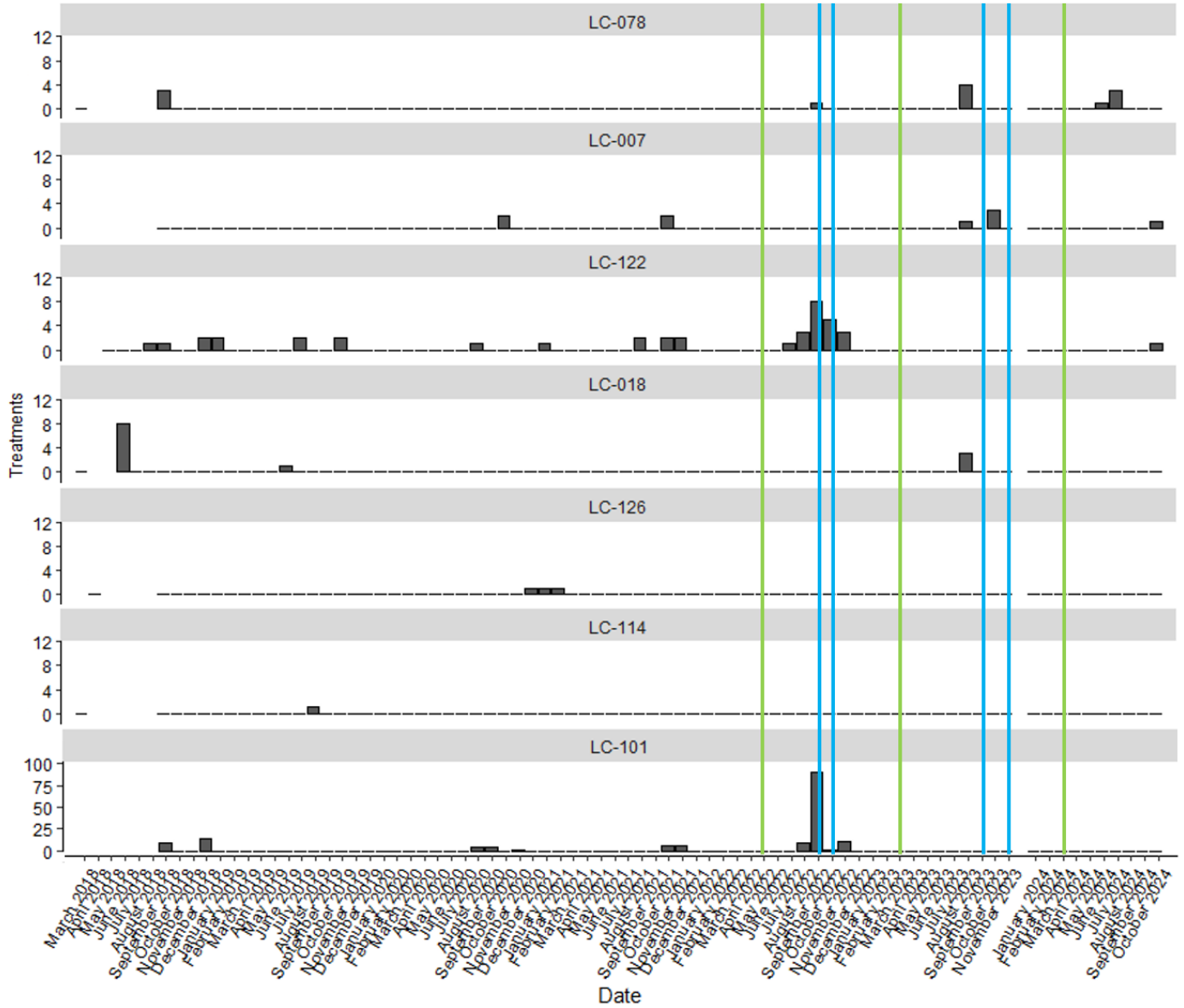

Figure 20. SCTLD treatment history of all corals. Corals were monitored for active SCTLD lesions which were treated with amoxicillin in Base2B monthly starting in 2018. Green and blue lines represent colony variability sampling timepoints in the dry and wet seasons, respectively.

Metabolomics – Organic extracts of tissue biopsies obtained from six *Orbicella faveolata* were analyzed via UHPLC-HRMS analysis across two analytical runs (data from sampling periods 3 & 4 and sampling periods 5 & 6 were acquired independently). All data were preprocessed with mzMine3 and the output was used to generate feature-based molecular networks (FBMN) to assist with unknown feature annotation. Chemometric analysis revealed statistically significant features between sampling period, dominant algal symbiont (*Breviolum* or *Durusdinium*), histology supported resistance categories (Wilcoxon signed-rank, $p < 0.05$) and colony (Kruskal-Wallis post-hoc Dunn, adjusted $p < 0.05$). Principal component analysis was performed to visualize the difference in metabolome between sampling periods and colony within sampling period (Figure 21, A). Temporally, the metabolome visually differs the most between February 2022 and September 2023, which could be indicative of a shift in metabolome between warm and cooler months. This finding is supported by the overlap of metabolomes between the later sampling periods, August 2023 and September 2023. Studies have shown that coral species have a metabolic response to heat stress [1-3], and in order to remove that confounding factor in statistical analysis inter-colony variability was assessed for each sampling period individually.

The PCAs display inter-colony variability in metabolome at each sampling period (Figure 21, B) with colony LC-126 displaying the greatest sub-clustering across all seasons (PERMANOVA, $F > 7.07$, p adj. < 0.01). ITS2 sequencing results for these samples determined the dominant Symbiodiniaceae genus *Durusdinium* is highly abundant in this colony while all other colonies are dominated by either *Breviolum* or *Cladocopium*. This finding prompted exploration of features differentiating between dominant algal symbiont genera.

PCAs of samples grouped by dominant Symbiodiniaceae genera (Figure 22) were constructed for samples dominated by either *Breviolum* or *Durusdinium* as the mixed dominant and *Cladocopium* dominant samples did not contain sufficient replicates for statistical analysis. Wilcoxon signed-rank test was performed to identify metabolite features that explain variation between *Durusdinium* and *Breviolum* dominant samples at each sampling period. Significant features were captured at each timepoint with TP3 containing 1344, TP4 containing 971, TP5 containing 584, and TP6 containing 563 ($p < 0.05$ for all groupings). GNPS spectral library matching was performed to identify these significant features which revealed several different classes of lipids including diacylglyerylcarboxyhydroxymethylcholine (DGCC), phosphatidylcholines (PC), platelet activating factors (PAF), phosphatidylethanolamines (PE), and vitamin E derivatives (Figure 23). For MolDiscovery and DEREPLICATOR+ workflows through GNPS were utilized to aid in feature annotation, and in cases where annotation could not be made, CANOPUS was used to provide class prediction (deliverable Table X1. *Breviolum* vs *Durusdinium* Significant Features.xlsx). DGCC, PC, PE, and PAF have been differentially detected in coral responding to various stressors. Lyso-DGCC 16:0 and Lyso-PE 18:1 were both detected in higher abundance in *Breviolum* when compared to *Durusdinium* dominant samples. A vitamin E analogue, α-tocomonoenol, was detected in higher abundance in *Durusdinium* versus *Breviolum* dominant samples during February. Studies have shown this compound to provide enhanced antioxidant protection in marine organisms[4]. It has also

been demonstrated that *Durusdinium* is a more thermally tolerant genus,[5] and the increased abundance of this compound in samples dominated by this genus could indicate that this compound is conferring this enhanced thermal tolerance.

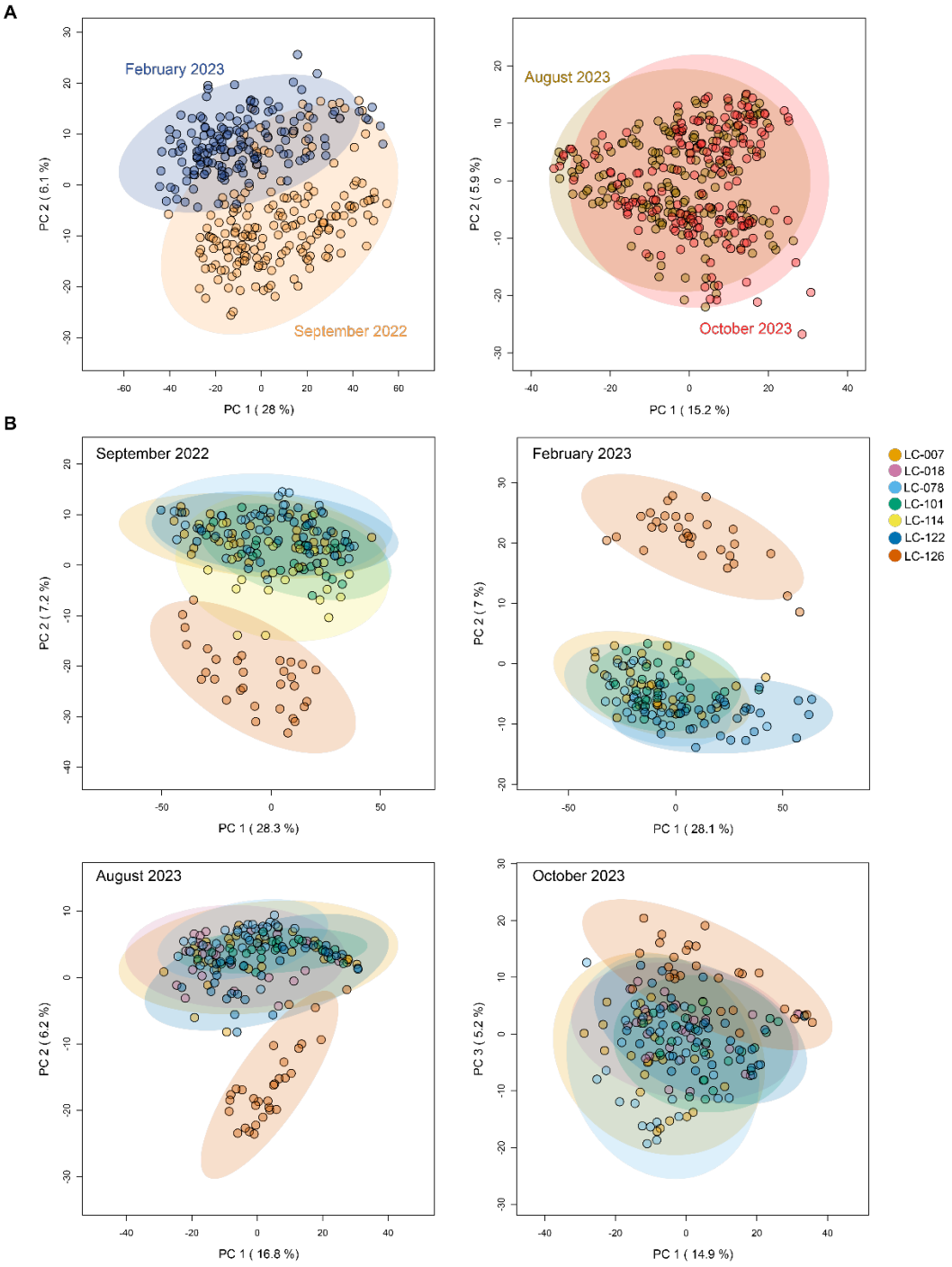

Figure 21. (A) PCA displaying colony variability at each sampling period. (B) PCA of intercolonial variability at each time point.

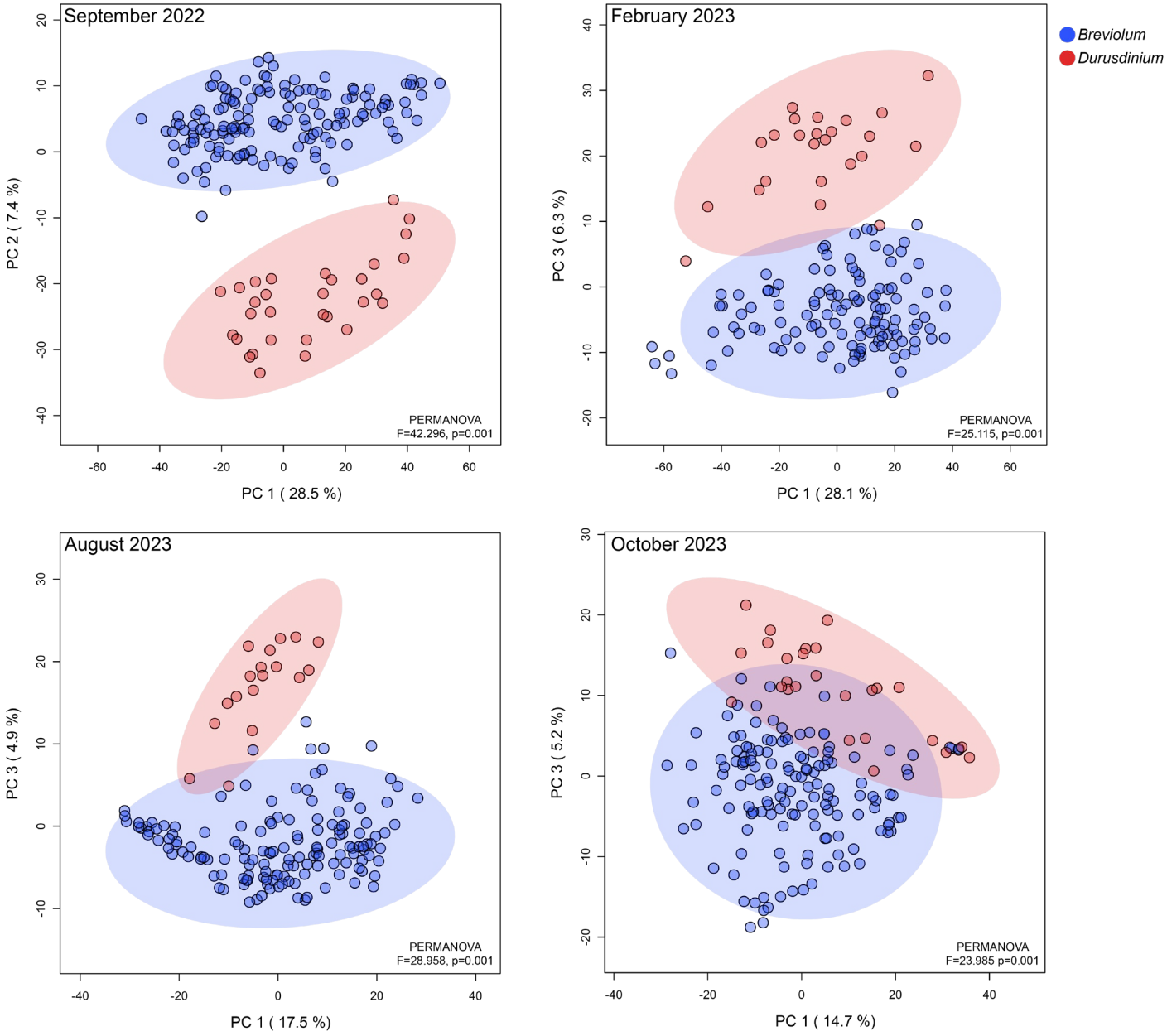

Figure 22. PCA of samples grouped by dominant algal symbiont *Breviolum* or *Durusdinium*.

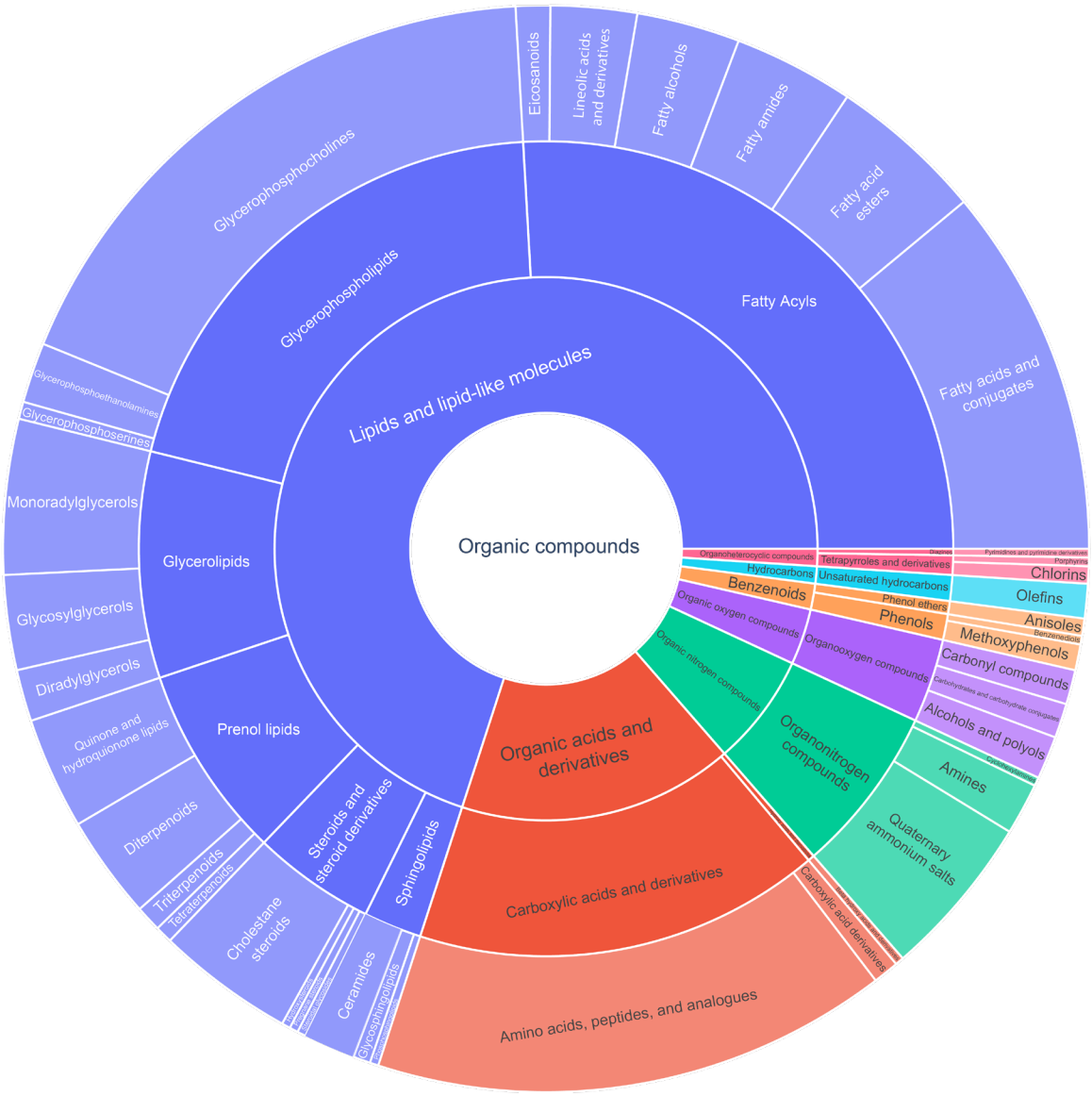

Figure 23. Sunburst plot of superclass, class, and subclass assignments from statistically significant features between *Breviolum* and *Durusdinium* at sampling period 3.

Additionally, we generated a PCA to visualize the metabolomic differences between the "Low" and "Some" histology supported resistance categories (Figure 24). Prior to generation of PCA for all sampling periods, we removed colony LC-126 because prior analysis has shown the metabolome of this colony is metabolically different than all others at this sampling period. While there is significant visual overlap in the PCA model, we were able to identify several features variably detected with Wilcoxon signed-rank test which revealed 560 statistically significant features at sampling period 3, 1470 at sampling period 4, 345 features in the sampling period 5, and 539 at sampling period 6. Further analysis of these identified features is necessary to provide annotations, however CANOPUS generated class prediction was performed on the identified features (deliverable Table X2. Resistance Categories Feature Annotations.xlsx).

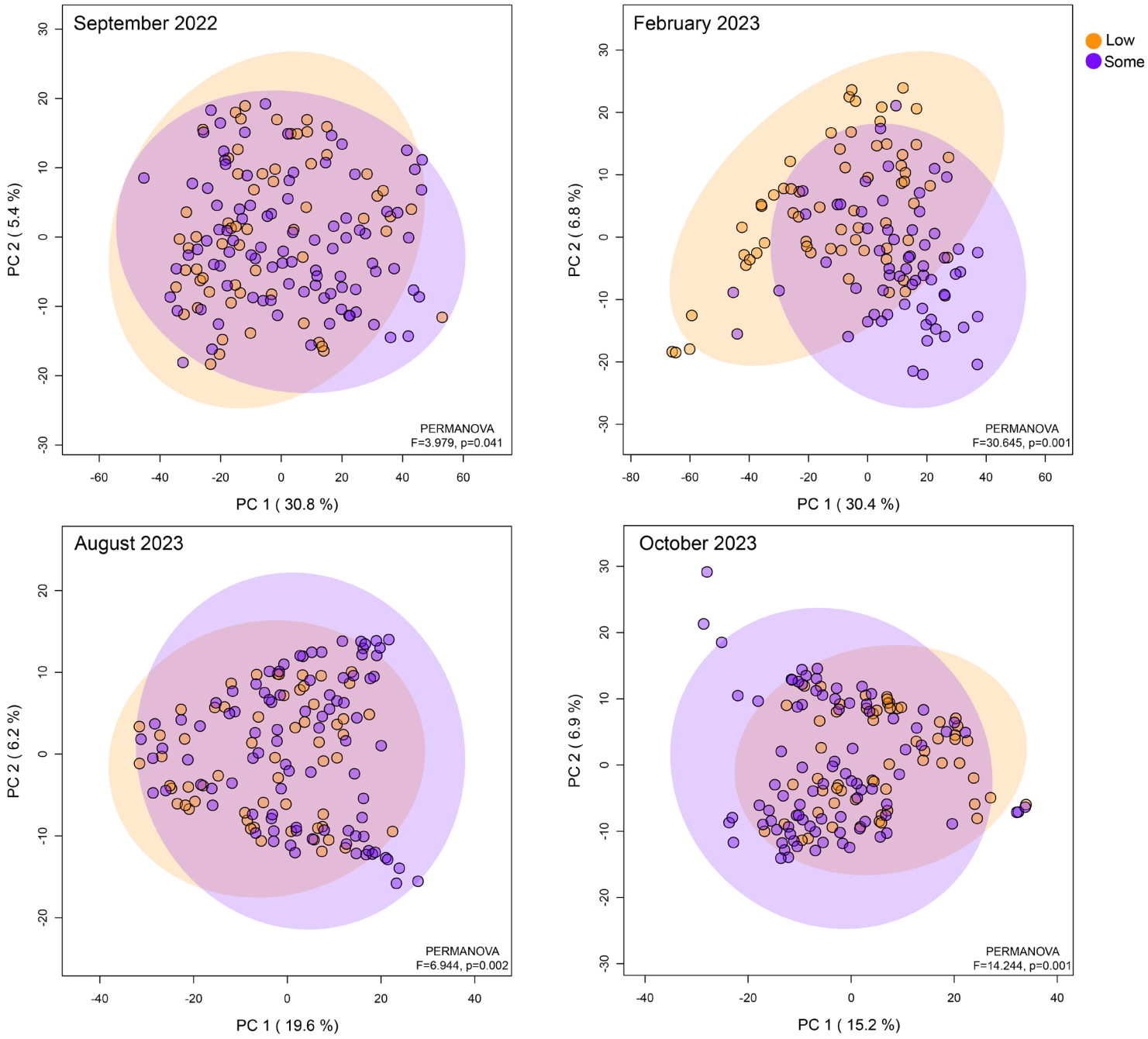

Figure 24. PCAs of Low vs Some histology supported resistance categories. All samples containing samples dominant in *Durusdinium* were removed prior to generation.

References

1. Haydon, T. D.; Matthews, J. L.; Seymour, J. R.; Raina, J.-B.; Seymour, J. E.; Chartrand, K.; Camp, E. F.; Suggett, D. J., Metabolomic signatures of corals thriving across extreme reef habitats reveal strategies of heat stress tolerance. *Proceedings of the Royal Society B: Biological Sciences* **2023,** *290* (1992), 20221877.

2. Huang, S.; Luo, L.; Wen, B.; Liu, X.; Yu, K.; Zhang, M., Metabolic signatures of two scleractinian corals from the northern South China sea in response to extreme high temperature events. *Marine Environmental Research* **2024,** *198*, 106490.

3. Rädecker, N.; Pogoreutz, C.; Gegner, H. M.; Cárdenas, A.; Roth, F.; Bougoure, J.; Guagliardo, P.; Wild, C.; Pernice, M.; Raina, J.-B.; Meibom, A.; Voolstra, C. R., Heat stress destabilizes symbiotic nutrient cycling in corals. *Proceedings of the National Academy of Sciences* **2021,** *118* (5), e2022653118.

4. Yamamoto, Y.; Fujisawa, A.; Hara, A.; Dunlap, W. C., An unusual vitamin E constituent (alpha-tocomonoenol) provides enhanced antioxidant protection in marine organisms adapted to cold-water environments. *Proc Natl Acad Sci U S A* **2001,** *98* (23), 13144-8.

5. Palacio-Castro, A. M.; Smith, T. B.; Brandtneris, V.; Snyder, G. A.; van Hooidonk, R.; Maté, J. L.; Manzello, D.; Glynn, P. W.; Fong, P.; Baker, A. C., Increased dominance of heat-tolerant symbionts creates resilient coral reefs in near-term ocean warming. *Proceedings of the National Academy of Sciences* **2023,** *120* (8), e2202388120.

3.5. Task 5a: Data analysis of RRC unified samples and participate in data synthesis (Andrade and Traylor-Knowles)

Goal: Develop a bioinformatic pipeline and focus on finding unique genetic signatures of *O. faveolata* genotypes that have been exposed to SCTLD.

Significant findings: *Orbicella favelota* colonies that have been visually affected by Stony Coral Tissue Loss Disease (SCTLD) have a distinct transcriptomic signature during winter compared to colonies that have never been visually affected by the disease.

Results:
KJCAP and Lower Keys SCTLD unaffected colonies show different patterns of expression than SCTLD affected colonies during winter. Most genes are down-regulated in colonies SCTLD unaffected colonies during winter in both regions. There are 33 genes differentially expressed between SCTLD affected and unaffected colonies from the Lower Key during winter (Figure 25). There are 169 genes differentially expressed between SCTLD affected and unaffected colonies from the KJCAP during winter (Figure 26).

After obtaining a list of 10,832 genes relevant to the samples of *O. faveolata* collected and processed to obtain 3'RNAseq data, we performed a network analysis with WGCNA package where we obtained 8 modules of co-express genes. We use these modules to find the correlation between gene expression and symbiont density collected per symbiont genus. We analyzed the correlation of *Breviolum*, *Cladocopium* and *Durusdinium*, and the correlation between a binary trait corresponding to SCTLD-affected corals equal to one and SCTLD-unaffected corals equal to 0. *Breviolum* and *Cladocopium* showed a significant correlation with some modules, and only one module, module green, was significantly correlated with SCTLD susceptibilities and the symbiont density (Figure 27). We also analyze the correlation of the biological metadata variables obtained by the microbiome analysis, metabolome and bioactivity data (Figure 28). Lyctic necrosis and EtOAc show significant correlation with the module that also shows correlation with SCTLD susceptibility state. The vibrio data showed a significant correlation but with a module corresponding to a different set of genes (ME turquoise).

Work is ongoing to identify patterns in the 299 genes that are correlated with SCTLD susceptibility and symbiont density. Of these, 125 are poorly annotated or lack annotation and need to be investigated further to understand their functions.

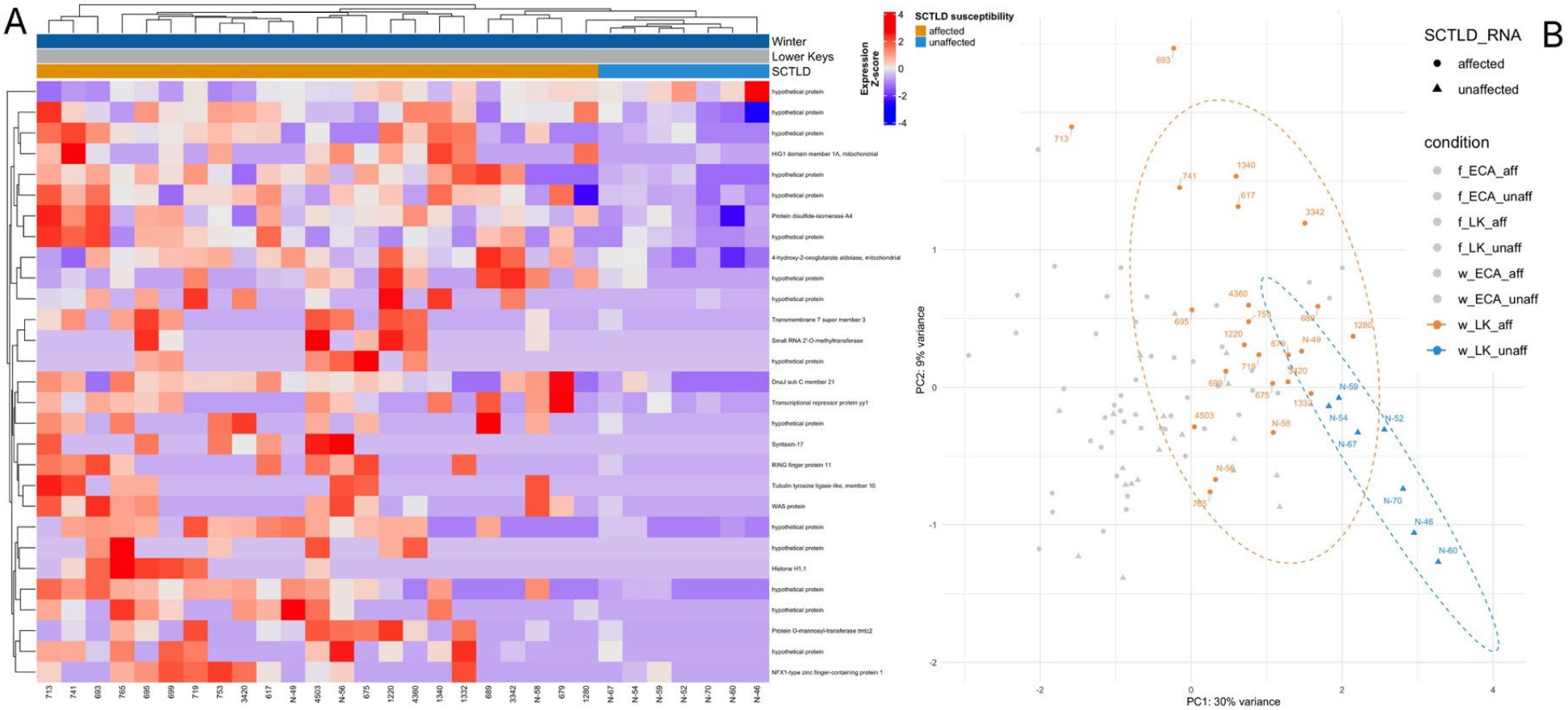

Figure 25. Differentially expressed genes (DEG) between SCTLD affected and unaffected colonies from Lower Key during winter sampling. A) Heatmap showing the expression of DEG only in samples collected during winter in the Lower Keys. B) PCA showing sample clustering only considering DEG expression, samples in orange correspond to SCTLD affected colonies and samples in blue to SCTLD unaffected colonies

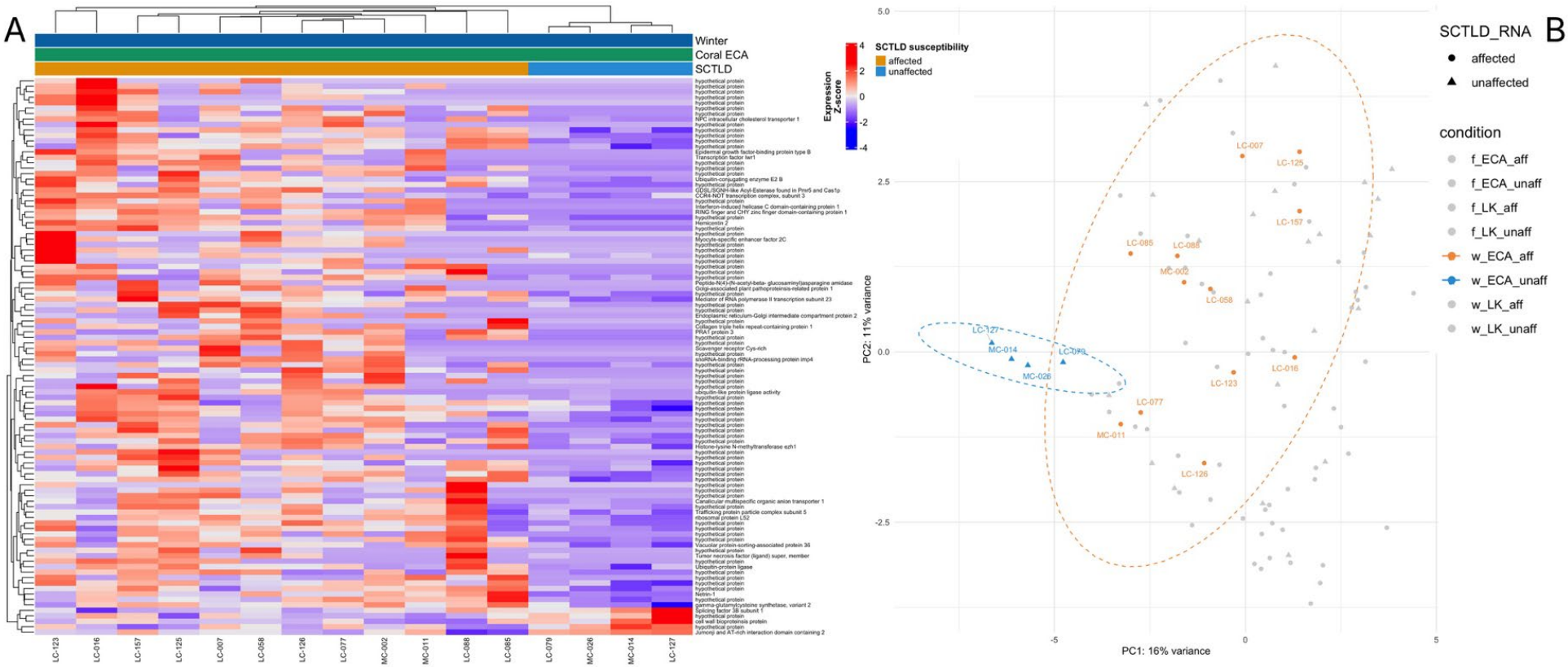

Figure 26. Differentially expressed genes (DEG) between SCTLD affected and unaffected colonies from KJCAP region during winter sampling. A) Heatmap showing the expression of DEG only in samples collected during winter in the KJCAP region B) PCA showing sample clustering only considering DEG expression, samples in orange correspond to SCTLD affected colonies and samples in blue to SCTLD unaffected colonies.

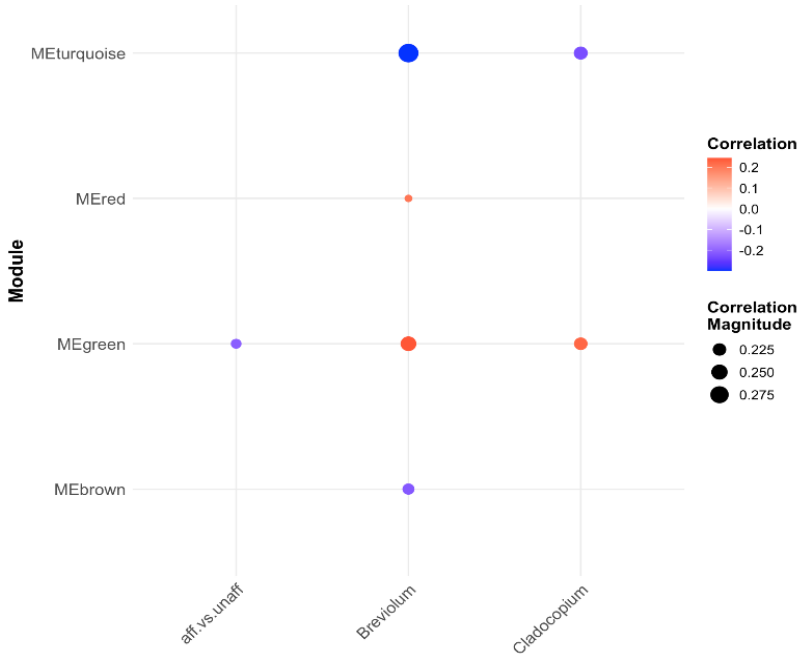

Figure 27. Dot plot showing significant symbiont abundance and module correlations, the size of the dot corresponds to the significance of the correlation. For both graphs, color scale corresponds to the correlation directionality, red being positively correlated and blue being negatively correlated.

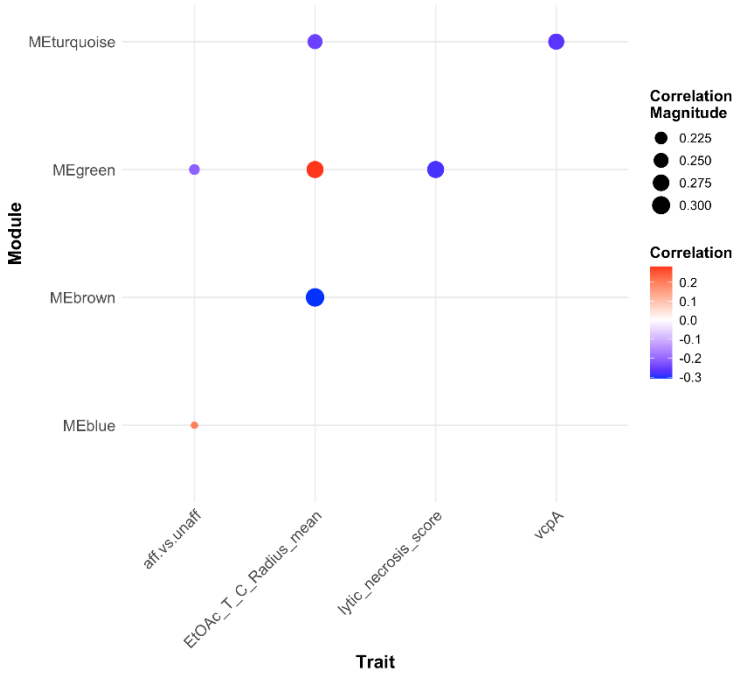

Figure 28. Dot plot showing significant biological traits and module correlations, the size of the dot corresponds to the significance of the correlation. For both graphs, color scale corresponds to the correlation directionality, red being positively correlated and blue being negatively correlated.

The model fitting process involving the suite of temperature metrics resulted in a single predictor model, with mean temperature over the prior 30 days explaining 18.0% of the variation in the transcriptomics data across the two sample periods (Figure 29). However, given the highly correlated nature of all the temperature metrics across these time periods, a more appropriate interpretation is that mean temperature across a period of 1-90 days prior to sampling explains ~18% of the variation in the transcriptomics data. Overall, higher temperatures in sample period 2 relative to sample period 3 correlated with significant shifts in the transcriptomic data.

The model fitting process involving the suite of rainfall metrics also resulted in a single predictor model, with summed rainfall over the prior 30 days coming out as the most effective predictor and explaining 18.6% of the underlying variation in the transcriptomics data (Figure 30). When the temperature metrics and rainfall metrics were normalized and both included simultaneously in the model-fitting process, the optimal model was a two-predictor model, with both mean temperature over the prior 30 days and summed rainfall over the prior 30 days explaining 19.8% of the variation in the transcriptomics data. However, given the high correlation between these two predictors, we cannot disentangle their relative effects. A more cautious interpretation here therefore, is that mean temperature or summed rainfall over the prior 30 days both offer equal explanatory power over the transcriptomic data.

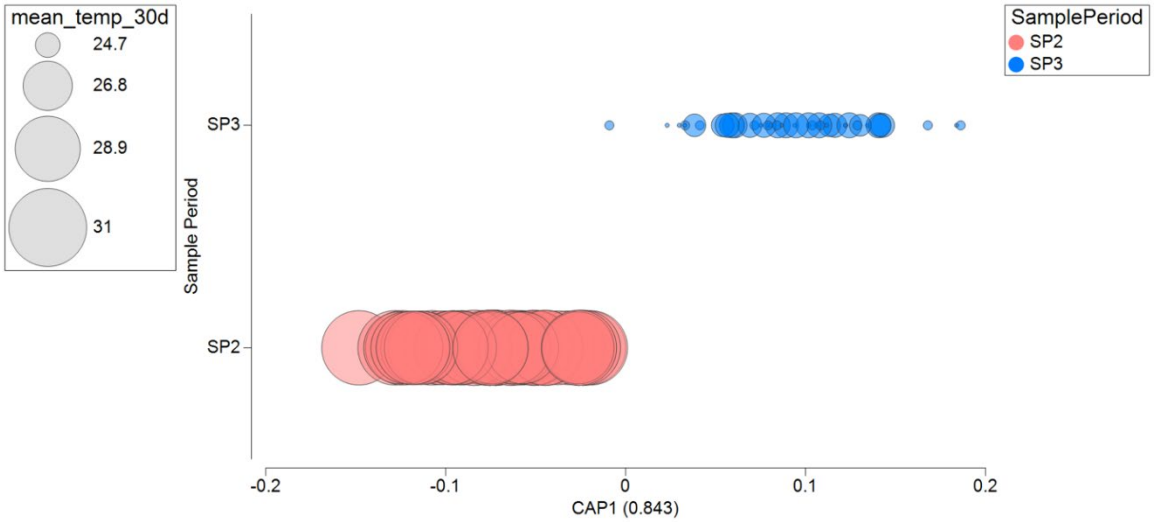

Figure 29. Relative similarity in the '160 gene' data between Sample Period (SP) two and three (visualized along the x axis) using the RRC corals as replicates. The performance (squared canonical correlation) of the constrained ordination axis is shown in parentheses. The mean in situ seawater temperature (in °C) for the 30-day period prior to sampling each coral is overlaid as a bubble plot (values shown in the bubble key).

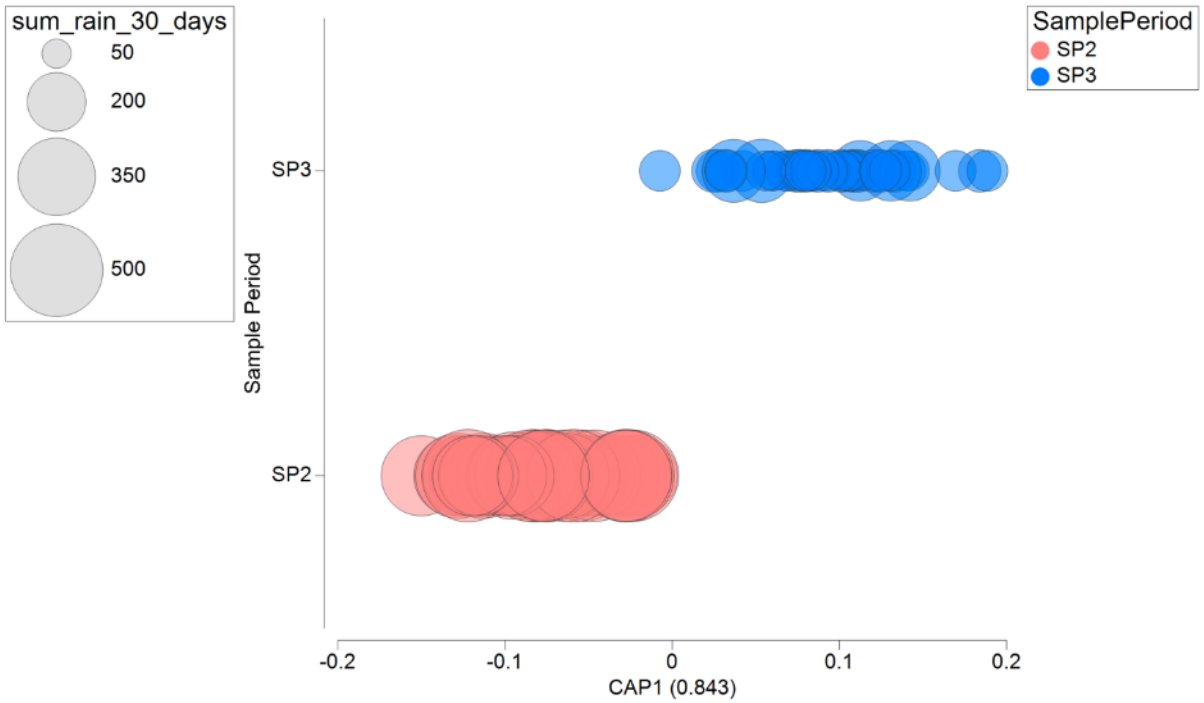

Figure 30. Relative similarity in the '160 gene' data between Sample Period (SP) two and three (visualized along the x axis) using the RRC corals as replicates. The performance (squared canonical correlation) of the constrained ordination axis is shown in parentheses. The summed rainfall (in mm) for the 30-day period prior to sampling each coral is overlaid as a bubble plot (values shown in the bubble key).

Discussion:
The two overarching findings based on the 3'RNAseq data are the following:

- Seasonality has an effect on coral transcriptomics based also on the fact that a coral has been visually unaffected by SCTLD.
- Colonies that have never been visually affected by SCTLD tend to down-regulate genes compared to colonies that have been visually affected by SCTLD.

Our findings demonstrate that SCTLD leaves a trace at a transcriptomic level, suggesting that colonies that have been affected by SCTLD and are, therefore, susceptible to reinfection, could potentially be identified based on their transcriptomic profiles.

Knowing which colonies are more susceptible and require more attention by management efforts could improve the efficiency of the conservation agencies when an outbreak occurs or even to prevent an outbreak of this disease.

The transcriptomic data collected so far create a solid base for improving our understanding of coral's response to SCTLD exposure. However, more data is needed to support these results and create a robust understanding of *O. faveolata*'s molecular and cellular response to SCTLD.

Understanding how *O. faveolata* responds to SCTLD is a steppingstone to direct the study of SCTLD response from other corals affected by this disease. There is a strong need to start exploring the transcriptomic patterns of other species affected by SCTLD to create a comprehensive action plan that could help various coral species survive this disease.

3.6. Task 5b: Long-read RNA sequencing from 3 *O. faveolata* colonies from each region based on their latest susceptibility status (Andrade and Traylor-Knowles)

Goal: To obtain long-read RNA sequencing data from SCTLD-affected and SCTLD-unaffected *Orbicella faveolata* colonies

Background and objectives:
The RRC group collected samples from the Lower Keys and Coral ECA during fall 2021 and winter 2022 for the DEP-funded project "Investigation of intraspecific factors driving resistance to SCTLD on Florida's Coral Reef." The objective of the current project was to use these previously collected samples to extract RNA for testing direct RNA sequencing (D-RNAseq) and long-read RNA sequencing (LR-RNAseq) using Oxford Nanopore Technology (ONT) protocols.

Both D-RNAseq and LR-RNAseq require specific RNA quality standards to preserve RNA length. Since previous RNA extraction methods were not standardized for these sequencing approaches, the first objective of this project was to establish and optimize a new RNA extraction method to obtain RNA of sufficient quality for D-RNAseq and LR-RNAseq.

Additionally, D-RNAseq has never been performed on Caribbean corals before, and long-read sequencing (ONT) has not yet been tested on *O. faveolata* samples. Therefore, the second objective was to evaluate these two sequencing methods to determine their effectiveness for our sample types. To analyze the data, we also aimed to develop a bioinformatic pipeline tailored for this data type. Finally, the third objective was to integrate gene lists from the previous project with those generated by these RNA sequencing techniques to assess data consistency.

In this report, we detail the standardization of RNA extraction for D/LR-RNAseq, provide an overview of the bioinformatic pipelines used, and present results from both sequencing methods along with comparisons to prior 3'RNAseq data. We also discuss the advantages of D-RNAseq and LR-RNAseq for analyzing differences between SCTLD-affected and unaffected colonies.

Significant findings:
- Direct-zol kit yielded better RNA quality results, but samples collected for the DEP project in 2021/2022 and homogenized might be too degraded to be suitable for D/LR-RNAseq.
- Archived samples might yield better RNA quality to be sequenced for D/LR-RNAseq.

- The RNA quality of the samples collected in January 2025 in RNA/DNA shield and processed with the bench RNA extraction protocol with Trizol also had low quality scores. These results illustrate the need to standardize not only the extraction protocol but also the sample collection protocol. *Orbicella faveolata* tissue sampling in the field needs to be revisited and tested to optimize the correct RNA preservation in this type of sample.
- Moderate quality data from D/LR-RNA sequencing can be obtained from an RNA extraction sample with non-optimal RNA quality.
- The sequencing results presented here showed that a significantly higher amount of reads can be obtained using a cDNA and PCR amplification approach library prep compared to D-RNAseq
- The fall-2021 sample from the affected Lower Key colony (colony ID 753) sequenced with the D-RNAseq kit yielded approximately 287,000 reads.
- Bioinformatic analysis revealed colony 753 (fall 2021) expressed:
    - 15 genes that were also differentially expressed in winter 2022 when comparing SCTLD-affected and SCTLD-unaffected Lower Keys colonies
    - 81 additional genes that were differentially expressed in winter 2022 when comparing SCTLD-affected and SCTLD-unaffected ECA colonies
- The 96 genes found in common between the two sequencing techniques suggest these genes might be highly expressed and could need further investigation to better understand their role in SCTLD susceptibility.

Results:

The RNA extraction protocol was standardized in two main phases. The first phase focused on identifying the most effective extraction method. To achieve this, we used positive control samples collected under laboratory conditions to compare protocols for obtaining high-quality RNA. We tested the Direct-zol RNA Miniprep Kit (Catalog #: R2051) and the Quick-RNA Miniprep Kit (Catalog #: R1054) and found that the Direct-zol protocol consistently produced higher-quality RNA (Table 5).

Table 5. Comparison of RNA quality metrics for two extraction kits. Green highlighted cells correspond to optimal values.

Method	Qubit (ng/ul)	260/280	260/230	RINe	28s/18s (Area)
Direct-zol	124	2.17	2.12	9	1.5
Quick-RNA	78.2	2.19	1.68	9.4	1.7

During the second phase, the objective was to test the RNA quality of the samples that were collected in 2021/2022. We had two types of tissue sample, one that was already homogenized and another that had been preserved at -80 °C since collection. A total of nine colonies were selected to process. The RNA from samples that had been previously homogenized was highly degraded based on the quality check metrics (Table 6).

Table 6. Quality check summary of RNA extraction from nine samples from previous experiment used in 2022. Expected good quality check values per measurement in parenthesis.

Colony ID	SCTLD susceptibility	Qubit Concentration (>50 ng/ul)	RINe (7 to 10)	260/280 (1.80 to 2.00)	260/230 (2.00 to 2.20)
699	affected	176	4.2	2.14	2.21
719	affected	64	6	2.06	2.14
741	affected	68.5	6.2	2.05	2.19
753	affected	132	4.4	2.08	2.37
N48	unaffected	98.8	4.8	1.93	2.15
N50	unaffected	70.4	6.3	2.07	2.27
N54	unaffected	130	3.9	2.08	2.34
N56	unaffected	190	3.7	2.13	2.37
N59	unaffected	120	4.1	2.07	2.31

A subset of archive cores from the same nine colonies was collected in TRI Reagent (Catalog #: R2050-1-50) at Nova Southeastern University and transported on dry ice to the University of Miami. At the Traylor-Knowles Laboratory, samples were homogenized and RNA was extracted using the Direct-zol RNA Miniprep Kit. All RNA extracts were further cleaned and concentrated using the RNA Clean & Concentrator Kit (Catalog #: R1017, Zymo Research). Although the resulting RNA still showed low quality based on standard quality checks, TapeStation profiles indicated reduced degradation compared to the original samples (Table 7).

Table 7. Summary of RNA quality metrics from nine archived samples. Expected quality thresholds for each metric are shown in parentheses.

Colony ID	SCTLD susceptibility	Qubit Concentration (>50 ng/ul)	RINe (7 to 10)	260/280 (1.80 to 2.00)	260/230 (2.00 to 2.20)
699	affected	122	4.7	2.11	2.28
719	affected	124	5.8	2.07	2.26
741	affected	106	7.1	2.06	2.28
753	affected	136	4.6	2.06	2.31
N48	unaffected	130	5.8	2.11	2.36
N50	unaffected	136	4.3	2.07	2.28
N54	unaffected	134	5.4	1.99	2.24
N56	unaffected	108	5.1	2.08	2.31
N59	unaffected	134	4.6	2.1	2.38

Building on the previous results, we evaluated the sequencing quality of RNA extracted from an archived tissue sample to determine the quality of recoverable RNA sequences. We selected a fall 2021 sample from SCTLD-affected colony 753 in the Lower Keys and performed direct RNA sequencing using the SQK-RNA002 kit. This run yielded approximately 287,000 reads (see HTML report in the shared folder).

To process this dataset, we developed a custom pipeline based on Oxford Nanopore Technologies (ONT) recommendations and workflows (available in the GitHub repository: LR_RNAseq_SCTLD). Briefly, we re-performed base-calling using ONT's Dorado software with a high-accuracy model to improve sequence quality. The base-called reads were then aligned to the *Orbicella faveolata* long-read genome (Young et al., 2023) using a modified version of ONT's wf-transcriptomes workflow. Gene-level quantification was performed using the subread package on the resulting BAM files.

The resulting gene count matrix was imported into R to identify genes expressed in colony 753 during fall 2021. These were compared to genes found to be differentially expressed between SCTLD-affected and unaffected colonies from winter 2022 based on 3′RNA-seq data. We found that at least 95 genes were shared between the direct RNA-seq dataset and the differentially expressed gene set (Table 8).

Table 8. Differentially expressed genes between SCTLD-affected and unaffected colonies during winter 2022 in ECA and the Lower Keys, also detected in the direct RNA-seq dataset. Red highlighted cells represent genes up-regulated during winter, and blue highlighted cells correspond to genes down-regulated during winter. (table link)

Finally, to improve RNA quality, 18 samples from SCTLD-affected and unaffected corals in the ECA region were collected in January 2025. Samples were preserved in DNA/RNA Shield to maintain RNA integrity and minimize degradation during homogenization. From these 18 samples, we process 6 tissue colonies (3 from SCTLD-affected corals and 3 from SCTLD-unaffected corals). We use a bench protocol that was standardized with tissue samples from the 18 colonies collected (Table 9).

Table 9. List of colonies collected in January 2025 from the ECA region.

Asses ID	Collection date	Field status	SCTLD_RNA	Long Reads
MC-005	1/13/2025	absent	unaffected	0
MC-027	1/13/2025	absent	unaffected	1
LC-018	1/13/2025	absent	affected	0
LC-024	1/13/2025	absent	affected	0
LC-064	1/13/2025	absent	unaffected	1
LC-077	1/13/2025	absent	affected	0
LC-077	1/13/2025	present	affected	1
LC-079	1/13/2025	absent	unaffected	1
LC-085	1/13/2025	absent	affected	1
LC-088	1/13/2025	absent	affected	1
LC-101	1/13/2025	absent	affected	1
LC-110	1/13/2025	absent	affected	1
LC-114	1/13/2025	absent	affected	1
LC-123	1/13/2025	absent	affected	0
LC-124	1/13/2025	absent	affected	0
LC-125	1/13/2025	absent	affected	0
LC-126	1/13/2025	absent	affected	0
LC-127	1/13/2025	absent	unaffected	0
LC-127	1/13/2025	present	unaffected	0
LC-139	1/13/2025	absent	unaffected	1

The RNA quality metrics for the 6 samples did not meet the optimal thresholds for Long-Read RNA sequencing, but the Tape Station gel and pick graphs showed a considerable concentration of long RNA (Figure 31). Therefore, to assess the quality of the RNA sequencing data, we sequenced the SCTLD-unaffected colony LC-079 that had a low RIN score of 2, but the gel showed the presence of long RNA.

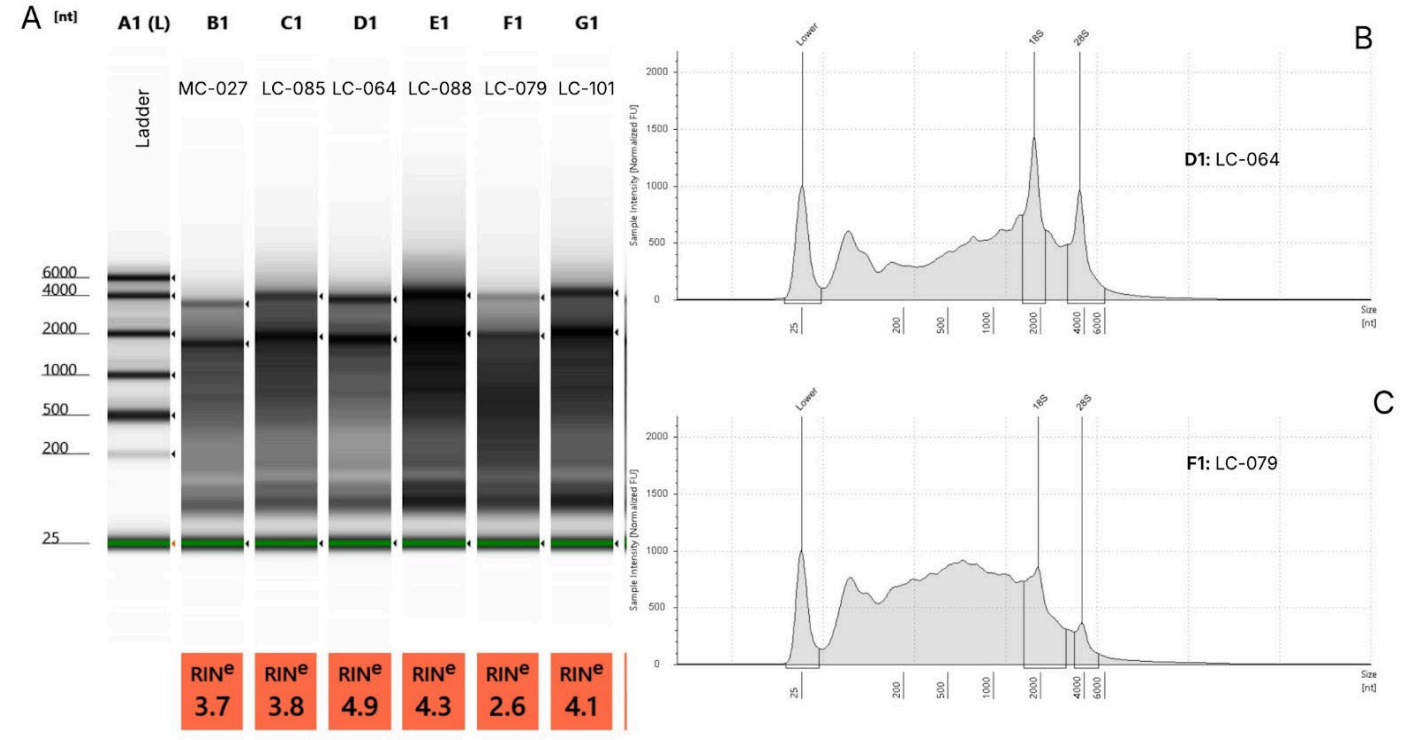

Figure 31. RNA quality assessment of Orbicella faveolata samples extracted using a bench Trizol protocol (January 2025 collection). (A) TapeStation gel image with electronic RNA Integrity Number (RINe) scores for six samples. (B–C) Electropherograms showing fragment size distribution (in nucleotides, nt) and relative fluorescence units (RFU) for representative samples LC-064 (B) and LC-079 (C). Lines indicate marker peaks.

We decided to test the cDNA kit SQK-PCS114 that has reverse transcription and PCR amplification steps during library preparation, due to the considerably high amount of reads/data that could potentially be obtained. The sequencing resulted in 4.71 million reads, which is around 16 times more reads than the direct RNAseq protocol.

A pipeline to analyze this data was also built by adapting the D-RNAseq pipeline developed before to the new kit and conditions (available in the GitHub repository: LR_RNAseq_SCTLD). Due to high-performance computing power, the gene counts for

this sample is not available yet. However, the higher number of reads suggests that SQK-PCS114 could be a better option for Long-Read RNAseq of our tissue type.

Discussion:

Orbicella faveolata tissue may contain high levels of RNases, which could lead to rapid RNA degradation. Our results indicate that standard RNA extraction methods are insufficient for obtaining high-quality RNA. Based on the Tape station results, some samples were degraded, while others appeared contaminated, leading to poor RNA quality metrics. We suspect that the tissue's high lipid content may interfere with RNA quality checks and contribute to the degradation of longer RNA fragments. To improve RNA quality from field samples, future research should optimize collection and extraction methods. This could include testing lipid removal techniques and size-selection steps during RNA extraction (Bouchard et al., 2020). Despite the low RNA quality scores, our successful D-RNAseq run suggests that factors other than RNA integrity (such as contamination) may not negatively impact sequencing. This means that the 2021/2022 and 2025 samples could still be sequenced, even with suboptimal quality metrics.

Having found 95 genes that were differentially expressed between SCTLD-affected and SCTLD-unaffected corals during winter, also express in a SCTLD-affected sample during fall serves as a proof of concept that using different RNA sequencing techniques can improve our understanding about genes involved in SCTLD response. These genes might be potential biomarkers that can be targeted for SCTLD susceptibility monitoring. Future research should focus on increasing the number of replications that can be sequenced from different colonies and timepoints to prove their involvement in SCTLD response. As mentioned earlier in this report, most of the functions of the highly up-regulated genes are related to an immune response; therefore, having these genes also found on the D-RNAseq data suggests that the SCTLD-affected corals' immune reaction to SCTLD might be constantly turned on. An extra sampling time point at different times of the year might help elucidate the role of these genes all year long.

Overall, these results demonstrate that D/LR-RNAseq is a technique that can be successfully applied to already collected samples with an average RNA quality. This flexibility on the quality of RNA use could allow the use of different samples that might bring more insights into how SCTLD susceptibility changes over time or if there is any genetic signature for resistant phenotypes. Additionally, we can consider the 96 genes found with both RNAseq techniques as potential future targets for SCTLD studies.

3.7. **Task 6a: Chemical defense data analysis and integration (Paul, Williams, Walker)**

Goals: Extract colonies for metabolomics analysis (Task 7 Garg), partition extracts for lipidomics of the EtOAc partition, and conduct antimicrobial assays of both the EtOAc and BuOH partitions against *Vibrio coralliilyticus* strain OFT6-21. Conduct statistical analyses of the antimicrobial assays and integrate these data with the other analytical data including metabolomics, lipidomics, *Vibrio* quantification, etc.

Significant findings: Findings show that antimicrobial activity of the EtOAc partitions was higher than for the BuOH partitions and weights of EtOAc partitions were also higher than weights of BuOH partitions, suggesting that the nonpolar compounds present in the extracts are driving the antimicrobial activity of these corals. Thus, the lipidomics results may be very important for analyzing the compounds responsible. Antimicrobial activity in the EtOAc partitions was highest in the Winter 2022 sampling period. There was a significant difference in EtOAc radius (T-C) between SCTLD affected and unaffected colonies in Winter 2022, and the same pattern was observed for the diseased presence or absence at coring data. Antimicrobial activities were higher for the corals that never had SCTLD suggesting some level of resistance in these corals may be due to their antimicrobial compounds.

Results and Discussion: For the antimicrobial activity of the EtOAc partitions, there was a significant interaction between Sample Period and SCTLD (Psuedo-$F_{1,260}$=3.95, p=0.025) on EtOAc radius (Table 10). There was a significant difference in EtOAc radius (T-C) between SCTLD affected and unaffected colonies in Winter 2022 (p=0.006), with unaffected colonies having a significantly higher mean radius (16.3 mm) than affected colonies (13.2 mm) (Figure 32). Within either SCTLD affected or unaffected colonies, EtOAc radius significantly increased through time, with all sample periods significantly different from each other (p=<0.004 for all pairwise comparisons, Table 11). In SCTLD affected colonies, mean EtOAc radius increased from 7.8 mm in Summer 2021, to 10.9 mm in Fall 2021, and then to 13.2 mm in Winter 2022. In SCTLD unaffected colonies, mean EtOAc radius increased from 7.7 mm in Summer 2021, to 12.2 mm in Fall 2021, and then to 16.3 mm in Winter 2022. This is an intriguing finding suggesting that corals that never showed presence of SCTLD had higher lipophilic antimicrobial compounds present, but this was only obvious during the cooler/drier winter sampling period when corals should be least stressed by environmental factors.

The same significant interaction occurred when examining antimicrobial activity of the EtOAc partitions by Disease presence or absence at coring, with a significant interaction between Sample Period and Disease at coring (Psuedo-$F_{1,260}$=3.72, p=0.026) on EtOAc mean radius (Table 10). The interpretation of this interaction remained the same as for Sample Period and SCTLD, with one exception: in Fall 2021 colonies with disease absent at coring had a significantly higher EtOAc radius (12.2 mm) than colonies with disease present at coring (10.8 mm) (p=0.029, Table 6) (Figure 33).

For EtOAc partition mgs (weights of extracts), there was a significant effect of Sample Period (Psuedo-$F_{1,260}$=50.41, p=0.001), and no significant effect of either Region or SCTLD, nor any significant interactions between the three fixed effects (Table 10). EtOAc partition weights were significantly higher in both Summer 2021 (12.6 mm) and Winter 2022 (11.6 mm) than in Fall 2021 (7.2 mm) (p=0.001 for both pairwise comparisons, Table 11) (Figure 34). The same single effect of Sample Period (and its pairwise comparisons) occurred on EtOAc partition mgs when substituting SCTLD for Disease presence at coring (Table 10). The most likely explanation for these results is that these samples were collected post spawning for many coral samples in Fall 2021, and this led to a reduction of fatty lipids that were in gravid colonies in the nonpolar EtOAc partitions. Alternatively, corals are more stressed in the Fall 2021 sampling period after exposure to summer warm water temperatures, rainfall, runoff, etc. and this might affect lipid concentrations.

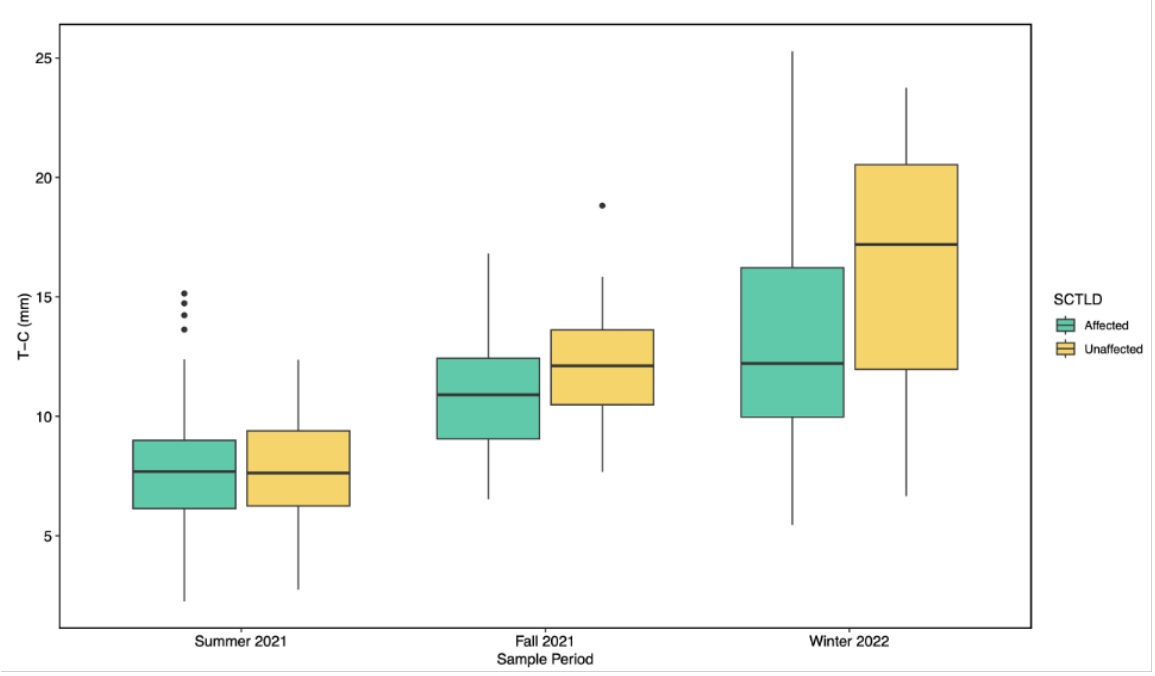

Figure 32**.** Variations in EtOAc Treatment-Control (T-C) mean radius (mm) across Sample Periods and SCTLD. Boxplots denote the median value (thick horizontal line), the interquartile range (thin horizontal lines), the minimum and maximum values (vertical thin lines), and any outliers.

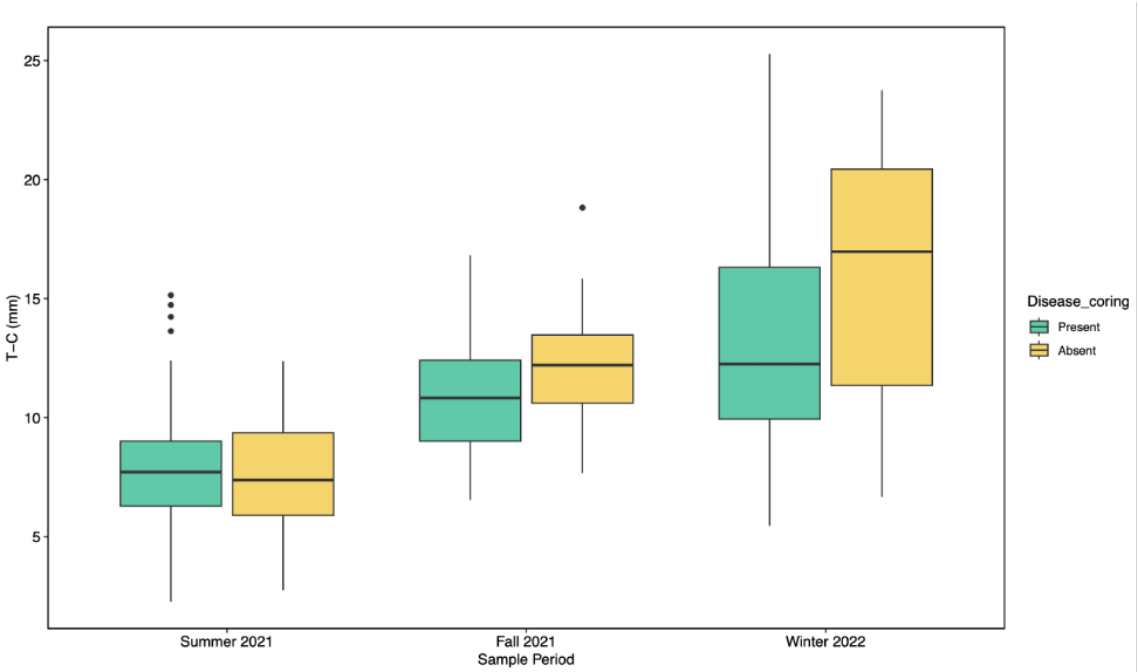

Figure 33. Variations in EtOAc Treatment-Control (T-C) mean radius (mm) across Sample Periods and Disease presence at coring. Boxplots denote the median value (thick horizontal line), the interquartile range (thin horizontal lines), the minimum and maximum values (vertical thin lines), and any outliers (black circles).

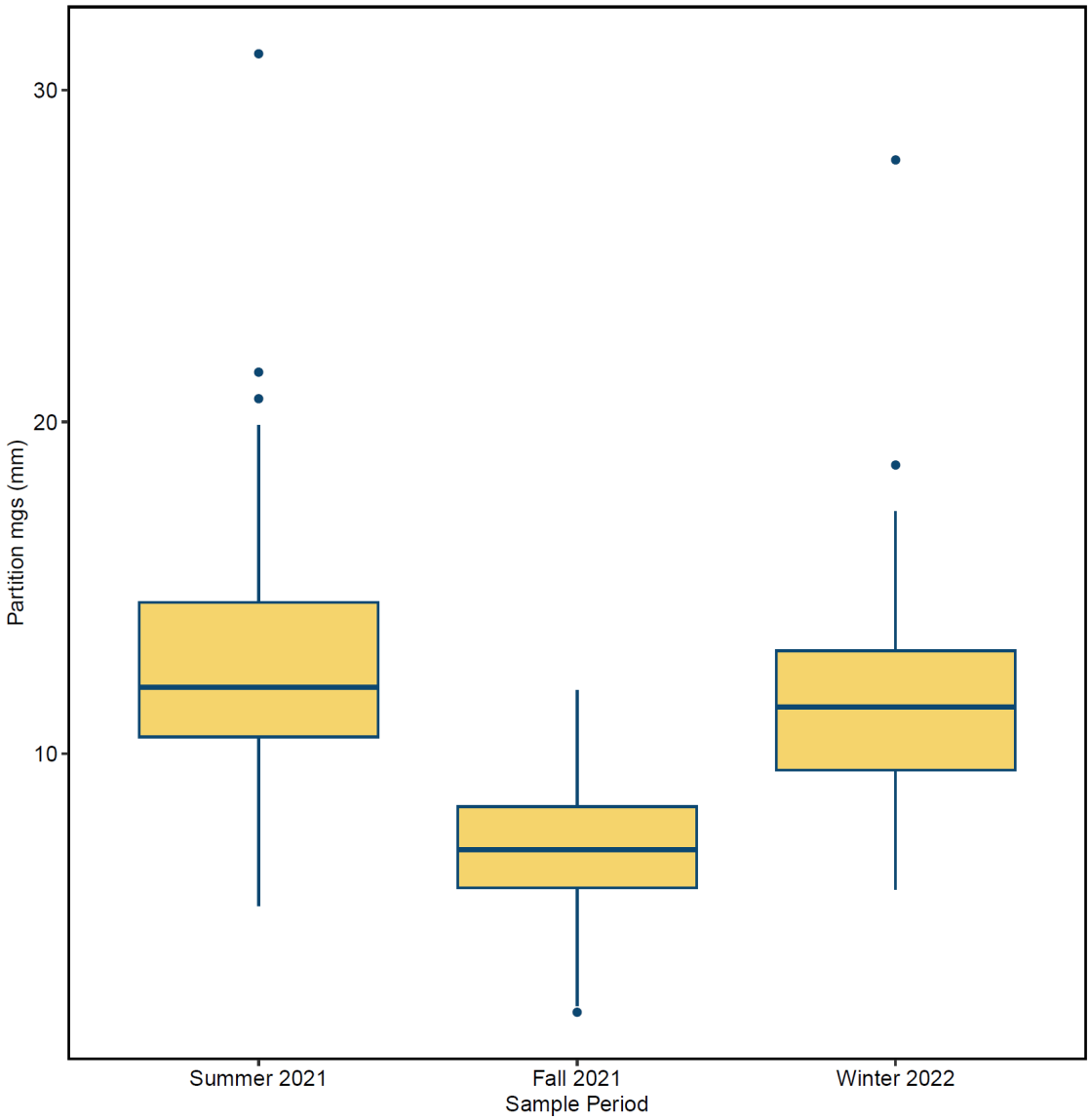

Figure 34. Variations in EtOAc Partition mgs (weights of partitions) across Sample Periods. Boxplots denote the median value (thick horizontal line), the interquartile range (thin horizontal lines), the minimum and maximum values (vertical thin lines), and any outliers (black circles).

For the antimicrobial effects of the BuOH partitions, there was a three-way significant interaction between Sample Period, Region, and SCTLD (Psuedo-$F_{1,260}$=3.46, p=0.044) on BuOH radius (Treatment-Control) making the results more challenging to interpret (Figure 35). Patterns for antimicrobial activity in response to presence or absence of SCTLD or disease presence at coring were only observed at some sampling periods or locations (Figure 36). It is worth noting that the BuOH partitions showed less antimicrobial activity and lower weights than the EtOAc partitions overall. The higher antimicrobial activity of the EtOAc partitions and their higher amounts suggest that the EtOAc partitions are explaining most of the antimicrobial activity of the whole colonies.

Table 10. Permutational analysis of variance (PERMANOVA) outputs testing for the main effects of Sample Period (fixed factor, three levels: Fall 2021, Summer 2021, Winter 2022), Region (fixed factor, two levels: ECA and Keys), and either SCTLD (fixed factor, two levels: affected, unaffected), or Disease at coring (fixed factor, two levels: present, absent) on EtOAc radius and EtOAc partition mgs.

Factor (EtOAc Radius mean)	df	SS	MS	Pseudo-F	P-value
Sample Period	2	1476.60	738.31	64.69	0.001
Region	1	16.53	16.53	1.45	0.231
SCTLD	1	101.18	101.18	8.86	0.004
Sample Period x Region	2	30.00	15.00	1.31	0.284
Sample Period x SCTLD	2	90.14	45.07	3.95	**0.025**
Region x SCTLD	1	8.19	8.19	0.72	0.404
Sample Period x Region x SCTLD	2	0.79	0.39	0.03	0.966
Residuals	249	2842.00	11.41		
Total	260	4738.60			

Factor (EtOAc Radius mean)	df	SS	MS	Pseudo-F	P-value
Sample Period	2	1517.30	758.63	66.13	0.001
Region	1	11.41	11.41	0.99	0.327
Disease coring	1	85.88	85.88	7.49	0.010
Sample Period x Region	2	22.51	11.26	0.98	0.361
Sample Period x Disease coring	2	85.29	42.65	3.72	**0.026**
Region x Disease coring	1	15.85	15.85	1.38	0.259
Sample Period x Region x Disease coring	2	0.77	0.38	0.03	0.969
Residuals	249	2856.40	11.47		
Total	260	4738.60			

Factor (EtOAc Partition mgs)	df	SS	MS	Pseudo-F	P-value
Sample Period	2	930.65	465.33	50.41	**0.001**
Region	1	1.75	1.75	0.19	0.676
SCTLD	1	0.03	0.03	0.00	0.950
Sample Period x Region	2	25.51	12.76	1.38	0.242
Sample Period x SCTLD	2	24.70	12.35	1.34	0.249
Region x SCTLD	1	3.56	3.56	0.39	0.520
Sample Period x Region x SCTLD	2	9.08	4.54	0.49	0.600
Residuals	249	2298.50	9.23		
Total	260	3800.60			

Factor (EtOAc Partition mgs)	df	SS	MS	Pseudo-F	P-value
Sample Period	2	931.94	465.97	50.80	**0.001**
Region	1	0.66	0.66	0.07	0.789
Disease coring	1	1.36	1.36	0.15	0.689
Sample Period x Region	2	28.23	14.11	1.54	0.224
Sample Period x Disease coring	2	41.99	20.99	2.29	0.091
Region x Disease coring	1	8.52	8.52	0.93	0.316
Sample Period x Region x Disease coring	2	2.29	1.15	0.12	0.899
Residuals	249	2284.20	9.17		
Total	260	3800.60			

Table 11. Permutational analysis of variance (PERMANOVA) pairwise comparisons of significant main effects for Sample Period (fixed factor, three levels: Fall 2021, Summer 2021, Winter 2022), Region (fixed factor, two levels: ECA and Keys), and either SCTLD (fixed factor, two levels: affected, unaffected), or Disease presence at coring (fixed factor, two levels: present, absent) on EtOAc radius and EtOAc partition mgs.

Pairwise test	Factor level comparison	t	P-value
EtOAc Radius mean			
Sample Period x SCTLD			
Within level 'Unaffected' of SCTLD	Fall 2021, Summer 2021	5.21	**0.001**
	Fall 2021, Winter 2022	3.14	**0.004**
	Summer 2021, Winter 2022	6.41	**0.001**
Within level 'Affected' of SCTLD	Fall 2021, Summer 2021	7.05	**0.001**
	Fall 2021, Winter 2022	3.66	**0.001**
	Summer 2021, Winter 2022	8.44	**0.001**
Within level 'Fall 2021' of Sample Period	Unaffected, Affected	2.01	0.058
Within level 'Summer 2021' of Sample Period	Unaffected, Affected	0.15	0.872
Within level 'Winter 2022' of Sample Period	Unaffected, Affected	2.80	**0.006**

Pairwise test	Factor level comparison	t	P-value
EtOAc Radius mean			
Sample Period x Disease coring			
Within level 'Absent' of Disease coring	Fall 2021, Summer 2021	5.74	**0.001**
	Fall 2021, Winter 2022	2.95	**0.006**
	Summer 2021, Winter 2022	6.50	**0.001**
Within level 'Present' of Disease coring	Fall 2021, Summer 2021	6.85	**0.001**
	Fall 2021, Winter 2022	3.74	**0.002**
	Summer 2021, Winter 2022	8.36	**0.001**
Within level 'Fall 2021' of Sample Period	Absent, Present	2.25	**0.029**
Within level 'Summer 2021' of Sample Period	Absent, Present	0.47	0.640
Within level 'Winter 2022' of Sample Period	Absent, Present	2.54	**0.008**

Pairwise test	Factor level comparison	t	P-value
EtOAc Partition mg			
Sample Period	Fall 2021, Summer 2021	9.14	**0.001**
	Fall 2021, Winter 2022	9.40	**0.001**
	Summer 2021, Winter 2022	0.89	0.376

Pairwise test	Factor level comparison	t	P-value
EtOAc Partition mg			
Sample Period	Fall 2021, Summer 2021	9.12	**0.001**
	Fall 2021, Winter 2022	9.51	**0.001**
	Summer 2021, Winter 2022	0.74	0.490

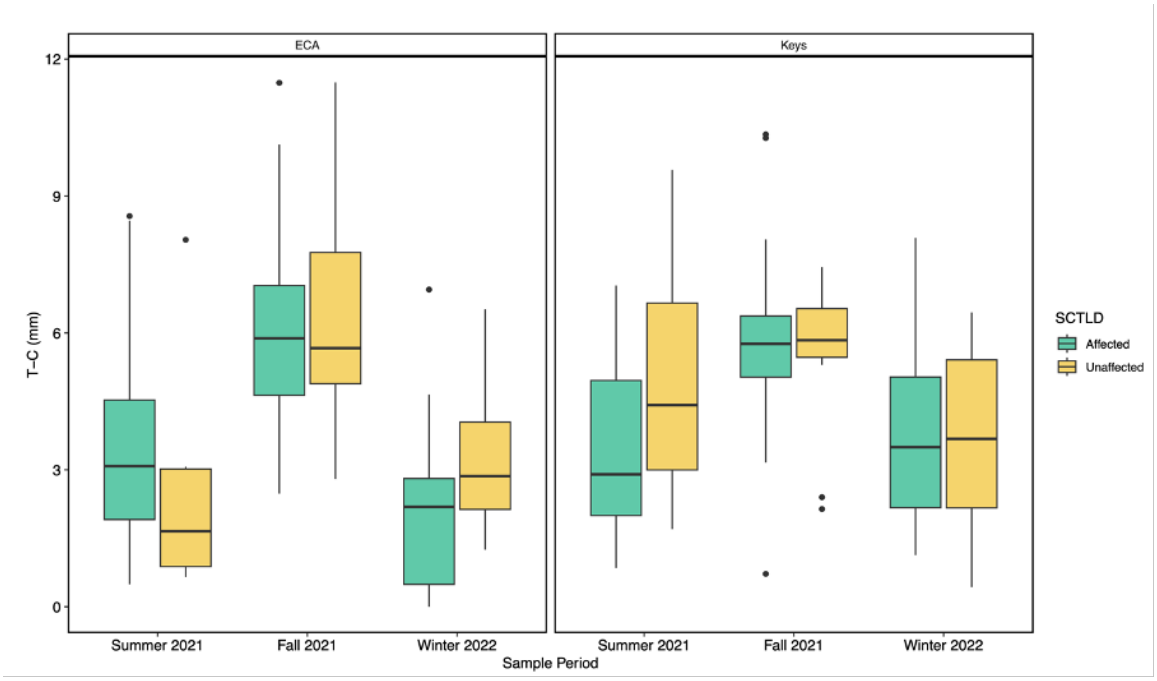

Figure 35. Variations in BuOH Treatment – Control radius mean (mm) by Sample Period and SCTLD. Boxplots denote the median value (thick horizontal line), the interquartile range (thin horizontal lines), the minimum and maximum values (vertical thin lines), and any outliers (black circles).

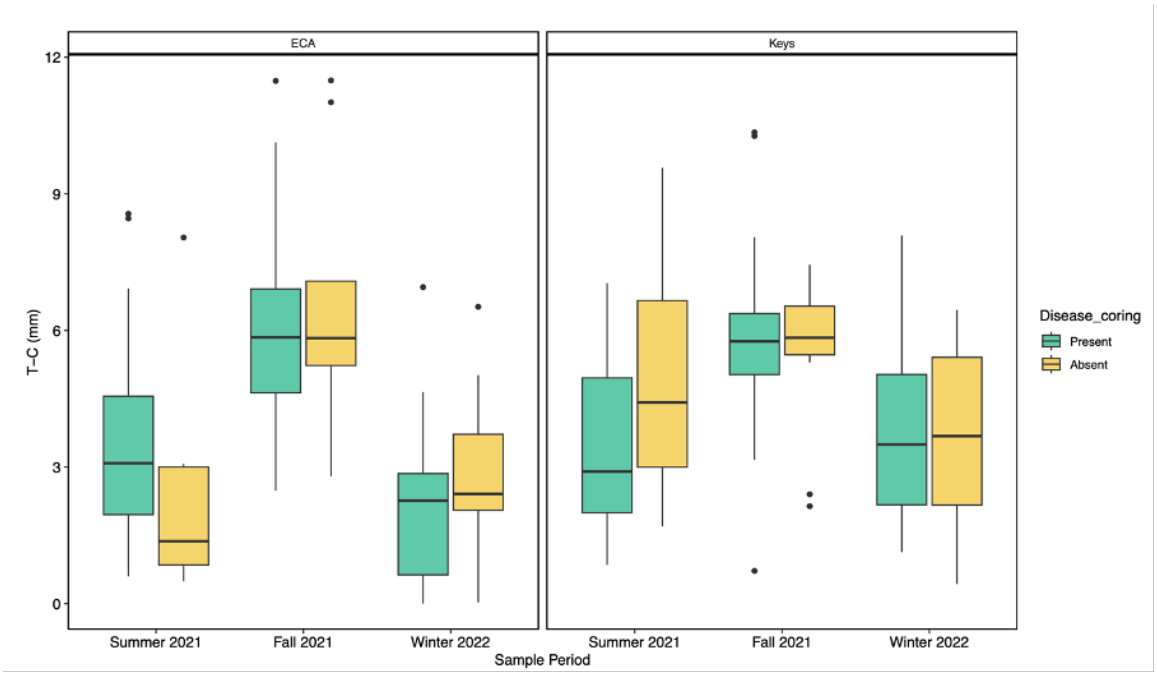

Figure 36. Variations in BuOH Treatment – Control radius mean (mm) by Sample Period and Disease coring. Boxplots denote the median value (thick horizontal line), the interquartile range (thin horizontal lines), the minimum and maximum values (vertical thin lines), and any outliers (black circles).

3.8. Task 6b: Characterizing compounds involved in antimicrobial chemical defenses (Paul, Garg)

Goals: 1) isolate compounds from RRC corals responsible for the antimicrobial activity using bioassay-guided fractionation and 2) extract and test *Symbiodiniaceae* from *O. faveolata* cultured at SMS.

Significant findings: Results of bioassay-guided fractionation of EtOAc partitions of RRC corals suggest that no single compound or related compounds are driving the antimicrobial patterns observed against *Vibrio coralliilyticus* OfT6-21. After chromatography, several fractions with different polarities showed antimicrobial activity. It is likely that diverse lipids are responsible for the antimicrobial activity of the corals.

Results and Discussion:

Ten of the ethyl acetate (EtOAC) partitions of *O. faveolata* extracts from the RRC samples were each separated into five fractions on silica gel columns using the same separation scheme (Figure 37). The samples fractionated were selected based on their disk diffusion assay activity and the amount of material remaining. We then tested the fifty fractions in the disk diffusion assays against our test strain, the coral pathogen *V. coralliilyticus* OfT6-21, to begin to resolve the chemistry driving the antimicrobial activity (Figure 38). A portion of the parent EtOAc partition material was retained prior to fractionating to test in tandem with the fractions. In general, the antimicrobial activity did not clearly resolve into one fraction, suggesting the separation was not efficient, or more likely that multiple compounds of different polarities were producing antimicrobial activity. In general, the most active fractions were fractions 2 and 4, indicating that compounds of different polarities were showing activity (Figure 38). Based on assay results, proton NMR spectra was obtained for two sets of fractions, and fraction 4 from Broward coral MC-002 was further separated by HPLC resolving three peaks for further analysis (Figure 38).

The amounts of extracts and subsequent partitions for the RRC corals were relatively small, and we wanted more coral extract to scale up to be able to isolate more of the antimicrobial compounds. We did not have live coral available to us but did have *O. faveolata* samples frozen at –80 °C from prior experimental work with SCTLD. Six coral pieces were extracted and partitioned in the same way as the RRC samples. Again, the EtOAc partitions were more active than the BuOH partitions, indicating that BuOH partitions are not worth further pursuit at this time. Interestingly, the partitions of the experimental corals that were exposed to SCTLD but never showed signs of disease were slightly more bioactive than those from the same corals never exposed to disease for 2 of 3 corals (Figure 39). Nonetheless, the antimicrobial differences among the samples are small, and the next step will be to combine all six of the EtOAc partitions to have more material for further compound isolation and antimicrobial testing.

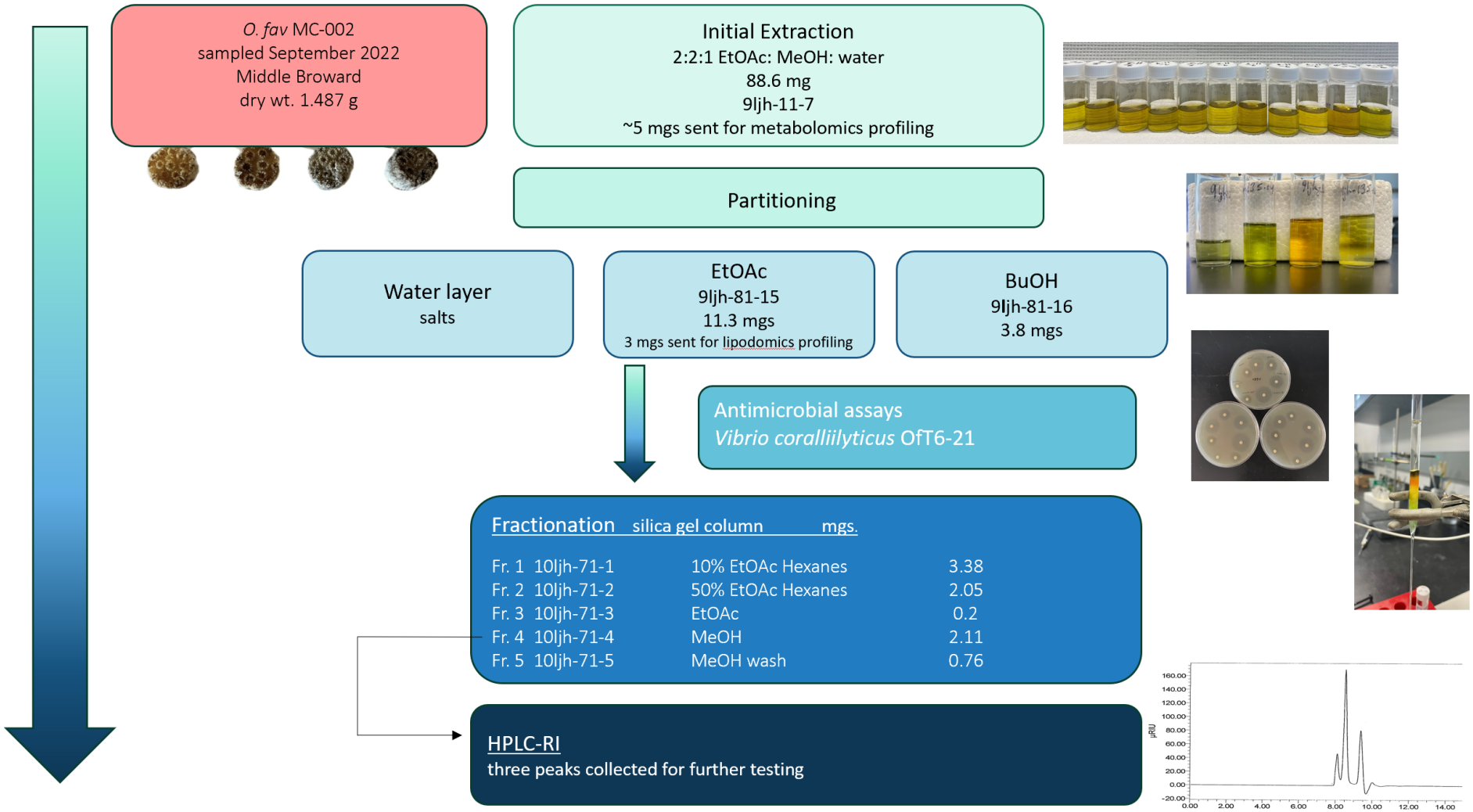

Figure 37. Overview of coral extraction, partition steps and fractionation of the samples. This is illustrated for one coral, MC-002, but the process was the same for the other nine.

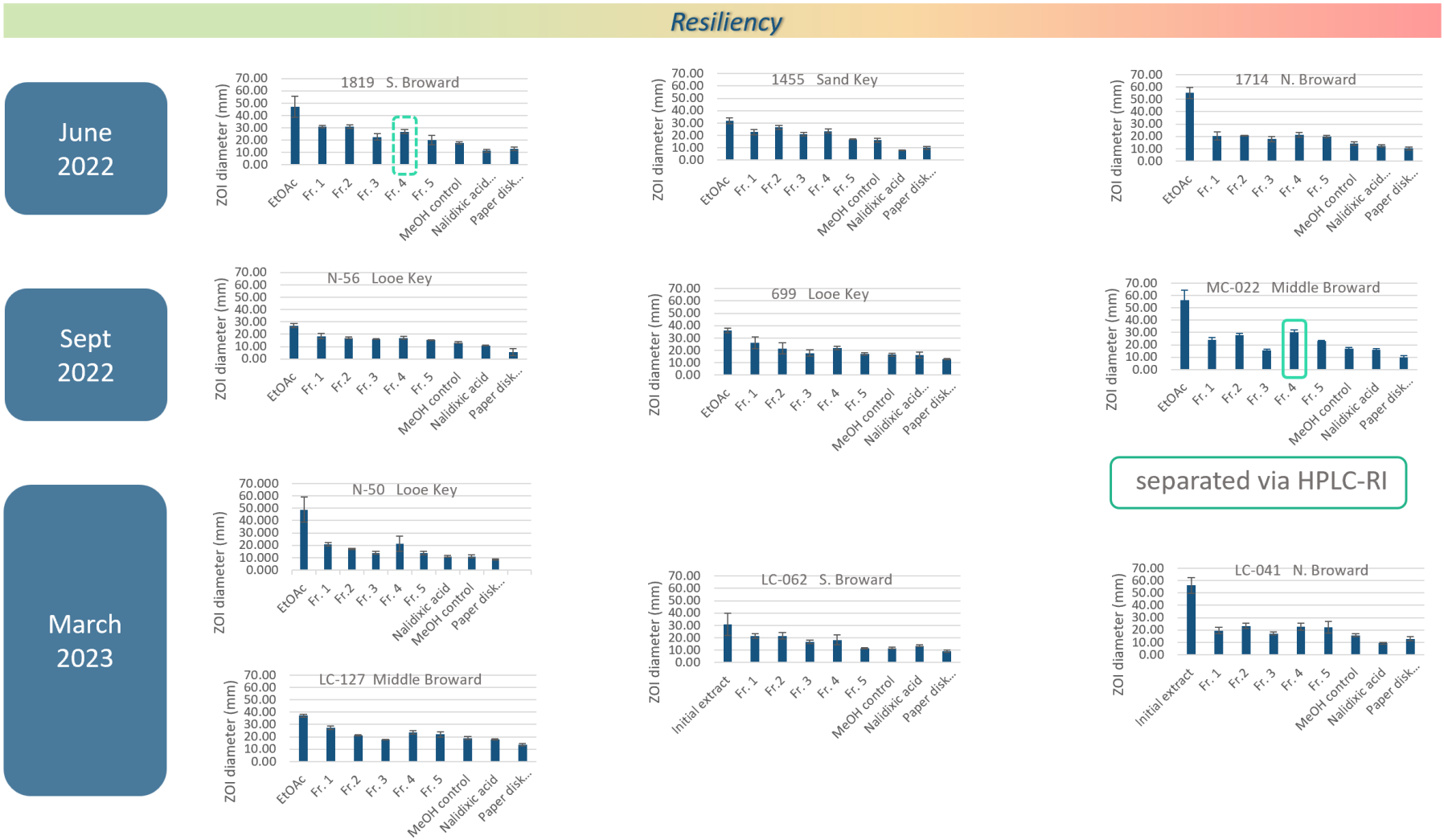

Figure 38. Results of disk diffusion assay with the coral pathogen *V. coralliilyticus* OfT6-21 for 10 of the *O. faveolata* samples that spanned all three resistance categories. The larger ZOI means the extract showed more antibacterial activity. There was considerable individual variation in antimicrobial activity and how it was distributed among the fractions but often fraction 4 (100% MeOH) was the highest. The resiliency categories correspond to SCTLD resistant (green) to the most susceptible (orange).

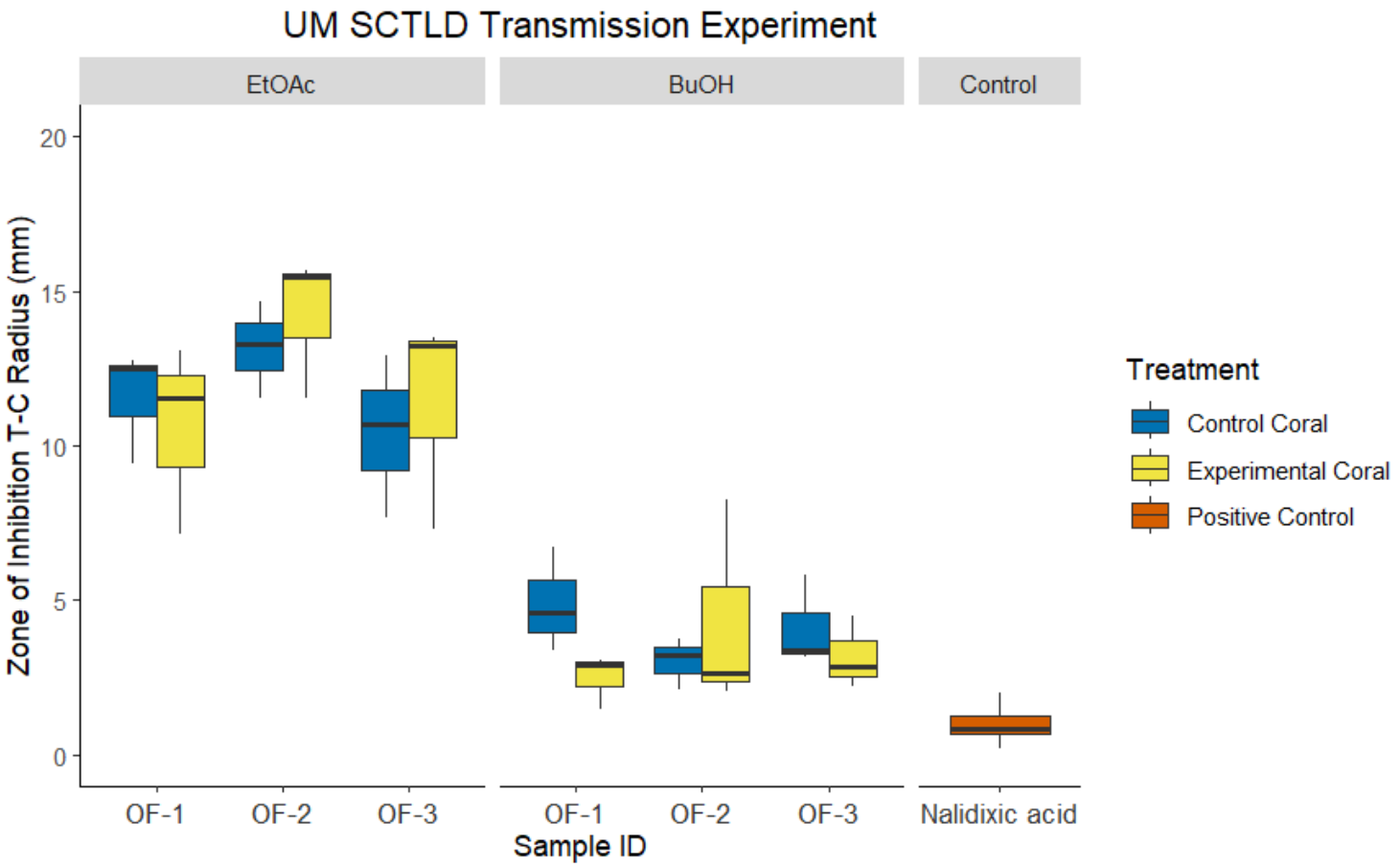

Figure 39. Disk diffusion assay results of *O. faveolata* ethyl acetate (EtOAc) and butanol (BuOH) partitions against *V. coralliilyticus* strain OFT7-21. Corals from 2020 disease transmission experiment, where *O. faveolata* were exposed to corals with SCTLD. Partitions dissolved in methanol at a concentration of 10 µg/disk. Results shown as the treatment radius from the disk to the edge of the ZOI minus the radius from the methanol control (T-C). Nalidixic acid was used as a positive control and methanol and a blank disk were used as a negative control. The boxes represent the range for three replicates and the middle line indicates the median. The bottom and top bars in the boxes represent the 25th and 75th percentiles; whiskers above and below the box are the 10th and 90th percentiles.

Additionally, four strains of *O. faveolata*-derived zooxanthellae (Symbiodiniaceae), *Breviolum* (MF1.05b01 SCI07-205), *Breviolum* (MF10.14.02 SCI), *Durusdinium* (MF 2.2 b-2), and *Symbiodinium* (MF 10.02a), were grown in culture after scaling up growth for one month. Cultures of the four strains of coral-derived of zooxanthellae were extracted, and the ethyl acetate (EtOAc) and butanol (BuOH) partitions of each were tested for antibacterial activity against the known coral pathogen *V. coralliilyticus* Of-T6-21. Overall, where larger amounts of extracts were partitioned, the BuOH partitions were more active than the EtOAc partitions. Now that we have more material we will be following up on both sets of partitions with bioassay-guided fractionation (Figure 40). We will maintain our scaled-up cultures so that we can continue to get more material for future analysis.

The ethyl acetate partitions were statistically profiled and metabolite feature annotations described herein. See more details below in the lipidomics section for Task 7d.

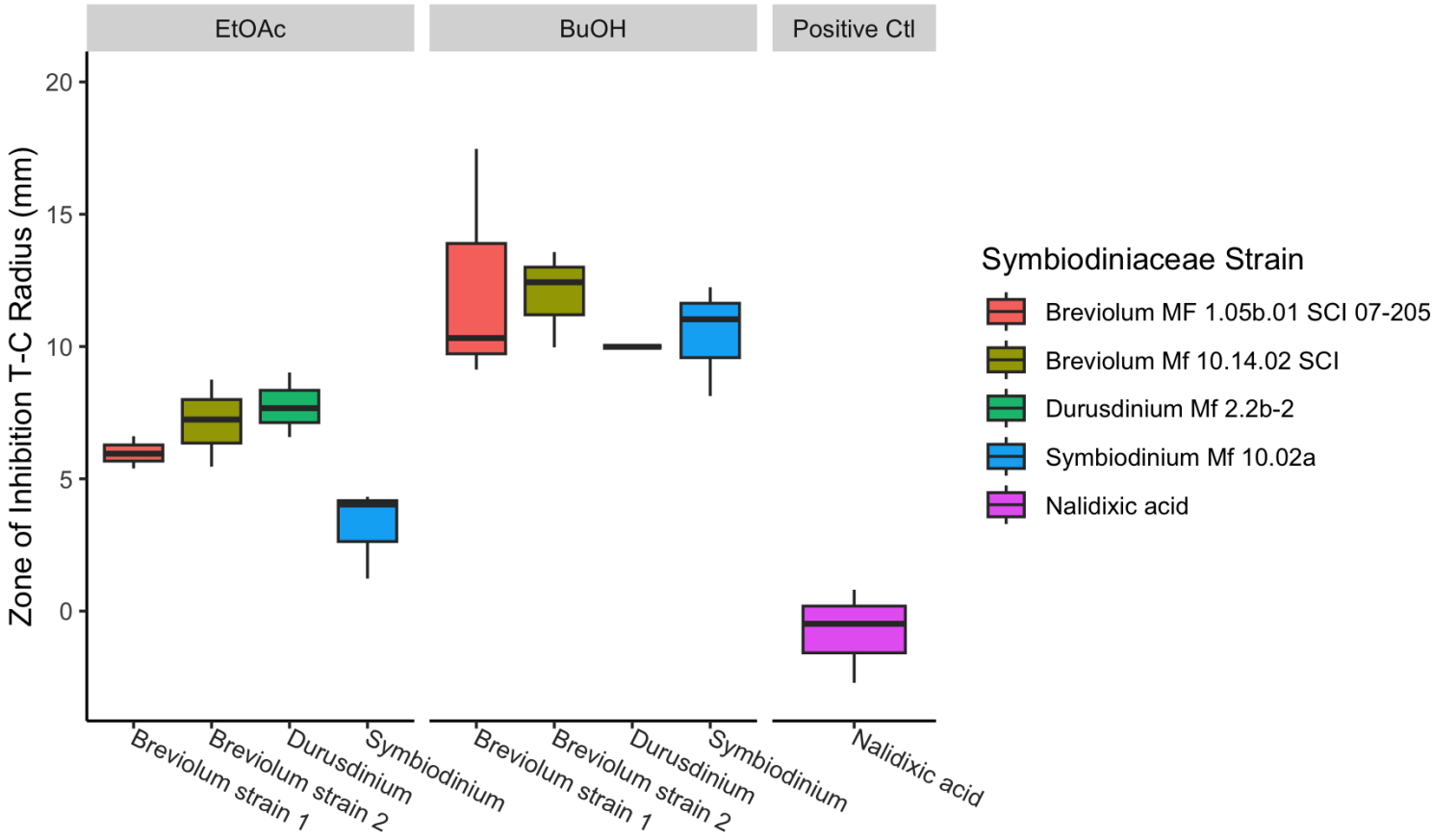

Figure 40. EtOAC and BuOH partitions of four Symbiodiniaceae strains representing 3 genera (*Breviolum*, *Durusdinium* and *Symbiodinium*). BuOH partitions were consistently more active than the EtOAc partitions for the partitions from the scaled-up symbiont extracts.

3.9. Task 7a: Continuation of metabolomics analysis and feature annotation to identify metabolic biomarkers of resilience (Garg)

Goal: continue the annotation of metabolite features detected in the RRC unified sample set with a variety of in silico tools and databases.

Significant findings: Statistical analyses revealed an evident environmental and temporal effect on the metabolome, which resulted in grouping the corals based on their sample period and reef location prior to subsequent analysis. The metabolites that drove differences in statistically significant SCTLD-based comparison groups were largely predicted as fatty acids. Annotations of these metabolite features included acylcarnitines, betaine lipids, phosphocholines, and peptidic-like natural products.

Results and Discussion: Using tandem mass spectrometry coupled with liquid chromatography, metabolites were extracted from 270 tissue cores with organic solvents by the Paul laboratory (Task 6) and analyzed via untargeted metabolomics (Figure 41). A suite of analysis tools aided metabolite feature annotations. In silico methods include tools that facilitate chemical substructure discovery, such as unsupervised substructure searches via MS2LDA[1] and user-defined spectral queries using MassQL.[2] Feature based molecular networking (FBMN) enables visualization of metabolite features that are clustered based on structural similarity, which allows for rapid propagation of metabolite identification.[3] In silico prediction tools such as MolDiscovery provide candidate metabolite identification, and where annotations cannot be proposed, the platforms SIRIUS45 with CSI:FingerID[4] and CANOPUS[5] provide putative chemical formulas and predicted chemical class to further inform the metabolome analysis.

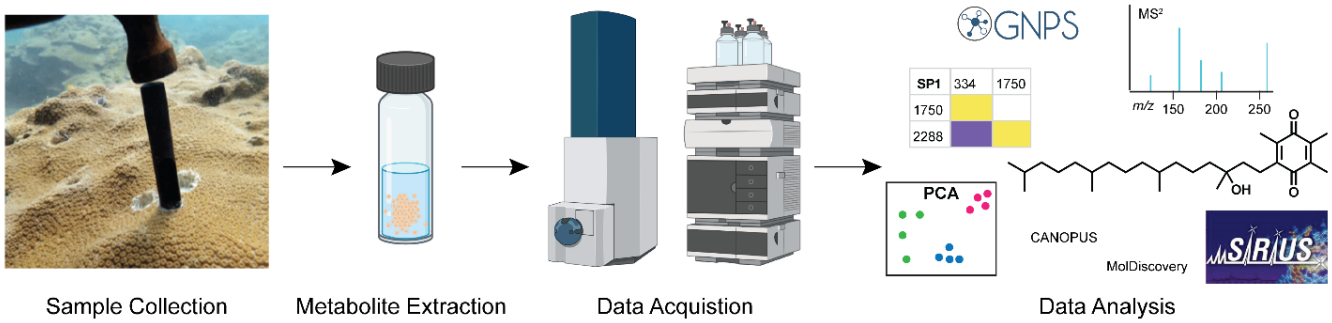

Figure 41. Metabolomics Analysis Workflow. Tissue cores of *O. faveolata* are collected, then metabolites are extracted using organic solvents. UPLC-MS/MS data is acquired on the metabolome extracts, then a variety of statistical methods are used to profile the coral metabolomes and prioritize metabolite features for annotations. Several in-silico tools were used to produce feature annotations.

Part 1: **Statistical Analysis of the Detected Metabolite Features from Coral Extracts**
Statistical analyses of all samples were performed to gauge factors driving metabolome variation. Three colonies from Sand Key were identified as *Orbicella franksi* in a genomics analysis[6] and were removed from all subsequent analysis to avoid metabolome variation attributed to cofounders. A variety of statistical analysis were performed to determine what factors may explain the variation captured within the detected metabolomes. Previous studies have shown spatial and temporal effects on metabolite composition among the

southern Florida coral reef system[7] and the Arraial do Cabo Bay reef (Brazil).[7] Therefore, we hypothesized that metabolome variation driven by sample period and reef region would be captured in our analysis. This sample set represents a unique opportunity to query both spatial (reef region/location) and temporal (sampling period) effects on the metabolome of field-sampled Caribbean stony corals.

The metabolome profiles of all corals (n=261, excluding the 3 corals identified as *O. franksi*) were visualized using unsupervised principal component analysis (PCA). Corals from the two regions formed separate clusters within each sample period (Figure 42 A-C) and the coral metabolomes from each sample period within the regions also formed distinct clusters (Figure 42 D-F). The PCA plot generated shows intragroup variation with either sampling period or location, with an exception for samples from KJCAP. Thus, metabolome variation was attributable to additional factors beyond reef region and sample period. We further queried the effect of reef location on the metabolome variation. For the Lower Keys, this includes differentiation of Sand Key and Looe Key. For the KJCAP, this differentiates the 'North', 'Middle' and 'South' designations within the reef. It is important to note that across reef regions and locations, "sample period" does not refer to a consistent date. Thus, the resulting 15 groups account for both temporal and spatial effects that drive variation of the metabolome and will be referred to by their sample period_location designation henceforth. The PCA analysis by location/sample date within the sample period (Figure 42 A-C) and by sample period within the location/sample date (Figure 42 D-F) reveals inter- and intragroup variation, with temporal sample period effects most evident at Looe Key and Sand Key.

We constructed a non-metric multidimensional scaling plot on the bootstrapped averages of each group. A bootstrap nMDS (bnMDS) plot helps visualize the confidence interval, variance, and mean of each group. The bnMDS plot is in agreement with the PCA analyses, illustrating the variance between sample periods and reef locations (Figure 43). It is also evident that some groups, such as SP2_North and SP2_Middle, have larger intragroup variation than other groups. Finally, non-parametric permutation multivariate analysis of variance (PERMANOVA) was performed. The results showed that the differences between sample period, region, and location/sample date were indeed significant ($p<0.02$ for all comparisons, Table X1). Thus, the corals were separated into this 15-group scheme prior to subsequent analysis.

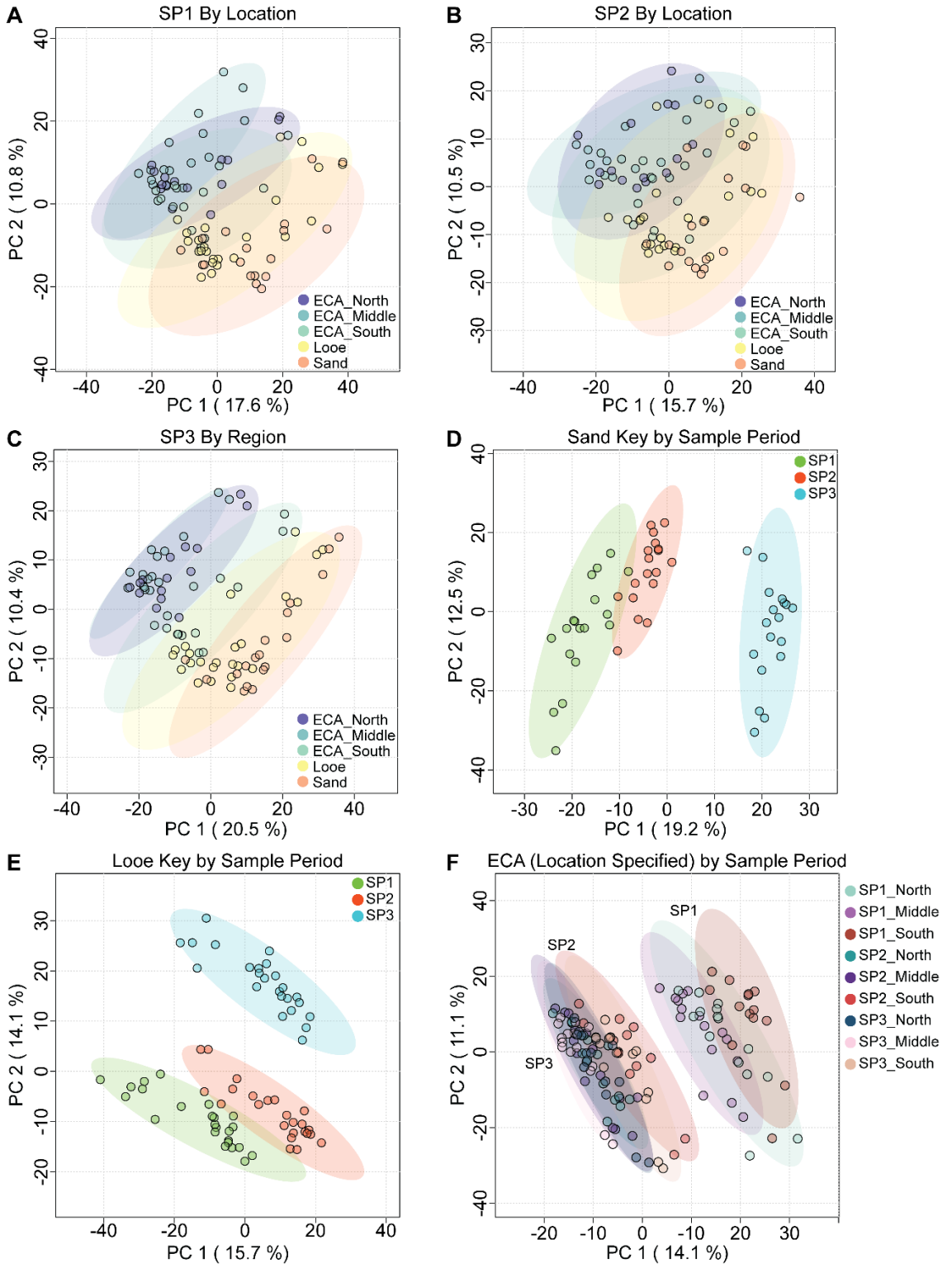

Figure 42. Principal Component Analysis (PCA) of Metabolome Data with Reef Location Specified. (A-C) PCA of the metabolome data for each sample period (SP= sample period) where the reef location of each coral is indicated. (D-F) PCA of each reef location with the sample period of each coral sample indicated. The sample periods are further labeled on (F) for clarification. The variation explained by each principal component is included on each axis.

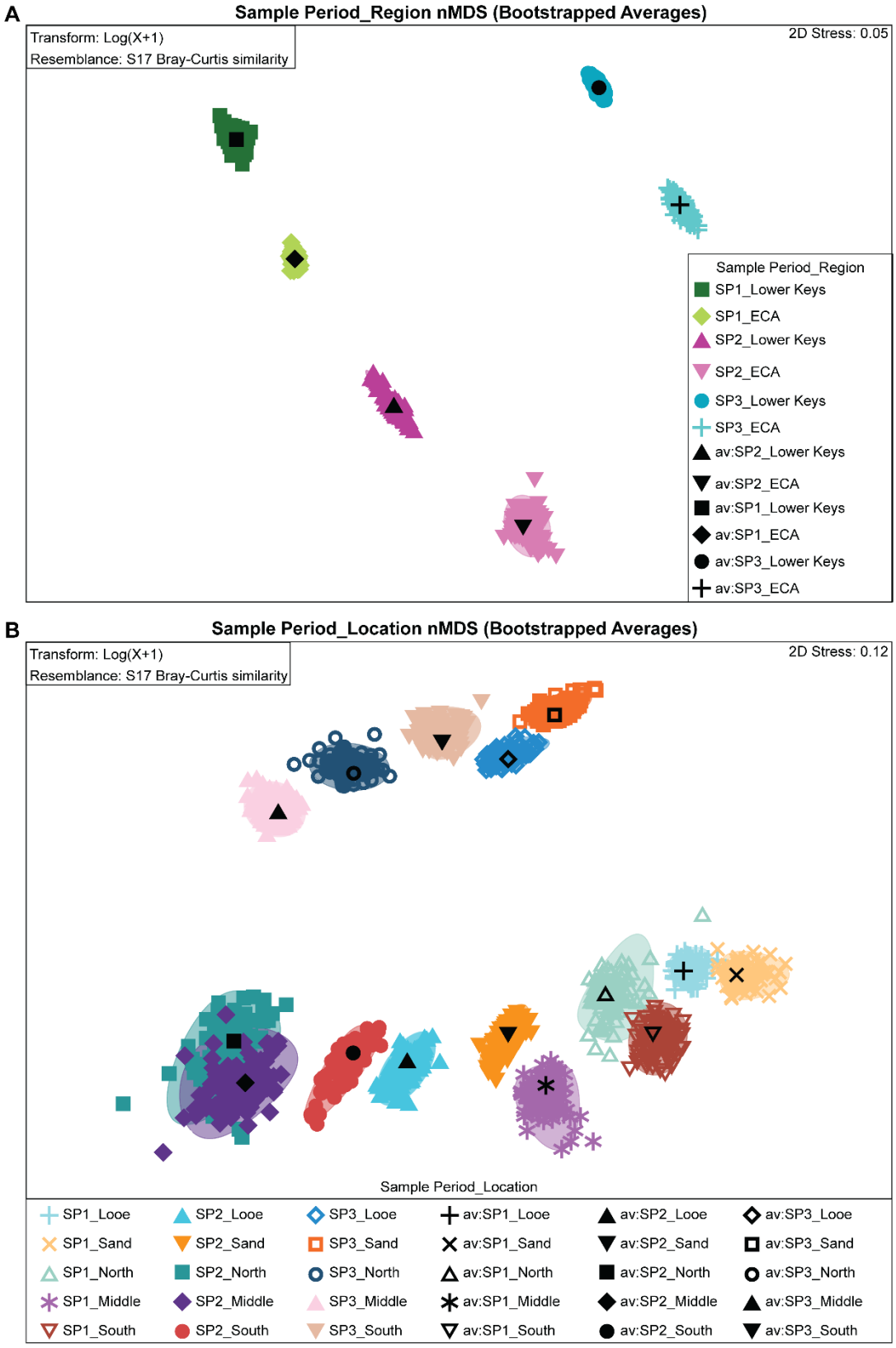

Figure 43. Bootstrapped nMDS Plot of Metabolome Data. The confidence interval, variance, and mean of each group based on bootstrapped averages are visualized through the (A) nMDS plot of the corals by sample period_region and (B) the nMDS plot of the corals by sample period_location.

Evaluation of Additional Discrete Metadata Categories

Additional classifications, related to SCTLD resilience or colony health status, were examined to determine which metabolites may be attributed to SCTLD resistance/resilience (Task 7 deliverable Table X2). Descriptors were created through results based on monitoring, histology results, proteomics analysis (credit to Janet Saunders for providing these groups), metabolomics considerations, and physical characteristics. Descriptors based on a tissue core analysis were considered to characterize the entire coral colony. PERMANOVA was run on all the relevant groups (e.g. for Dynamic Disease State, only SP3 corals have this designation) and statistically significant comparisons are reported in Task 7 deliverable Table X3. An UpSet Plot was generated to show the distribution of these metabolite features across the significant comparisons (Figure 44). The largest intersection consisted of several disease descriptors in SP1_Sand, which is explained by the similarity of groupings in several disease descriptors. There is some environmental specificity in the features that contribute to the group differences as the next largest intersections are unique to the sample period_location. The subsequent largest intersections show overlap between reef locations from the KJCAP, generally within the same sample period. The subsequent largest intersections show overlap between reef locations from the KJCAP, generally within the same sample period. There was no single feature detected in all intersections.

Similarity percentage (SIMPER) was run to quantify the contribution of metabolite features to the dissimilarity between the significant comparisons[8], with a cutoff of 10% cumulative contribution. CANOPUS was used to predict the natural products class pathway for the features selected through SIMPER, where predictions were filtered for a probability greater than 0.8. The majority of the features that differentiated statistically significant comparisons were predicted as fatty acids (Figure 44A). Generally, more features as predicted as fatty acids in the resistant (or less severe) phenotype compared to the more severe phenotype (Figure 44B). Annotations include betaine lipids, acylcarnitines, phosphocholines, and peptidic-like natural products (partially annotated). As metabolite function is dictated by chemical structure, it will be necessary to annotate the metabolites confirmed as fatty acids to determine which fatty acids are present. We have partitioned the whole coral metabolome extracts into organic solvents and acquired LC-MS/MS data on the ethyl acetate partitions. The data acquired on these ethyl acetate partitions will enable us to increase identifications of metabolites from these coral holobionts, particularly the less polar portion (which fatty acids tend to be) of the metabolome.

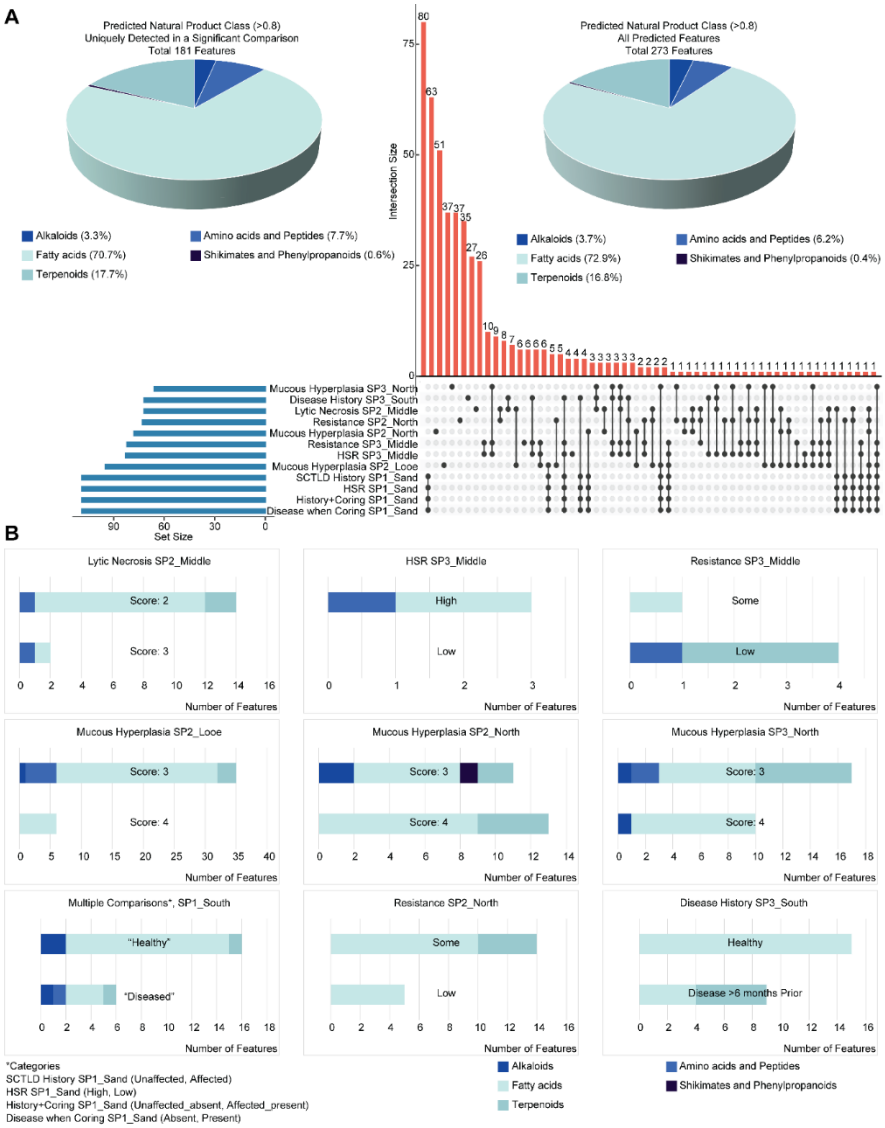

C

Score	0	1	2	3	4
Lytic necrosis	No lytic lesions in section	Rare, small area(s) of lytic necrosis within gastrodermis and not crossing body wall	Lesion that crosses body wall and/or small but multiple areas of lysis	Larger, more common lesions that cross body wall and/or extend across the gastrovascular space	Large, multiple areas of lytic necrosis with loss of gastrodermis and/or body wall
Mucous Hyperplasia	Not hypertrophic, no increase	Mild hypertrophy	Moderate hypertrophy, mucous release	Marked hypertrophy, some ruptured and necrotic mucocytes	Extensively hypertrophic and ruptured mucocytes, poor tissue integrity

Reproduced from Walker *et al*, 2023.

Figure 44. Metabolite Features Identified Through SIMPER Analysis. (A) UpSet Plot showing the distribution of metabolite features that contribute to 10% of the variance of each comparison group that was found statistically different through PERMANOVA ($p<0.05$). The number above each bar represents the number of features in that intersection. "Set Size" denotes the total number of features detected in comparison group. The predicted natural product pathway (probability > 0.8) using CANOPUS for 273 of the 488 features identified through SIMPER t group is included (pie chart, right). The features detected in the SP1_Sand groups are considered a unique intersection since the makeup of the groups compared within these categories is identical. Natural product pathway predictions for the 181 features that comprise the unique intersections are indicated (pie chart, left). The percentages indicate how many of the features were predicted as that pathway. (B) Shows the directionality for the features with a predicted natural product class (probability > 0.8) for each group. The healthy (or comparatively healthier) condition is listed above the diseased (or comparatively diseased) condition in each group. (C) Definitions for Lytic Necrosis scores and Mucous Hyperplasia scores, reproduced from Walker et al 2023.[8]

Tocopherols

We have previously reported detection patterns of α-tocopherol analogues (vitamin E) where the saturation of the dominant analogues corresponded to the health state of the sampled coral tissue.[9, 10] Vitamin E analogues are antioxidants that play a role in regulating lipid oxidation and may be responsible for preventing apoptosis.[11] Thus, we searched for the presence of tocopherols in this dataset and annotated several analogues based on our previous annotations,[9] FBMN, MassQL, and literature[12] (Task 7 deliverable Table X5). These include the monounsaturated α- and β/γ-tocomonoenols, hydroxy-α-tocopherol, and α-tocopherolquinone derivatives (Figure 45). An analytical standard was used to confirm MS2 and retention time to support the annotation of α-tocopherolquinone for feature 447.383_20.3 min. No feature annotated as a tocopherol analogue was present in the SIMPER output; therefore, of the SCTLD-associated categories we have queried, the tocopherols don't contribute towards the variance between statistically different groups. Detection of α-tocopherolquinone in healthy *O. faveolata* tissue may be indicative of a commonly utilized biochemical pathway to prevent apoptosis in response to stressors. The presence of these molecules in healthy tissue may also suggest frontloading, in which the corals are dedicating metabolic resources to chemical defenses.

Since vitamin E analogs do not drive variance between *O. faveolata* colonies with varying SCTLD-affectedness where metabolites were extracted from healthy tissue, we queried whether the analogues differed based on sample period_location groups. A heatmap generated on the log transformed abundances revealed ubiquitous detection of α-tocopherolquinone as the most dominant annotated analogue (Figure 45A). In SP1, the North and South KJCAP are most similar to each other. During SP2 the North and Middle KJCAP reef regions have the most similar analogue profile to each other, followed by the South KJCAP. In SP3, North and Middle KJCAP continue to share the greatest similarity in their profiles. There are no other obvious trends attributable to sample period_location. Kruskal Wallis with Dunn's Post Test ($p<0.05$, with Benjamin-Hochberg correction) was conducted to determine whether statistically significant differences existed between the sample period_location groups. All but two features were found significant (Task 7 deliverable Table X6), with analogues differing within and between the sample period_location groups without any clear detection pattern, except the feature at 415.357_19.7 min (annotated as β/γ-tocomonoenol) that is detected in Middle KJCAP in all sample periods. (Figure 45B). This may indicate that the vitamin E pathway in corals is readily active, dynamic, and responsive to environment specific stressors. While we do not detect α-tocopherol in this study, the abundance of α-tocopherolquinone (the proposed activated form[11] decreases from SP1 ('summer') to SP2 ('fall'). This suggests as reef temperatures decrease, the activated form of α-tocopherol also decreases. It is also interesting to note that in SP2 the fewest number of comparisons of tocopherol analogues were statistically differentiating. This observation suggests that the corals pre- (KJCAP) and post- (Lower Keys) spawning dedicate more metabolic resources towards reproduction rather than chemical defenses. We can conclude from this study that in healthy coral tissue, the mono/unsaturated tocopherol analogues, including α-tocopherolquinone, are dominant regardless of the SCTLD status of the rest of the colony.

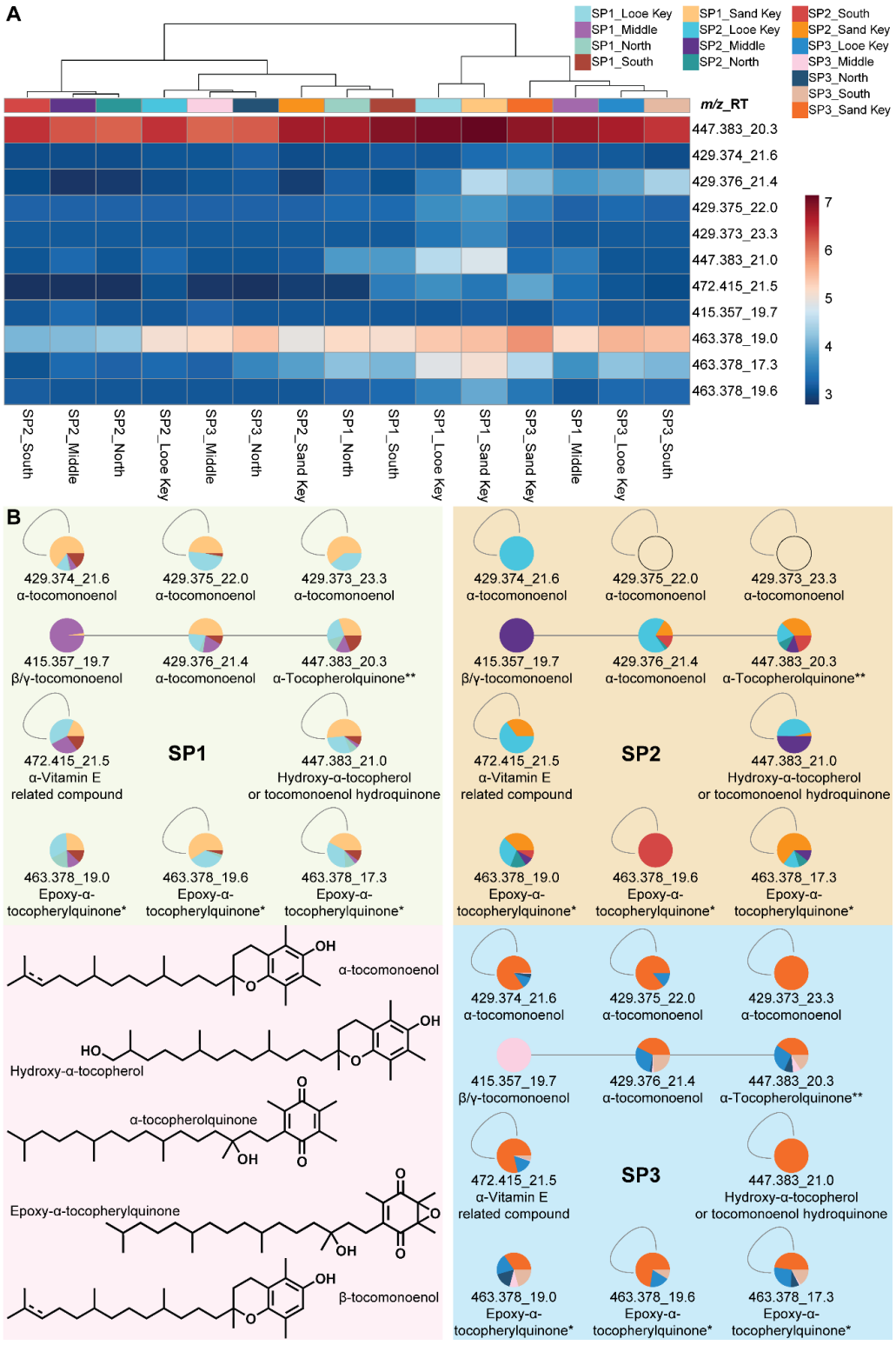

Figure 45. Tocopherols. (A) The heatmap of the log transformed abundances averaged for each sample period_location is compared for all features annotated as tocopherol analogues in this study. (B) Each metabolite feature annotated a tocopherol derivative is represented by a node showing the detected abundance in each reef location (see (A) for key). Each sample period is represented separately. The nodes are labeled with the m/z_RT and the putative annotation. * and ** indicates that this feature may be an isomeric species of the proposed annotation. The chemical structures of a subset of the annotated tocopherol derivatives is also included.

Acylcarnitines

Several metabolite features identified in the SIMPER analysis were annotated as acylcarnitines (Figure 46). We have previously reported acylcarnitines differentially detected between healthy coral species from the Dry Tortugas National Park, FL.[10] Acylcarnitines are usually synthesized by the host, and were previously not detected in metabolome extracts of coral-derived Symbiodiniaceae.[10] Feature 400.342_14.8 min was a GNPS library match to palmitoylcarnitine (CAR 16:0). Many features were identified as acylcarnitines containing fatty acid esters of hydroxy fatty acids (FAHFAs),[10] with characteristic acylcarnitine fragment peaks[13, 14] at m/z 85.028 and 144.102 supporting the annotation. We used the output of the FBMN to propagate annotations. The general detection pattern of the differentiating acylcarnitines, with a few exceptions, is higher intensity in corals with lower scores (corresponding to a less severe phenotype) in the mucous hyperplasia and lytic necrosis analysis (provided by Aine Hawthorne.[15] The majority of the differentiating acylcarnitines were annotated as FAHFA-acylcarnitines with three exceptions; CAR 16:0, CAR 18:3, and CAR 22:4. It should also be noted that this metabolite class differentiated SCTLD-based comparisons across sample period_ locations, with some analogues such as CAR 14:1-(O-18:0) differentiating at several sample period_locations. The general trend is that the acylcarnitines are detected at higher intensity in the healthier or less severe phenotypes within the comparative group (Figure 46). There are a few exceptions, where the detection appears almost equal (for SP1_Sand, SP3_Middle Histology Supported Resilience, and CAR 16:0 for SP2_Looe). Since these FAHFA-acylcarnitines differentiated healthy tissue on corals with various SCTLD-based classifications, and are more abundant in corals with a less severe (less necrotic) phenotype, they may be indicative of healthy functioning tissue that can readily and efficiently regulate cellular processes. The decrease in detection may indicate loss of regulatory functions, declined cellular processes and/or cell death. Investigations into the FAHFA-acylcarnitine presence in SCTLD-affected tissue and potential flux as a result of SCTLD exposure must be conducted to provide further insight into the function(s) of these molecules Thus, we will extensively annotate this metabolite class using the metabolome data acquired on EtOAc partitions of the whole coral metabolomes, as we can capture a broader set of acylcarnitines and generate a more extensive description of the detection pattern of this chemical class.

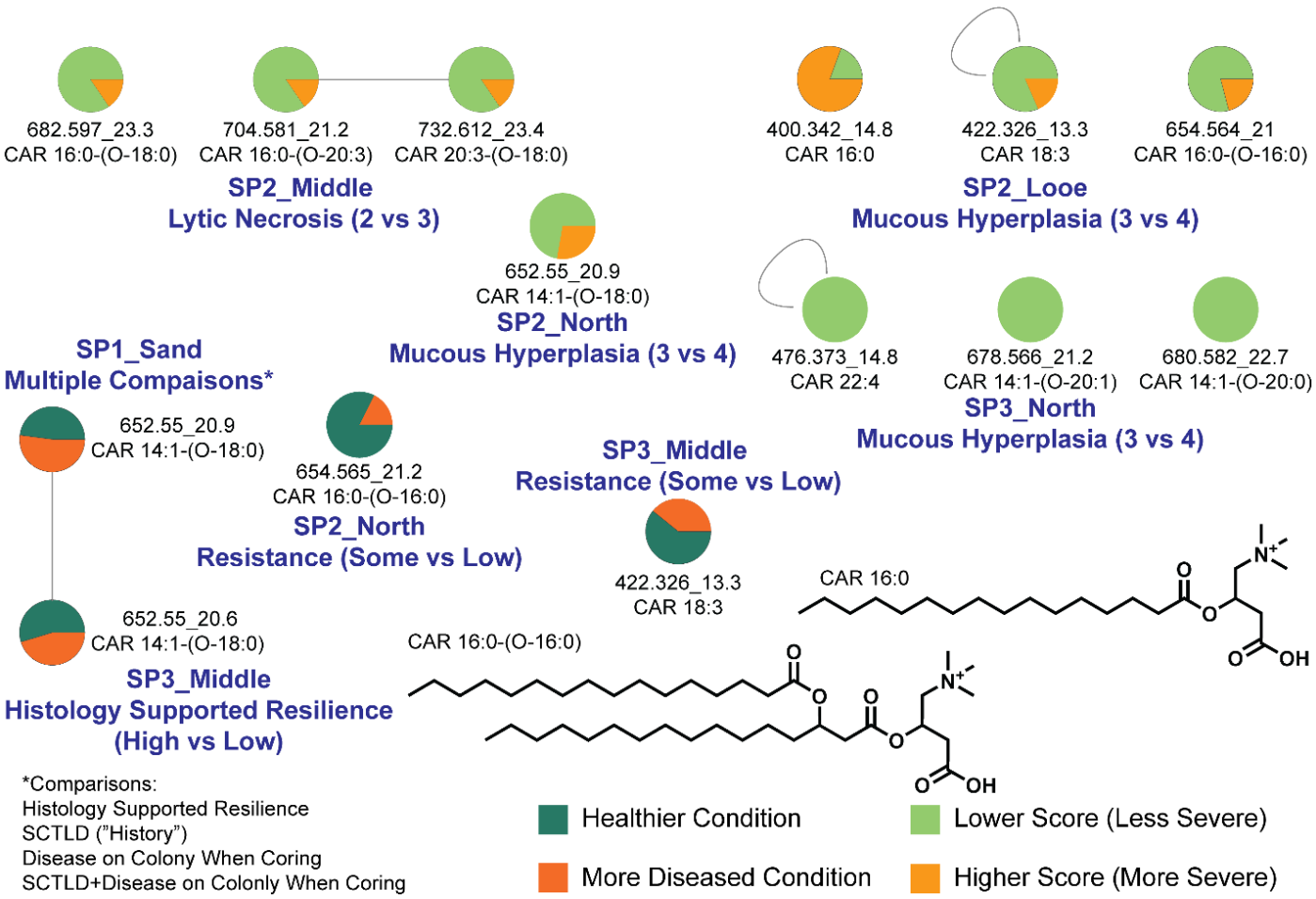

Figure 46. Acylcarnitines driving variation between SCTLD-based comparisons. Each metabolite feature annotated as an acylcarnitine is represented by a node showing abundance in each group. The nodes are labeled with the corresponding m/z_RT (min) and annotation, and organized by the sample period_location in which they were identified as differentiating based on SIMPER analysis. Some features (ex. 652.55_20.9 min) were identified in several sample period_location comparisons. The scores are included for the histology-based categories for reference. Representative structures of palmitoylcarnitine (CAR 16:0) and an acylcarnitine containing a fatty acid ester of hydroxy fatty acid (CAR 16:0-(O-16:0)) are included.

Conclusion: An untargeted metabolomics workflow to profile the metabolomes from healthy tissue of 261 *O. faveolata* with varied SCTLD susceptibility across three sample periods and five reef locations. The environmental signal, attributable to the sample period and reef location, evidently drove metabolome variation between the samples as shown in the unsupervised statistical analyses. Opportunistic metabolome analyses of naturally occurring genetic clones, different genomic lineages, and corals affected by Fast Lesion Progression were enabled by the analysis of RRC experts. Additionally, the RRC analyses provided several SCTLD-based categorizations that we tested for metabolome differences. Metabolites that underlay variation of statistically different groups within these comparisons (as identified by SIMPER and PERMANOVA, respectively) included

acylcarnitines, betaine lipids, peptidic-like molecules, and fatty acids. Analysis of tocopherol analogues detected in this study revealed a ubiquitous detection of mono- and saturated analogues of α-tocopherol, while no α-tocotrienol derivatives were detected in the metabolome extracts. Thus, regardless of the SCTLD disease state of the rest of the colony, the dominant tocopherol analogues in healthy tissue are mono/saturated. A time course study will resolve at what point in SCTLD progression the dominant analogues switch to unsaturated derivatives.

There are several additional avenues of inquiry that can be pursued in this study. This includes extensive annotation of the acylcarnitines, betaine lipids, and other features identified through the SIMPER analysis. Structural confirmation of the FAHFA-acylcarnitines will be conducted through biosynthesis of an FAHFA analogue and subsequent LC-MS/MS analysis to match retention times and MS2 spectra. Additional metadata categories, such as symbiont density, can be considered in the metabolome analysis to determine if other factors underlie the captured metabolome variation. Additionally, a portion of the whole coral metabolome extract for each sample was partitioned in organic solvents (ethyl acetate and butanol) to increase the breadth of described metabolites and test bioactivity against coral pathogen *Vibrio coralliilyticus* OfT6-21.[16] The observed zones of inhibition were larger for the ethyl acetate partitions compared to the butanol partitions, thus metabolomics data was acquired on ethyl acetate partitions (n=270) with the assistance of the Mass Spectrometry Core at the Georgia Institute of Technology and is currently being analyzed. The analysis of this data will provide further insight into the biochemical processes of *O. faveolata* with varying SCTLD susceptibility and may help us understand why fatty acids were the largest predicted chemical class that drove differences between corals based on SCTLD-related categorizations.

References:

1. Dührkop, K.; Fleischauer, M.; Ludwig, M.; Aksenov, A. A.; Melnik, A. V.; Meusel, M.; Dorrestein, P. C.; Rousu, J.; Böcker, S. SIRIUS 4: a rapid tool for turning tandem mass spectra into metabolite structure information. *Nature Methods* **2019**, *16* (4), 299-302. DOI: 10.1038/s41592-019-0344-8.

2. Jarmusch, A. K.; Aron, A. T.; Petras, D.; Phelan, V. V.; Bittremieux, W.; Acharya, D. D.; Ahmed, M. M. A.; Bauermeister, A.; Bertin, M. J.; Boudreau, P. D.; et al. A Universal Language for Finding Mass Spectrometry Data Patterns. *bioRxiv* **2022**, 2022.2008.2006.503000. DOI: 10.1101/2022.08.06.503000.

3. Nothias, L.-F.; Petras, D.; Schmid, R.; Dührkop, K.; Rainer, J.; Sarvepalli, A.; Protsyuk, I.; Ernst, M.; Tsugawa, H.; Fleischauer, M.; et al. Feature-based molecular networking in the GNPS analysis environment. *Nature Methods* **2020**, *17* (9), 905-908. DOI: 10.1038/s41592-020-0933-6.

4. Dührkop, K.; Shen, H.; Meusel, M.; Rousu, J.; Böcker, S. Searching molecular structure databases with tandem mass spectra using CSI:FingerID. *Proceedings of the National Academy of Sciences* **2015**, *112* (41), 12580-12585. DOI: doi:10.1073/pnas.1509788112.

5. Dührkop, K.; Nothias, L.-F.; Fleischauer, M.; Reher, R.; Ludwig, M.; Hoffmann, M. A.; Petras, D.; Gerwick, W. H.; Rousu, J.; Dorrestein, P. C.; et al. Systematic classification of unknown

metabolites using high-resolution fragmentation mass spectra. *Nature Biotechnology* **2021**, *39* (4), 462-471. DOI: 10.1038/s41587-020-0740-8.

6. Neely, K. *Observatons of rapidly progressing lesions on corals within the Florida Keys Natonal Marine Sanctuary: a Quicklook report*; Nova Southeastern University, 2023. https://www.agrra.org/wp-content/uploads/2023/03/FLP-Report_Neely_20230321.pdf.

7. Becker, C. C.; Weber, L.; Zgliczynski, B.; Sullivan, C.; Sandin, S.; Muller, E.; Clark, A. S.; Kido Soule, M. C.; Longnecker, K.; Kujawinski, E. B.; et al. Microorganisms and dissolved metabolites distinguish Florida's Coral Reef habitats. *PNAS Nexus* **2023**, *2* (9). DOI: 10.1093/pnasnexus/pgad287 (acccessed 3/22/2025).

8. CLARKE, K. R. Non-parametric multivariate analyses of changes in community structure. *Australian Journal of Ecology* **1993**, *18* (1), 117-143. DOI: https://doi.org/10.1111/j.1442-9993.1993.tb00438.x.

9. Deutsch, J. M.; Jaiyesimi, O. A.; Pitts, K. A.; Houk, J.; Ushijima, B.; Walker, B. K.; Paul, V. J.; Garg, N. Metabolomics of Healthy and Stony Coral Tissue Loss Disease Affected Montastraea cavernosa Corals. *Frontiers in Marine Science* **2021**, *8*. DOI: 10.3389/fmars.2021.714778.

10. Deutsch, J. D., A.; Jaiyesimi, O.; Foster, G.; Kindler, A.; Pitts, K.; Vekich, T.; Williams, G.;Walker, B.; Paul, V.; Garg, N. Metabolomic profiles of stony coral species from the Dry Tortugas National Park display inter-and intraspecific variation. **.submitted 2024**.

11. Hinman, A.; Holst, C. R.; Latham, J. C.; Bruegger, J. J.; Ulas, G.; McCusker, K. P.; Amagata, A.; Davis, D.; Hoff, K. G.; Kahn-Kirby, A. H.; et al. Vitamin E hydroquinone is an endogenous regulator of ferroptosis via redox control of 15-lipoxygenase. *PLOS ONE* **2018**, *13* (8), e0201369. DOI: 10.1371/journal.pone.0201369.

12. Terentis, A. C.; Thomas, S. R.; Burr, J. A.; Liebler, D. C.; Stocker, R. Vitamin E Oxidation in Human Atherosclerotic Lesions. *Circulation Research* **2002**, *90* (3), 333-339. DOI: doi:10.1161/hh0302.104454.

13. Yan, X.; Markey, S. P.; Marupaka, R.; Dong, Q.; Cooper, B. T.; Mirokhin, Y. A.; Wallace, W. E.; Stein, S. E. Mass Spectral Library of Acylcarnitines Derived from Human Urine. *Analytical Chemistry* **2020**, *92* (9), 6521-6528. DOI: 10.1021/acs.analchem.0c00129.

14. Vissing, C. R.; Dunø, M.; Wibrand, F.; Christensen, M.; Vissing, J. Hydroxylated Long-Chain Acylcarnitines are Biomarkers of Mitochondrial Myopathy. *The Journal of Clinical Endocrinology & Metabolism* **2019**, *104* (12), 5968-5976. DOI: 10.1210/jc.2019-00721 (acccessed 3/22/2025).

15. Walker, B. K.; Aeby, G. S.; Baker, A. C.; Buckley, S.; Garg, N.; Hawthorne, A.; Meyer, J.; Neely, K.; Noren, H.; Paul, V. J.; et al. *SCTLD Resistance Research Consortium Summary Report through May 2023*; Florida DEP, Miami, FL, 2023.

16. Ushijima, B.; Meyer, J. L.; Thompson, S.; Pitts, K.; Marusich, M. F.; Tittl, J.; Weatherup, E.; Reu, J.; Wetzell, R.; Aeby, G. S.; et al. Disease Diagnostics and Potential Coinfections by Vibrio coralliilyticus During an Ongoing Coral Disease Outbreak in Florida. *Frontiers in Microbiology* **2020**, *11*, Original Research. DOI: 10.3389/fmicb.2020.569354.

3.10. Task 7b: Co-relation of metabolomics data with microbiome, transcriptomics, proteomics, and bioactivity data (Garg, Williams, Walker)

Goal: co-relate the metabolomics data with results from the microbiome, transcriptomics, proteomics, and bioactivity analyses.

Significant findings: Variations in 'Bioactivity' (two predictor model) explained between 43.3% and 47.9% of the underlying variation in the RRC metabolome data depending on the data transformation applied to the multivariate metabolome data (Table 12).

Results: The two 'Bioactivity' predictors correlated differently with the metabolomics data. EtOAc steadily increased from SP1 to SP2 to SP3, separating out metabolomic changes between Sample Period 1 and Sample Periods 2 and 3 along the first db-RDA axis (Figure 47, top). In contrast, BuOH showed the highest increase in Sample Period 2, separating out metabolomic changes between Sample Periods 1 and 3, and Sample Period 2 along the second db-RDA axis (Figure 47, bottom).

Table 12. Model summaries testing for correlations between two measures of 'Bioactivity' (EtOAc and BuOH+695 Treatment-Control radius mean) and changes in coral metabolomics across Sample Periods (n=3, Sample Periods 1-3) and Locations (n=5, North ECA, Middle ECA, South ECA, Looe Key, Sand Key). % Expl., percentage variation in the metabolomic data explained by each predictor and their cumulative percentage explained (Cumul. %). The model was run on untransformed, 4th-root, and presence/absence transformed metabolomics data.

Response	Predictor	AICc	Pseudo-F	P-value	% Expl.	Cumul. %
Untransformed	EtOAc	92.6	4.287	0.009	24.8	
	BuOH	91.6	3.923	0.029	18.5	43.3
4th root	EtOAc	84.9	5.229	0.002	28.7	
	BuOH	83.4	4.441	0.011	19.3	47.9
Presence/Absence	EtOAc	69.1	4.869	0.002	27.2	
	BuOH	68.2	3.694	0.009	17.1	44.3

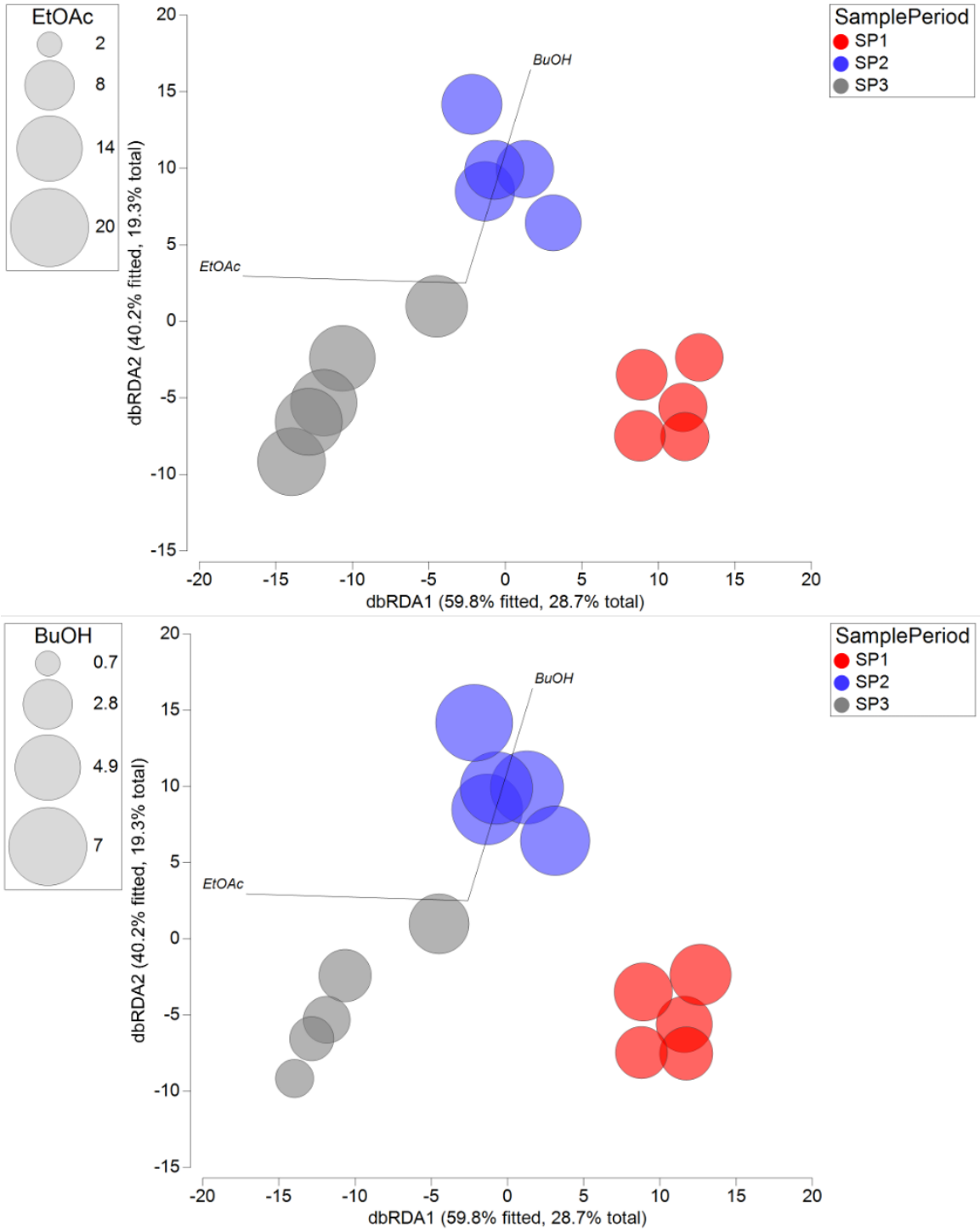

Figure 47. Relative similarity in metabolomic profiles across the RRC corals in relation to gradients in 'Bioactivity' (Top: EtOAc, Bottom: BuOH), averaged by all unique combinations of sample period and location (n=15 groups) and color-coded by Sample Period. The directional correlation of each predictor across the two db-RDA axes are shown by the vectors. Bioactivity values (in mm) are shown using a bubble plot. The fitted and total percentage variation in the metabolomic data explained by each db-RDA axis is shown in parentheses.

3.11. **Task 7c: Analysis of new Symbiodiniaceae variability metabolomics data (Garg)**

Goal: annotate metabolite features detected within the samples collected from Task 6B to understand the underlying chemical communication in which the Symbiodiniaceae participate.

Significant findings: Metabolomics analysis unveils that Lyso- 1,2-diacylglyceryl-3-O-carboxy-(hydroxymethyl)-choline (DGCC) are responsible for driving differences in the coral metabolome based on algal composition.

Results and Discussion:

A large scale -omics study can provide a holistic view of the biochemical processes that are occurring within the coral organism, thus Task 7c aims to combine metabolomic and genomic data to understand the chemical mechanisms occurring within each sample based on the dominate algal symbiont. Samples collected from various ECA and Florida Key reef locations were classified of predominantly comprising of *Cladocopium*, *Durusdinium*, *Breviolum*, or a combination of two genera.

Statistical analysis reveals several Lyso-DGCCs driving differences between algal symbiont colonization. DGCCs are a class of betaine lipids that have been detected in symbiotic dinoflagellates of the family *Symbiodiniaceae* and previous studies have correlated the presence of lyso-lipids with coral bleaching (Roach et al., 2021). Lyso-DGCCs are expressed by bacteria exposed warmer temperature and play a role in the renaturation of proteins (Rosset et al., 2019). Therefore, the accumulation of this metabolite maybe involved in a mechanism responsible for heat stress tolerance (Rosset et al., 2019). Additionally, this class of molecules have previously been reported as more abundant in *Durusdinium* than another genus (Rosset et al., 2019), which provides rational of why this molecule class is driving differences between the dominate *Symbiodiniaceae* colonization.

Roach, T.N.F., Dilworth, J., H., C.M. et al. Metabolomic signatures of coral bleaching history. Nat Ecol Evol 5, 495–503 (2021). https://doi.org/10.1038/s41559-020-01388-07

Rosset, S., Koster, G., Brandsma, J. *et al.* Lipidome analysis of *Symbiodiniaceae* reveals possible mechanisms of heat stress tolerance in reef coral symbionts. *Coral Reefs* **38**, 1241–1253 (2019). https://doi.org/10.1007/s00338-019-01865-x

3.12. **Task 7d: Lipidomics data acquisition and analysis (Garg)**

Goal: Analyze the organic extracts generated and further fractionated by partitioning the extract between EtOAc and water in the laboratory of Valerie Paul on samples previously collected for this project using the institute's Thermo Fisher Scientific Orbitrap ID-X Tribrid mass spectrometer coupled to an ultra-high-performance liquid chromatograph to obtain a comprehensive lipidome of the EtOAc partitions of this coral species.

Significant findings: Preliminary lipidome analysis of KJCAP and Florida Key corals reveals the detection of several monogalactosyldiacylglycerol (MGDG) and digalactosyldiacylglycerol (DGDG) lipids. These lipids are a major component of the symbiont thylakoid membrane and higher unsaturation of the fatty acyl tails is indicative of higher thermal tolerance. Additional analysis is needed to determine statistical significance of these metabolite features across group categories.

Preliminary Results: The chemical signature of *Orbicella faveolata* collected from various KJCAP and Florida Key reef locations is currently being accessed to understand the variability of resilient coral. Samples were extracted using a 2:2:1 mixture of ethyl acetate, methanol, and water. Partitions were tested for antimicrobial activity against the known coral pathogen, *Vibrio coralliilyticus* OfT6-2170. The partition found to have the greatest bioactivity against the pathogen was the EtOAc partition, which was then selected for lipidomic analysis.

Based on past studies, the presence of galactolipids has been correlated with heat tolerant coral. Specifically, the galactolipid ratio of the monogalactosyldiacylglycerol (MGDG) to digalactosyldiacylglycerol (DGDG) has been shown to change during periods of stress in resilient coral. The MGDG/DGDG ratio is critical for proper photosynthetic and physiological function of thylakoid membranes in Symbiodiniaceae. Thus, analyzing the MGDG/DGDG presence, as well as the saturation of their acyl tails, in the samples collected for this study will likely provide insight to the chemical resilience of thermotolerant coral.

Preliminary analysis of these features has led to the putative annotation of 51 species of MGDG and DGDG lipids. Once an exhaustive library of these features has been annotated exploration of detection trends between group categories (sampling period, location, resistance) will be attempted to determine their effect on galactolipid detection.

3.13. **Task 8a: Characterize functional genes of microbial communities (Meyer, Cauvin, Becker)**

Goal: continue bioinformatic analysis of these metagenomes among *O. faveolata* colonies with varying resistance to SCTLD and work with other project members to integrate the analysis and interpretation of different datasets for a holobiont-wide view of the dynamics of disease resistance.

Significant findings: Bacterial functions in *O. faveolata* colonies in both regions varied with both the presence of disease and with Symbiodiniaceae composition. Location within the KJCAP also explained variation in bacterial functions. Although the bacterial functions responded to disease state in both regions, responses differed between the Florida Keys sites where half the colonies had active disease at the time of sampling and the KJCAP sites where only two of 45 colonies had active disease at the time of sampling.

Results:
Because disease presentation varied so strongly between the Lower Keys and the KJCAP, we analyzed bacterial functions within regions.

Florida Keys (SCTLD present for 2-3 years): At the time of sampling for bacterial metagenomes (May/June 2021), 21 colonies were unaffected by SCTLD, and 20 colonies were diseased. Overall, variability in the composition of bacterial functional genes was explained by both disease at sampling (8% of variation) and Symbiodiniaceae composition (33% of variation) (Figure 48). Bacterial communities in colonies with active disease at the time of sampling showed higher variability in their functional gene content than colonies without disease (Figure 48b). This means that the bacterial communities in apparently healthy tissue of diseased colonies showed signs of disturbance even though the disease lesion was not sampled. In addition, variability in the functional composition of bacterial communities was explained by the Symbiodiniaceae composition. When the Symbiodiniaceae community was more variable, the bacterial community functions were also more variable (Figure 48d).

To examine what genes drove the differences in bacterial functions between unaffected and diseased colonies, we tested for differentially abundant genes. A total of 327 genes were differential abundant in healthy tissues between unaffected and diseased colonies, of which 312 genes were enriched in corals that were unaffected by SCTLD at the time of sampling. In contrast, only 15 genes were enriched in apparently healthy tissue of diseased colonies. This is likely due to the higher variability of bacterial functional genes in diseased colonies, where bacterial functions changed stochastically (each colony changed in its own way), thus fewer shared changes were detected. Bacterial genes enriched in unaffected colonies included genes for the biosynthesis of multiple antibiotics that may serve as defense against bacterial pathogens.

KJCAP (SCTLD present for 7 years): In the KJCAP, only two colonies showed signs of active disease at the time of sampling, therefore we tested bacterial functional variation based on whether the colony was diseased prior to sampling or not. At the time of sampling for bacterial metagenomes (June 2021), 16 colonies had no previous signs of disease, and 29 colonies had SCTLD prior to sampling. The average time since the last observed lesion

was 12 months for colonies with SCTLD prior to sampling. Overall, variability in the composition of bacterial functional genes was explained by whether the colony was diseased prior to sampling or not (5% of variation), location within the KJCAP (16% of variation), and Symbiodiniaceae composition (36% of variation) (Figure 49). Bacterial functional gene composition in colonies with only *Breviolum* symbionts or predominantly *Breviolum* with *Cladocopium* were more variable than colonies that also contained *Durusdinium* (Figure 50A). Bacterial functions in colonies with no prior disease were more variable than in colonies that had SCTLD prior to sampling (Figure 50B).

To examine what genes drove the differences in bacterial functions between colonies with or without SCTLD prior to sampling, we tested for differentially abundant genes. A total of 85 genes were differential abundant in healthy tissues between colonies with or without SCTLD prior to sampling, of which 72 genes were enriched in colonies with prior disease. In contrast, only 13 genes were enriched in colonies without prior disease. This is likely due to the higher variability of bacterial functional genes in colonies without prior disease, where bacterial functions changed stochastically (each colony changed in its own way), thus fewer shared changes were detected. Many of the differentially abundant genes had unknown functions and while genes for the biosynthesis of antibiotics were present, they were not statistically different based on prior disease.

Discussion: These results demonstrate that bacterial functions change when the host is diseased and with changes in Symbiodiniaceae community composition. In the KJCAP, bacterial functions were also associated with location suggesting that the bacterial community responds to local environmental differences. However, bacterial responses to disease differed between the Florida Keys sites where SCTLD had been present two to three years at the time of sampling and the KJCAP sites where SCTLD had been present for seven years. In both regions, disease explained a similar amount of variation among bacterial functions in apparently healthy tissue, but in the Florida Keys the presence of active disease lesions on the coral colony coincided with more variable bacterial functions while in the KJCAP colonies without prior disease had more variable bacterial functions. Together, these results suggest that while SCTLD disrupts bacterial functions in apparently healthy tissue on actively diseased colonies, this effect is temporary and is outweighed by the influence of the Symbiodiniaceae composition or local environmental conditions.

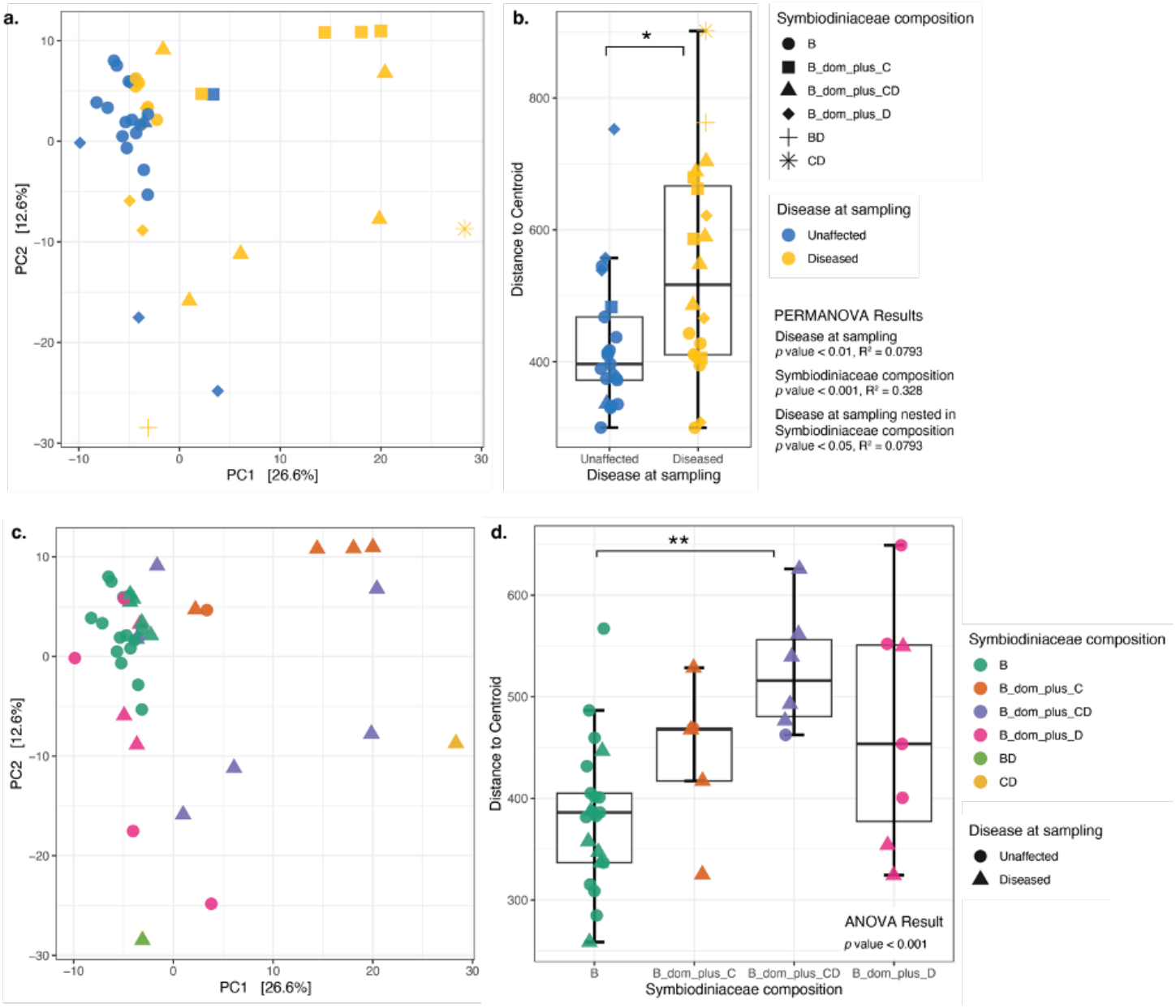

Figure 48. Bacterial functional gene composition varied with both Symbiodiniaceae composition and disease state (panels a and c). Bacterial functions in colonies that were diseased at the time of sampling were more variable (panel b), suggesting disturbance in the microbiome. Bacterial functions in colonies with only Breviolum symbionts were less variable, while colonies with more diverse Symbiodiniaceae composition were more variable (panel d). B = Breviolum, C = Cladocopium, and D = Durusdinium.

Figure 49. Comparison of the bacterial functional gene composition in *O. faveolata* based on their disease history, Symbiodiniaceae composition, and location within the Southeast Florida Ecosystem Conservation Area. B = *Breviolum*, C = *Cladocopium*, and D = *Durusdinium*, N = North, M = Middle, S = South.

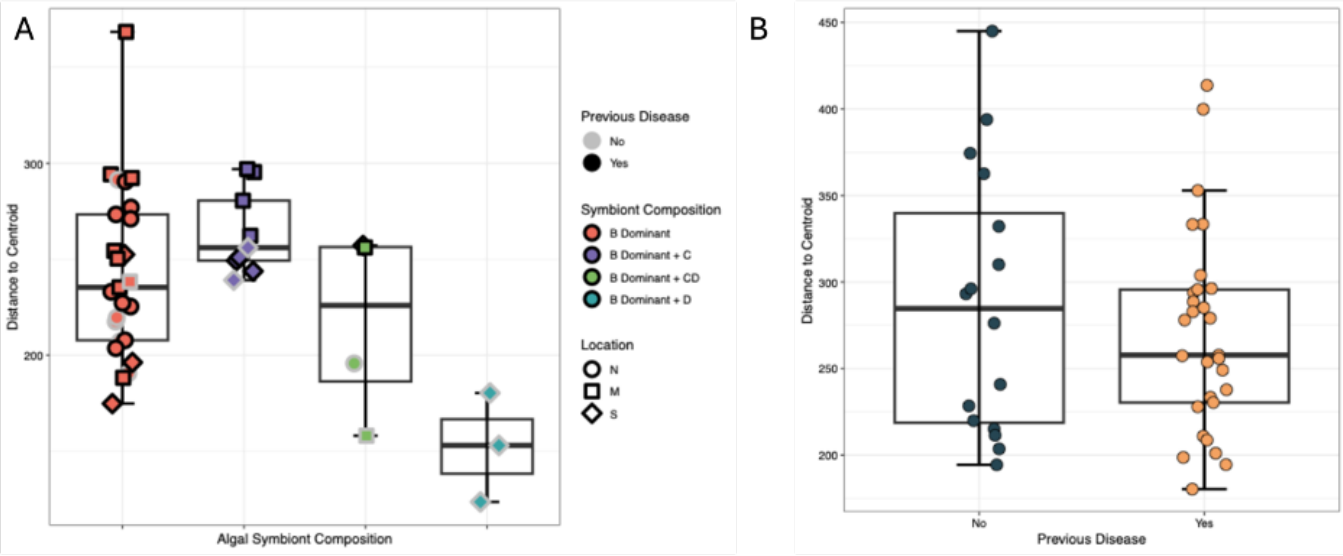

Figure 50. Bacterial functional gene composition varied with both Symbiodiniaceae composition and disease state. Bacterial functions in colonies with only *Breviolum* symbionts or predominantly *Breviolum* with *Cladocopium* were more variable than colonies that also contained *Durusdinium* (panel A). B = *Breviolum*, C = *Cladocopium*, and D = *Durusdinium*. Bacterial functions in colonies with no prior disease were more variable than in colonies that had SCTLD prior to sampling (panel B).

3.14. **Task 8b: Microbiomes (Klein, Meyer, and Voss)**

Goal: use already extracted DNA to quantitatively characterize and track *O. faveolata* microbiomes for each coral and all three sample periods.

Significant findings: Microbial communities vary through time, space, and lineage. Shifts in the corals' microbiomes may serve as early indicators of disease susceptibility or resilience in *O. faveolata*

Results: Dr. Josh Voss's team at the Harbor Branch Oceanographic Institute has recently begun exploring patterns in the RRC microbial sequencing data between healthy-looking *Orbicella faveolata* samples collected in May/ June 2021, Aug/Sept 2021, and Feb/March 2022 on the same colonies across Florida's Coral Reef. Scratching the surface of this large dataset reveals that microbial community structure was significantly influenced by the time of sample collection, sample location, and genetic lineage, along with their interactions. There were 37 Bacterial Orders observed across all samples, with no bacterial order unique to Timepoint, Lineage, or Disease status. Figure 51 illustrates the variation in microbial orders across sample periods (T1, T2, T3).

74 orders exhibited significant differential abundance; 21 had increased abundance with SCTLD affected, 53 had deceased abundance with SCTLD affected (Figure 52). Two orders had both positive and negative log fold change suggesting that taxa within these orders have differing interactions with disease status. Research continues on this extensive dataset including finding associations between these data and the data gathered by the other teams (e.g. transcriptome, proteome, metabolome, chemical defenses, environmental factors, tissue recovery rates, etc).

Discussion: These preliminary results suggest that shifts in the corals' microbiomes could serve as early indicators of disease susceptibility or resilience in *O. faveolata*. The significant effects of time, space, and genetic lineage on microbial community structure highlights the dynamic nature of coral-associated microbial communities and their potential role in coral health. Overall, 74 bacterial orders exhibited differential abundance based on disease status, with some orders increasing and others decreasing in conjunction with SCTLD activity. It is possible that specific microbial signatures may be predictive of disease onset or progression, however a larger data set or discrete experimental SCTLD infections would be needed to further evaluate this hypothesis. Further integration of microbial data with other omics datasets (e.g., transcriptomics, metabolomics) and coral recovery metrics may allow for the development of diagnostic tools to identify corals at greater risk of disease before visible symptoms appear, offering new avenues for proactive reef management and intervention strategies.

Figure 51. Bar plots depicting the relative abundance of microbial orders in SCTLD Affected samples. The plot is faceted by Timepoint, showing variations in microbial community composition. The x-axis represents different samples, and the y-axis shows the relative abundance of orders, stacked to represent the total abundance for each sample. The plot uses a custom color palette for order differentiation, with sample names on the x-axis rotated for clarity. There were no orders unique to a specific timepoint, disease status, or the intersection of the two.

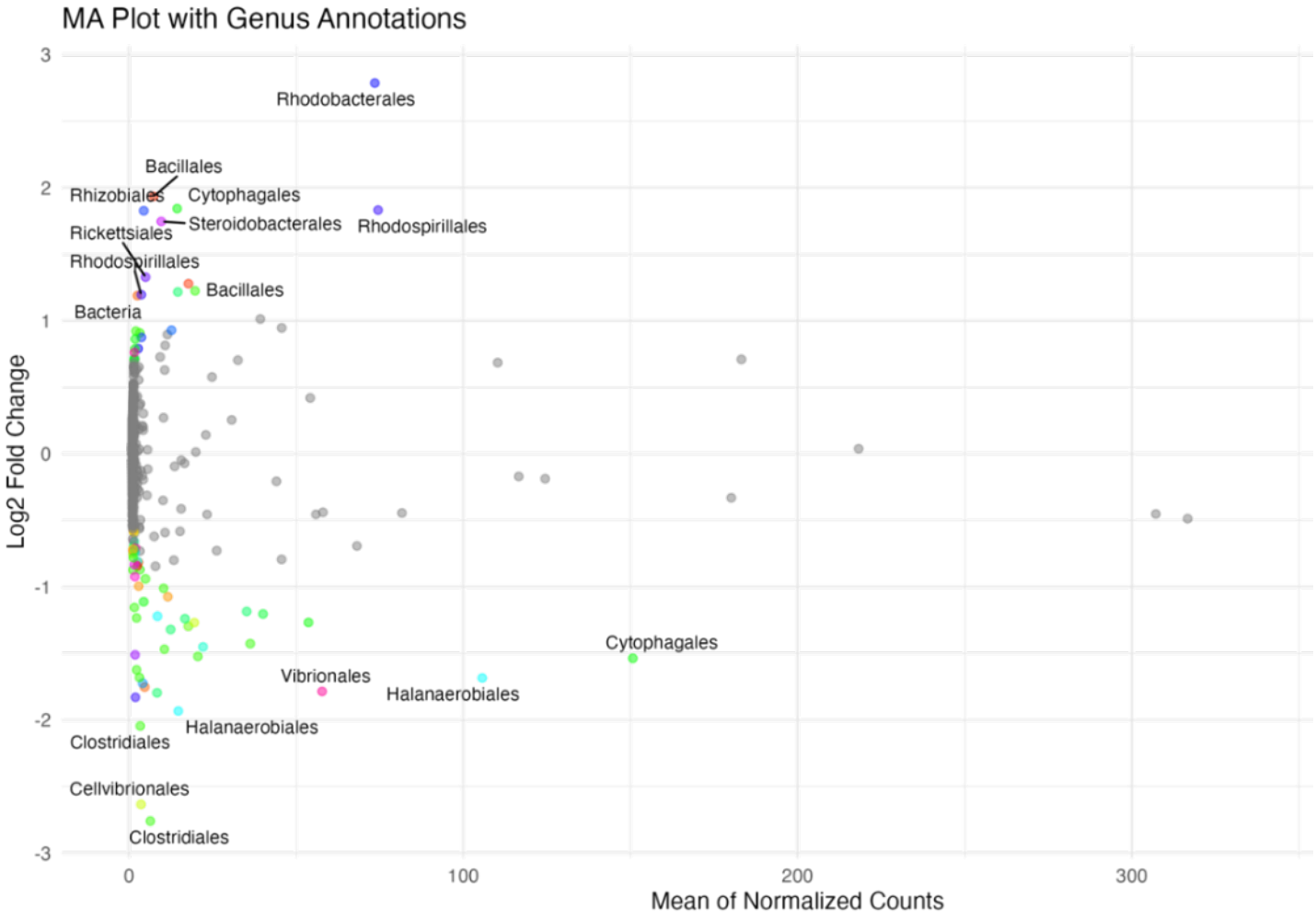

Figure 52. MA plot illustrates the differential abundance of microbial taxa with annotations for each order. The x-axis shows the mean of normalized counts, and the y-axis displays the log2 fold change between conditions. Points are colored by taxonomic order, with some orders labeled. Due to overlapping, not all orders are labeled. The plot is zoomed to visualize taxa with mean counts between 0 and 400.

3.15. **Task 9a – Summarizing Sample Period 3 RRC coral environmental drivers for machine learning models (Williams and Maynard)**

Goals: Incorporate the third RRC sampling period and build a series of statistical models to identify the proximate factors involved in driving differences between colony infection rates.

Significant findings: Environmental conditions (seawater temperature, inlet outflow, rainfall, wind) varied significantly during the three sampling periods. Sample period 1 (SP1) occurred during moderate inlet outflow (in the KJCAP), high rainfall, and moderate winds. Sample period 2 (SP2) saw peak seawater temperatures, moderate rainfall, and low wind speeds. Sample period 3 (SP3) experienced the lowest inlet outflow (in the KJCAP), lowest temperatures, minimal rainfall, and stronger seaward winds. Not surprisingly, all metrics of local human impacts were higher in the KJCAP than the Keys. Within the KJCAP, high intensity land use and population density appeared slightly higher in the North and Middle KJCAP than the South at the broadest scale, while septic tanks were slightly more abundant in the Middle KJCAP. Environmental conditions also varied across locations prior to each sampling period. Leading up to SP1, the North KJCAP showed the lowest seawater temperatures over both the short-term (7-days prior) and longer-term (90-days prior). During SP2, temperature differences across locations were minimal. Prior to SP3, Looe and Sand Key had lower temperatures over the shorter-term compared to the KJCAP, but the South KJCAP had the lowest temperatures over the longer-term. These patterns highlight the spatial and temporal complexity of environmental stressors, such as seawater temperature, that influence coral health. Rainfall patterns were similarly dynamic. Before SP1, the Middle and South KJCAP recorded higher rainfall levels than other locations over both the shorter- and longer-term. In SP2, rainfall distribution was highly variable, with no location experiencing consistently higher or lower amounts. By SP3, rainfall patterns stabilized, with the Middle and North KJCAP receiving the most rainfall. Wind conditions followed a more stable pattern, with the North and Middle KJCAP experiencing the highest winds across all sample periods, while Looe and Sand Key had the lowest winds. Incorporating the gradients in environmental conditions across the three sampling periods into predictive statistical models explained some variations in coral health. For SP1, models explained limited variation, with no significant predictors for polyp fecundity. However, longer-term exposure to extreme seawater temperatures emerged as a potential driver for lytic necrosis and zooxanthellae degeneration, warranting further research. In SP2, polyp fecundity was significantly correlated with local human population density, explaining nearly 40% of its variation. This finding suggests a potential link between anthropogenic stressors and coral reproductive health. SP3 models were weaker overall, with minimal predictive power across all coral health metrics.

Results:

Environmental conditions appeared quite unique across the three sample periods. Sample period 1 occurred during a period of moderate outflow from the inlet contributing areas (Figure 53A), during moderate seawater temperatures (Figure 53B), during some of the highest peaks in summed rainfall of any of the sample periods (Figure 53C), and during moderate wind speeds of a predominantly landward direction (Figure 54). Sample period 2 also occurred during moderate inlet outflow (although consistently higher from Government Cut) (Figure 53A), during peak seawater temperatures across the entire study

period (Figure 53B), moderate but temporally consistent levels of rainfall (Figure 53C), and moderate to low wind speeds of a predominantly landward direction (Figure 54). Sample period 3 occurred during the lowest inlet outflow of the three sample periods and some of the lowest over the entire study period (Figure 53A), when seawater temperatures were ~5°C lower than the other two sample periods (Figure 53B), during some of the lowest levels of rainfall (Figure 53C), and windier and more seaward blowing conditions than the other two sample periods (Figure 54). Not surprisingly, all metrics of local human impacts were higher in the KJCAP than the Keys (Figure 55). Within the KJCAP, high intensity land use and population density appeared slightly higher in the North and Middle KJCAP than the South at broadest scale, while septic tanks were slightly more abundant in the Middle KJCAP (Figure 55).

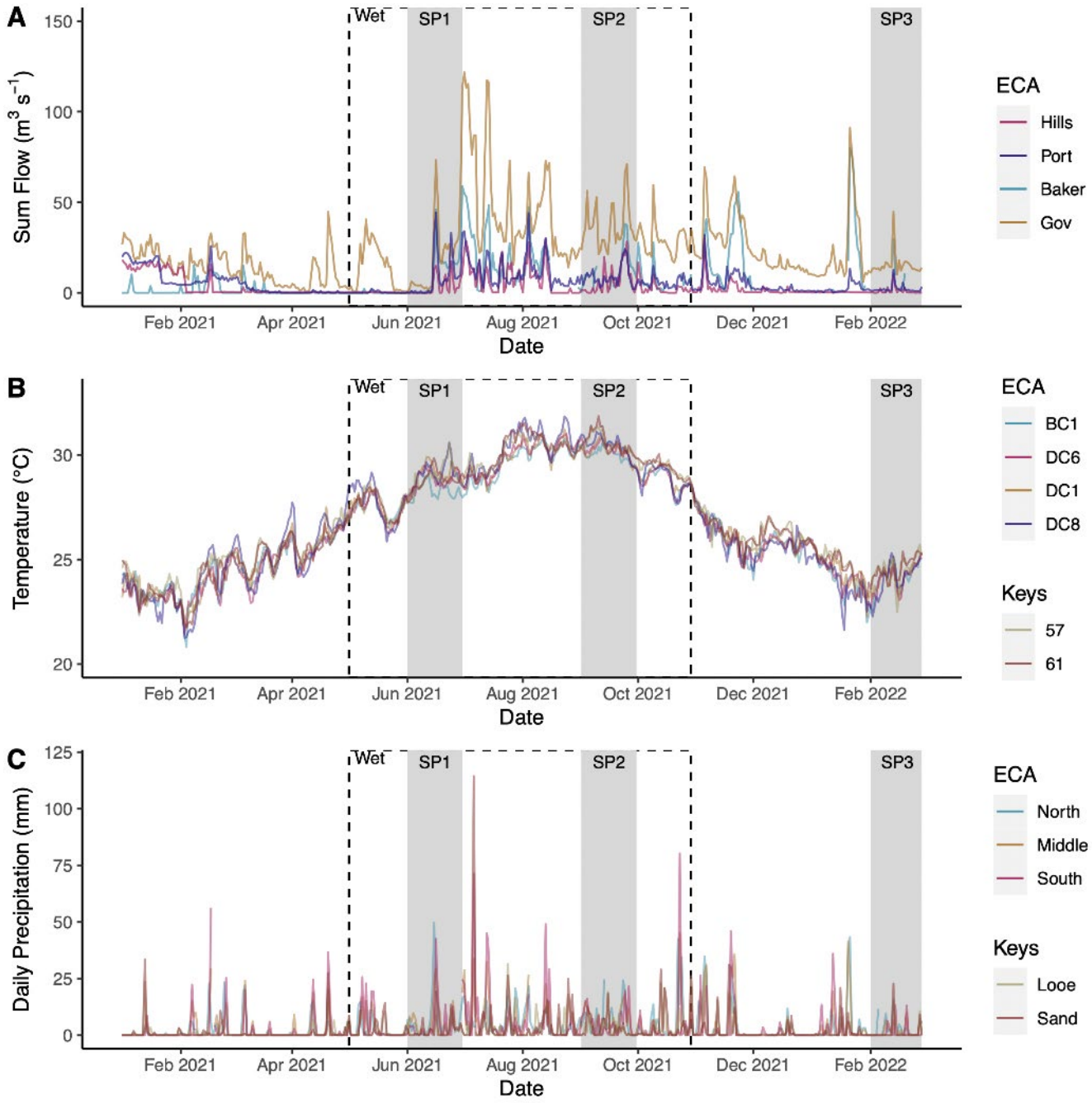

Figure 53. Temporal variations in A) inlet contributing area outflow (for the KJCAP), B) *in situ* temperature at the depth of the reef, and C) precipitation for the KJCAP and Keys. Wet season is denoted within the dotted lines, and the three sampling periods (SP1-3) of the RRC corals shown in grey shading (with of the shading represents the earliest and latest sample date).

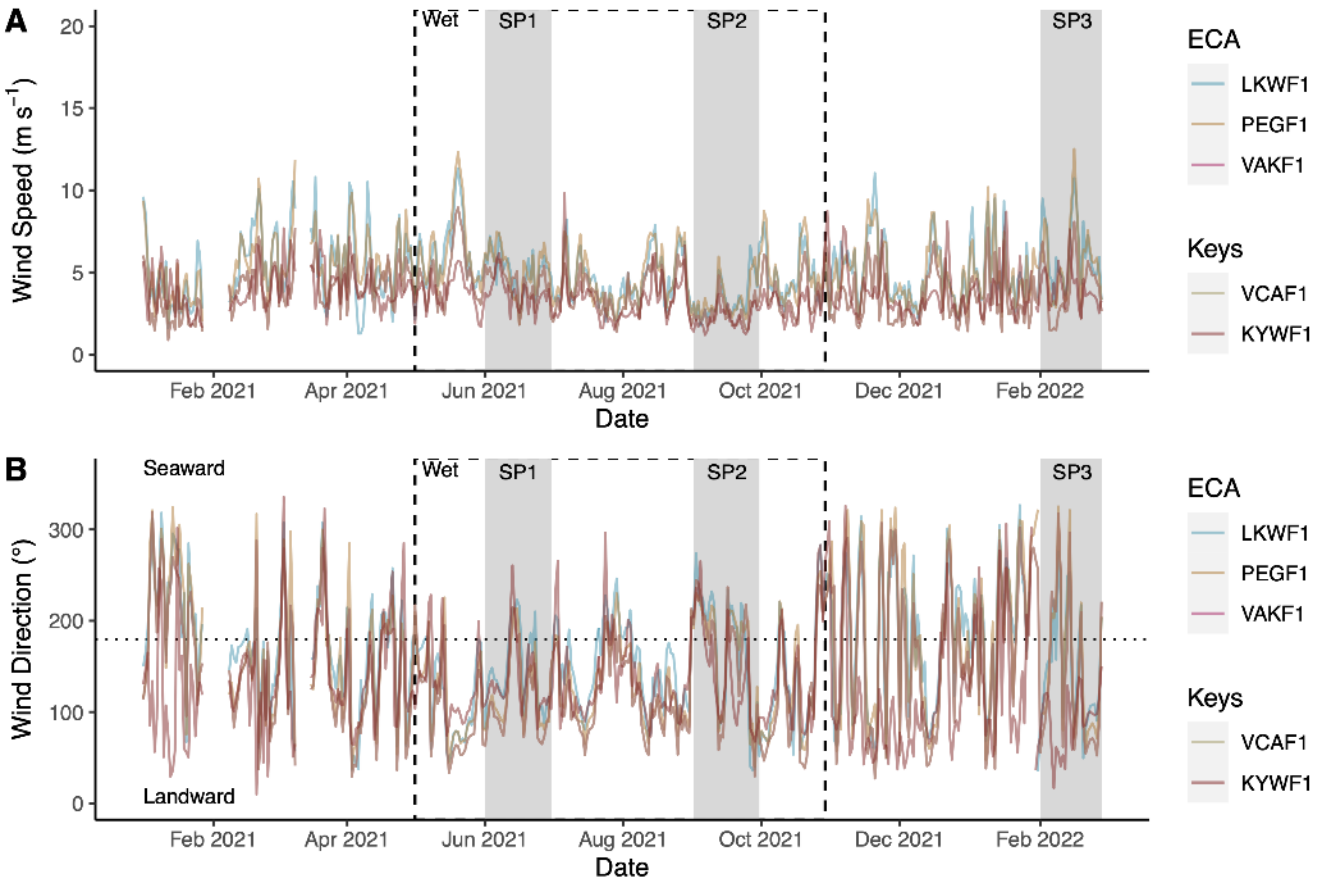

Figure 54. Temporal variations in A) wind speed and B) wind direction for the KJCAP and Keys. Wet season is denoted within the dotted lines, and the three sampling periods (SP1-3) of the RRC corals shown in grey shading (with of the shading represents the earliest and latest sample date). The horizontal dotted line in B represents the split between seaward wind (i.e., blowing out to sea, above the line) and landward wind (i.e., blowing towards the land, below the line).

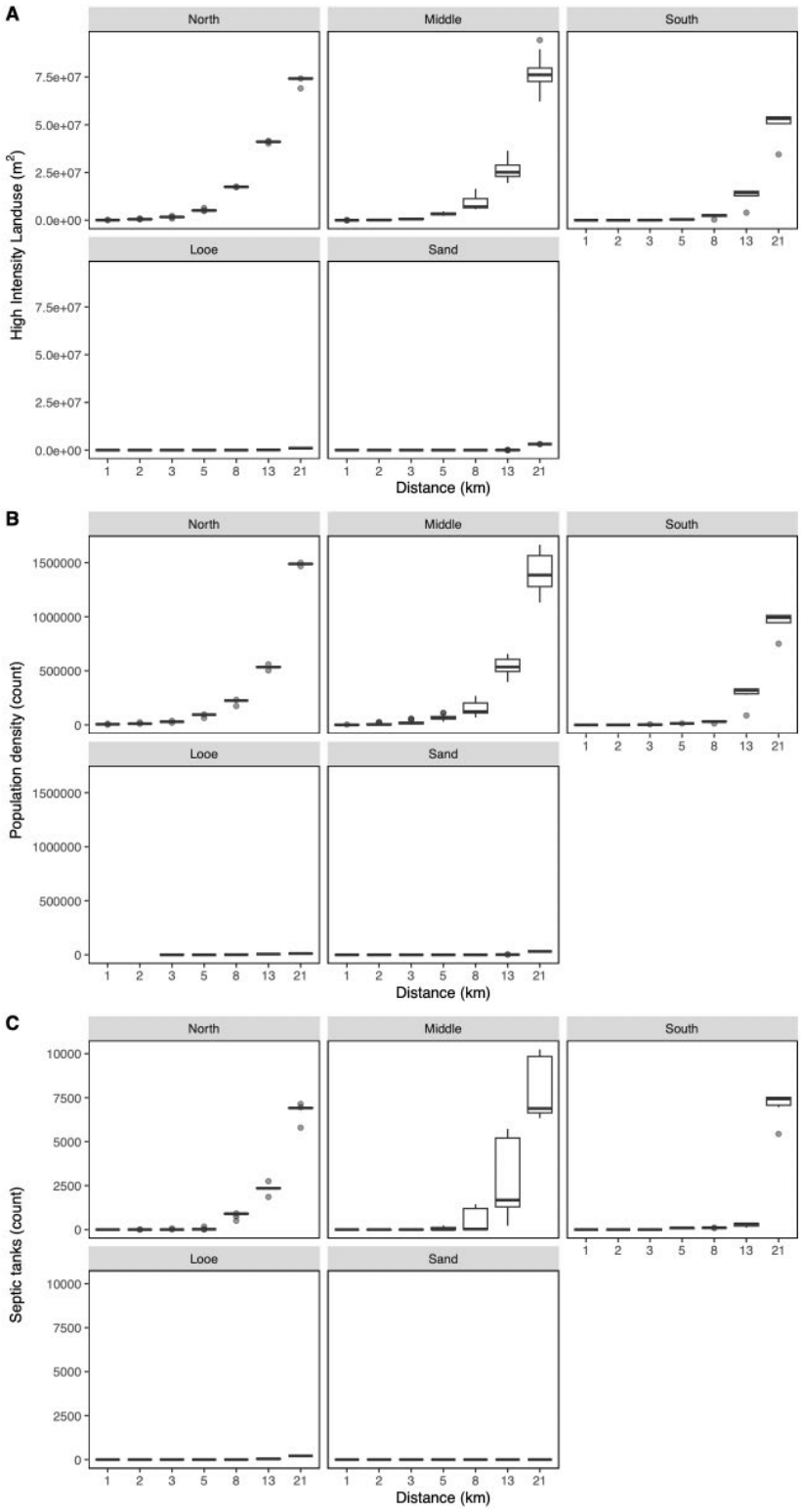

Figure 55. Spatial patterns in A) high intensity land use, B) human population density, and C) number of septic tanks over a series of expanding radial buffers (x axes) from the RRC corals. KJCAP is shown as North, Middle, South and the Keys as Looe and Sand Key. Medium intensity land use is not shown as the patterns were nearly identical to high intensity.

Temporal patterns of key environmental variables across sampling periods

There we clear differences in environmental conditions among regions, as well as across locations within regions leading up to each sample period (SP1-3). Leading up to SP1, mean seawater temperature was lower in the North KJCAP compared to all other locations for both short and longer-term time windows (Figure 56). Leading up to SP2, there was less difference in mean temperature among locations, but for both 7- and 90-days prior Looe and Sand Key appeared to experience slightly higher temperatures (Figure 56). Leading up to SP3, temperatures were lower at Looe and Sand compared to the KJCAP for the 7-days prior, but this pattern was the inverse for the 90-days prior, and the South KJCAP experienced the lowest temperatures (Figure 56). These flips in temperature patterns across different time windows highlight the dynamic nature of these *in situ* conditions.

Patterns of rainfall leading up to the sample periods were also highly dynamic, with clear intra-location differences across all sample periods. Leading up to SP1, the Middle and South KJCAP experienced more rain than all other locations over both 7- and 90-days prior (Figure 57). Leading up to SP2, patterns of rainfall within locations were highly variable, with no single location experiencing more or less than another (Figure 57).

Leading up to SP3, rainfall patterns were relatively consistent across both 7- and 90-days prior, with the middle KJCAP (and to a lesser extent the North KJCAP) experiencing more rain than elsewhere (Figure 57). Patterns of wind leading up to the sample periods were also unique among locations, but less so across sample periods. Leading up to SP1, the North and Middle KJCAP experienced the highest number of high wind events, and Looe and Sand the lowest over both 7- and 90-days prior (Figure 58). This general intra-location pattern then held leading up to both SP2 and SP3 (Figure 58). All these patterns and interpretations were backed up by the CAP allocation success results. All locations had a 100% correct allocation score for each sample period, highlighting the highly distinct environmental regimes each location experienced leading up to each sample period. The only exception was the Middle KJCAP leading up to SP2 (6.3% allocation success), highlighting that this location did not experience particularly unique environmental conditions compared to all other locations.

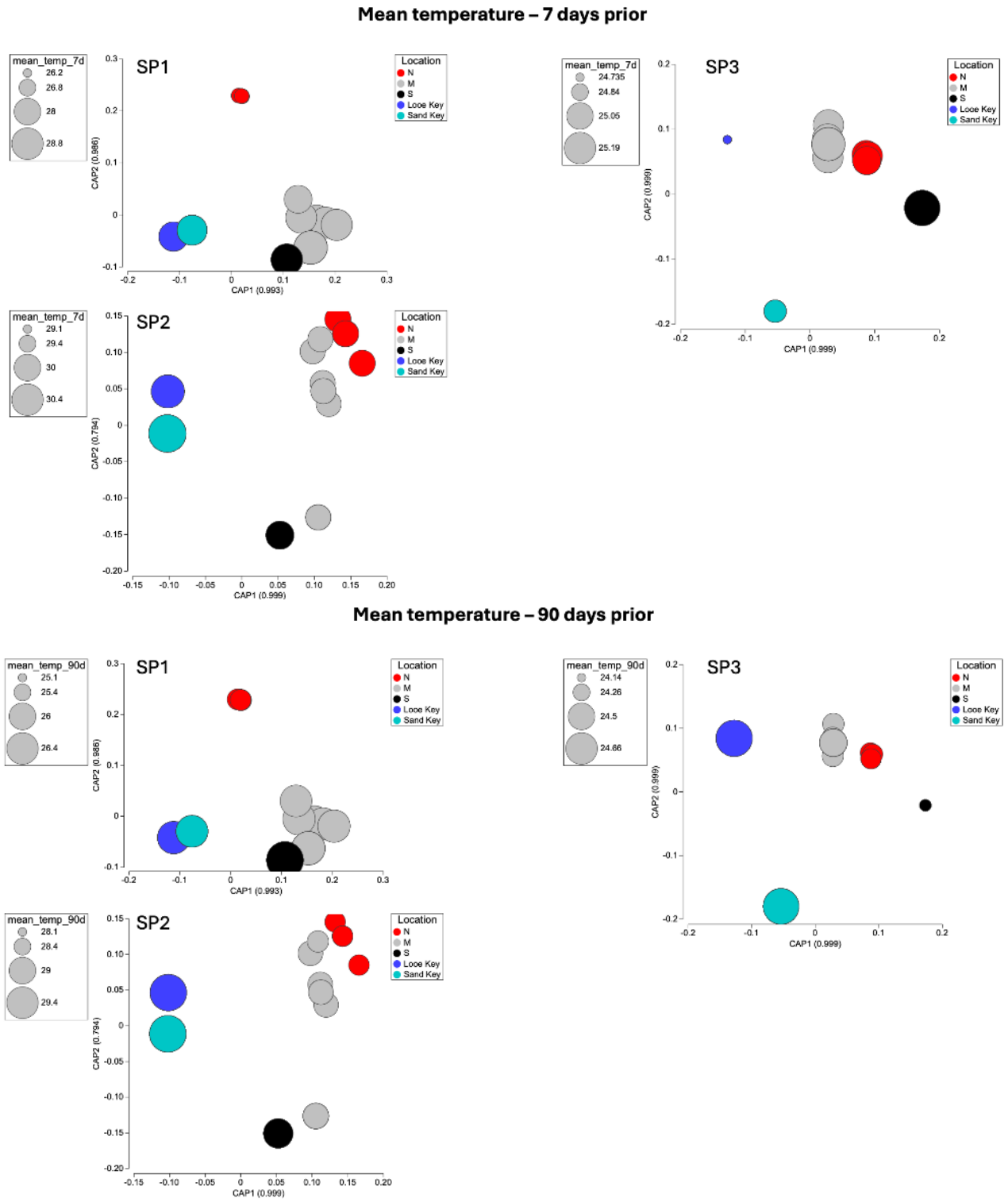

Figure 56. Relative similarity in mean seawater temperature patterns experienced by the RRC corals across the three sampling periods (SP1-3) within the KJCAP (North-N, Middle-M, South-S) and Keys (Looe and Sand) over a 7- and 90-day period prior to sampling (top and bottom plots, respectively). The performance (squared canonical correlation) of the constrained ordination axes for each plot are shown in parentheses. Size of bubbles correspond to temperature values (shown in the bubble keys).

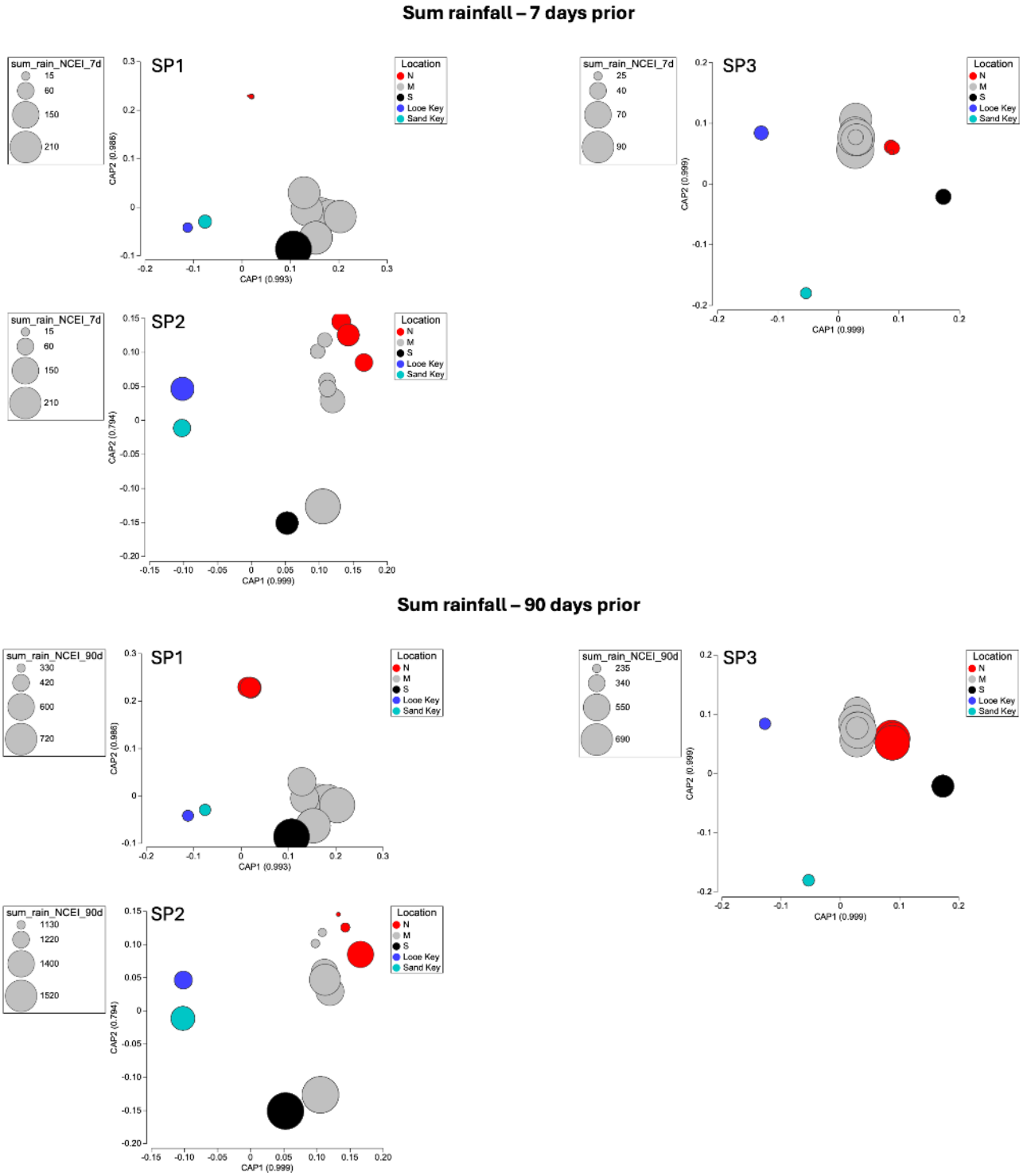

Figure 57. Relative similarity in summed rainfall patterns experienced by the RRC corals across the three sampling periods (SP1-3) within the KJCAP (North-N, Middle-M, South-S) and Keys (Looe and Sand) over a 7- and 90-day period prior to sampling (top and bottom plots, respectively). The performance (squared canonical correlation) of the constrained ordination axes for each plot are shown in parentheses. Size of bubbles correspond to temperature values (shown in the bubble keys).

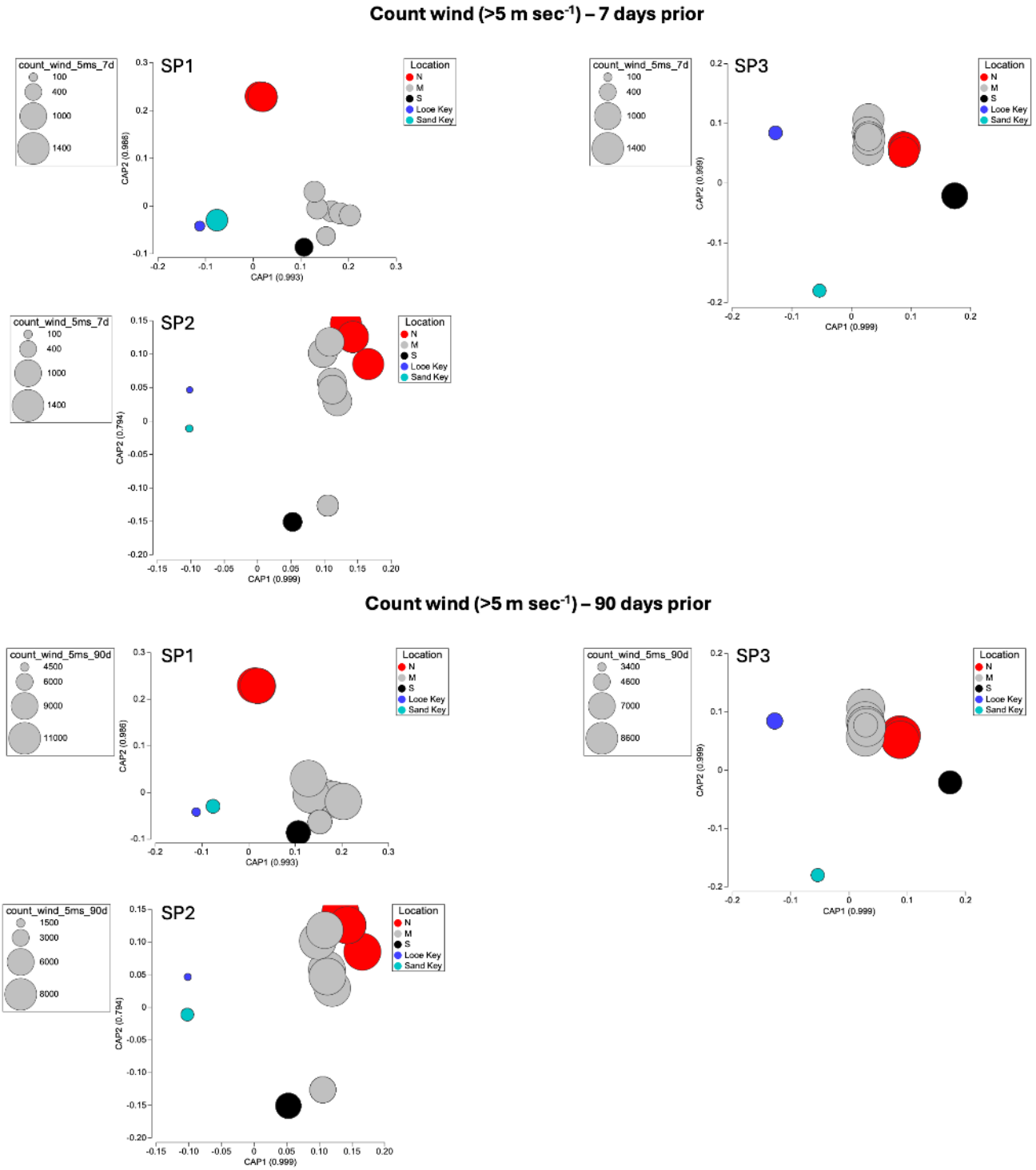

Figure 58. Relative similarity in high wind event patterns (regardless of direction) experienced by the RRC corals across the three sampling periods (SP1-3) within the KJCAP (North-N, Middle-M, South-S) and Keys (Looe and Sand) over a 7- and 90-day period prior to sampling (top and bottom plots, respectively). The performance (squared canonical correlation) of the constrained ordination axes for each plot are shown in parentheses. Size of bubbles correspond to temperature values (shown in the bubble keys).

Correlation between environmental/human factors and host resistance or resilience to SCTLD

Sample period 1: Using the temporal predictors over the 1-90 days prior to sample collection, overall model performance equaled 4.8% variation explained for EtOAc, and 15.8% and 16.8% for zooxanthellae degeneration and lytic necrosis, respectively (Table 13). However, the models for zooxanthellae degeneration and lytic necrosis both contained three predictors, and no single predictor contributed more than 9% to overall model performance, and most contributed less than 6% (Table 13). No variation in polyp fecundity was explained and the predictors were unable to explain significant variation across the four measurements of coral health as a multivariate response (Table 13).

Using the temporal predictors over 12 months prior to sample collection in 1-month increments, overall model performance equaled 12.6% for EtOAc, 15.8% for lytic necrosis, and 16.8% for zooxanthellae degeneration (Table 14). The model for EtoAc contained four predictors and each contributed less than 5% to overall model performance. However, the models for lytic necrosis and zooxanthellae degeneration each contained only two predictors, and in both models the Hot Snap exposure hours over the prior 11 months was the optimal predictor, each time contributing ~12% to overall model performance (Table 14). While still limited in terms of model performance, this result warrants further investigation into the directionality of the relationship between long-term Hot Snap exposure and lytic necrosis and zooxanthellae degeneration. No variation in polyp fecundity was explained and the predictors were unable to explain significant variation across the four measurements of coral health as a multivariate response (Table 14).

Sample period 2: Using the temporal predictors over the 1-90 days prior to sample collection, the models for EtOAc and lytic necrosis were the poorest performing (3.2% and 4.9% overall variation explained, respectively), while the models for zooxanthellae degeneration and all four health measurements as a multivariate response were slightly improved (10.7% and 16.3% overall variation explained, respectively) (Table 13). The model for polyp fecundity was the best performing, explaining 39.8% of the overall variation, with total human population numbers within 3 km and 13 km explaining 12.7% and 19.8% of the overall variation, respectively (Table 13). This result warrants further investigation into the directionality of the relationship between local human population density and polyp fecundity. Using the temporal predictors over 12 months prior to sample collection in 1-month increments, the same overall results held. The model for polyp fecundity remained the best performing and the models for EtoAc and lytic necrosis remained the poorest performing (Table 14).

Sample period 3: Using the temporal predictors over the 1-90 days prior to sample collection, overall model performance equaled 5.0% variation explained for EtOAc and 12.6% for zooxanthellae degeneration (Table 13). No variation was explained in lytic necrosis or the four measurements of coral health as a multivariate response (Table 13). Using the temporal predictors over 12 months prior to sample collection in 1-month increments, both the EtOAc and zooxanthellae degeneration models decreased in performance (Table 14). This approach did, however, lead to models for lytic necrosis and

the four measurements of coral health as a multivariate response, which explained 7.8 and 5.3%, respectively (Table 14).

Coral host-specific factors

In general, models explained less than 8% of the overall variation in the four measurements of coral health, as well as their simultaneous multivariate response (Table 15). The exceptions were the polyp fecundity for SP1 which explained 21.7% of the overall variation, however no single predictor explained more than 10%. The second exception was the zooxanthellae degeneration model for SP2 which explained 13.6% of the overall variation, with colony length contributing 10.7% to the overall model performance. While limited in terms of model performance, these results do suggest that host-specific morphometrics may be directly or indirectly linked to polyp fecundity and to a lesser extent zooxanthellae degeneration. Future work should focus on how host-specific factors may interact with other changes within the coral microbiome that occur from SCTLD and whether these interactions help to explain host resistance.

Table 13. Model summaries testing for correlations between four measurements of coral health (EtoAc, lytic necrosis, zooxanthellae degeneration, and polyp fecundity, as well as their simultaneous multivariate response) and **a series of local environmental (1, 3, 7, 14, 30, 60, 90 days prior to sample collection) and human factors**, showing statistics for the predictors included in the optimal models, the proportion of variation in the response variable they explain (Prop) and their cumulative proportion of variation they explain (Cumul). Model selection was based on Akaike Information Criterion with a second-order bias correction applied (AICc). SP, sampling period.

SP	Response	Predictor	SS(trace)	Pseudo-F	P	Percen	Cumul
1	Multivariate	*No model*					
	EtoAc	Wind (3 days)	27.353	4.46	0.038	4.8	**4.8**
	Lytic necrosis	Wind (3 days)	4.668	5.09	0.027	5.9	5.9
		Mean temperature (7 days)	4.089	4.88	0.047	5.2	11.1
		Wind (7 days)	3.989	4.54	0.028	5.0	**16.1**
	Zoox. Degen.	Land use (medium 2 km)	5.775	8.14	0.004	8.8	8.8
		Mean temperature (1 day)	3.035	3.93	0.051	4.6	13.4
		Mean temperature (30 days)	1.541	2.21	0.150	2.4	**15.8**
	Polyp Fecund.	*No model*					
2	Multivariate	Mean temperature (30 days)	9.042	8.83	0.007	9.1	9.1
		Septics (3 km)	4.610	4.78	0.057	4.7	13.8
		Wind (1 day)	2.576	2.56	0.160	2.5	**16.3**
	EtoAc	Hot Snap (1 day)	18.456	2.90	0.079	3.2	**3.2**
	Lytic necrosis	Mean rain (30 days)	4.268	4.34	0.049	4.9	**4.9**
	Zoox. Degen.	Hot Snap (1 day)	3.382	6.47	0.010	7.2	7.2
		Sum rain (7 days)	1.690	3.33	0.069	3.6	**10.7**
	Polyp Fecund.	Human Pop. (13 km)	12513.0	10.61	0.005	19.8	19.8
		Human Pop. (3 km)	8001.7	7.87	0.008	12.7	32.4
		Septics (3 km)	4675.8	5.04	0.018	7.4	**39.8**
3	Multivariate	*No model*					
	EtoAc	Mean temperature (7 day)	0.521	4.67	0.033	5.0	**5.0**
	Lytic necrosis	*No model*					
	Zoox. Degen.	Wind (1 day)	0.7838	2.40	0.121	3.1	3.1
		Human Pop. (2 km)	1.5088	4.85	0.034	5.9	8.9
		Human Pop. (13 km)	0.9364	3.09	0.083	3.7	**12.6**

Table 14. Model summaries testing for correlations between four measurements of coral health (EtoAc, lytic necrosis, zooxanthellae degeneration, and polyp fecundity, as well as their simultaneous multivariate response) and **a series of local environmental (1-12 months prior to sample collection in 1-month increments) and human factors**, showing statistics for the predictors included in the optimal models, the proportion of variation in the response variable they explain (Prop) and their cumulative proportion of variation they explain (Cumul). Model selection was based on Akaike Information Criterion with a second-order bias correction applied (AICc). SP, sampling period.

SP	Response	Predictor	SS(trace)	Pseudo-F	P	Percen	Cumul
1	Multivariate	*No model*					
	EtoAc	Mean rain (7 mo)	23.96	3.88	0.050	4.2	4.2
		Human Pop. (3 km)	18.02	2.98	0.104	3.2	7.4
		Septics (2 km)	15.37	2.63	0.105	2.7	10.1
		Human Pop. (8 km)	14.34	2.41	0.146	2.5	**12.6**
	Lytic necrosis	Hot Snap (11 mo)	9.96	11.69	0.001	12.6	12.6
		Wind (12 mo)	2.55	3.07	0.067	3.2	**15.8**
	Zoox. Degen.	Hot Snap (11 mo)	7.93	11.15	0.001	12.1	12.1
		Human Pop. (2 km)	3.11	4.57	0.032	4.7	**16.8**
	Polyp Fecund.	*No model*					
2	Multivariate	Mean temperature (1 mo)	9.04	8.83	0.009	9.1	9.1
		Septics (3 km)	2.54	2.52	0.153	2.6	11.7
		Land use (medium 1 km)	5.10	5.32	0.028	5.1	**16.8**
	EtoAc	Hot Snap (12 mo)	15.78	2.47	0.105	2.7	**2.7**
	Lytic necrosis	Mean rain (1 mo)	4.27	4.34	0.030	4.9	**4.9**
	Zoox. Degen.	Hot Snap (12 mo)	2.83	5.35	0.028	6.0	**6.0**
	Polyp Fecund.	Human Pop. (13 km)	12513.0	10.608	0.005	19.8	19.8
		Human Pop. (3 km)	8001.7	7.8669	0.008	12.7	32.4
		Septics (3 km)	4675.8	5.0392	0.016	7.4	**39.8**
3	Multivariate	Hot Snap (8 mo)	2.3591	2.4692	0.126	2.7	2.7
		Septics (2 km)	2.2059	2.3441	0.114	2.6	**5.3**
	EtoAc	Summed rain (9 mo)	0.45873	4.0871	0.038	4.4	**4.4**
	Lytic necrosis	Hot Snap (8 mo)	2.4788	3.4915	0.067	4.4	4.4
		Septics (2 km)	1.9467	2.8073	0.106	3.4	**7.8**
	Zoox. Degen.	Hot Snap (8 mo)	1.009	3.1161	0.095	3.9	**3.9**

Table 15. Model summaries testing for correlations between four measurements of coral health (EtoAc, lytic necrosis, zooxanthellae degeneration, and polyp fecundity, as well as their simultaneous multivariate response) **and a series of colony-specific host characteristics**, showing statistics for the predictors included in the optimal models, the proportion of variation in the response variable they explain (Prop) and their cumulative proportion of variation they explain (Cumul). Model selection was based on Akaike Information Criterion with a second-order bias correction applied (AICc). SP, sampling period.

SP	Response	Predictor	SS(trace)	Pseudo-F	P	Percen	Cumul
1	Multivariate	Height	5.27	4.01	0.065	0.044	4.4
		Depth	3.53	2.74	0.138	0.029	**7.3**
	EtoAc	*No model*					
	Lytic necrosis	Depth	4.38	4.76	0.048	0.055	**5.5**
	Zoox. Degen.	Depth	3.69	4.83	0.033	0.056	**5.6**
	Polyp Fecund.	Depth	341.98	4.57	0.035	0.098	9.8
		Length	224.24	3.29	0.068	0.064	16.2
		Height	189.99	2.64	0.116	0.055	**21.7**
2	Multivariate	Surface area	2.51	2.29	0.190	0.025	**2.5**
	EtoAc	Depth	17.99	2.82	0.097	0.031	**3.1**
	Lytic necrosis	Length	4.31	4.39	0.042	0.050	**5.0**
	Zoox. Degen.	Length	5.06	10.07	0.001	0.107	10.7
		Width	1.37	2.78	0.1	0.029	**13.6**
	Polyp Fecund.	*No model*					
3	Multivariate	*No model*					
	EtoAc	Treatments (2 mo)	0.81375	7.5205	0.009	7.9	**7.9**
	Lytic necrosis	*No model*					
	Zoox. Degen.	Width	0.83919	2.5738	0.118	3.3	**3.3**

3.16. **Task 9b – Classifying RRC corals by potential nutrient pollution exposure in the KJCAP (Williams and Maynard)**

Goals: Collaborate to build hydrographic models to quantify connections between inland waterways and the RRC corals and DEP water quality reef monitoring sites in the KJCAP.

Significant findings: N/A.

Results:
Here our task was to generate high-resolution inlet contributing area outflow data for the KJCAP and estimates of water quality analytes coming directly out of the inlets to parameterize the hydrographic model built and reported on by Dobbelaere et al. (2024).

For the flow data, using the same 20 selected stations as in Task 9a, we sourced all flow data and calculated the time difference between each row grouped by the station. On average, most stations reported a flow rate every 2 min, however, this was highly variable through time, (minimum time was as fast as 1 sec, maximum was several days or even weeks if a station went down). To account for this, we binned the data into 5-min intervals and calculated mean flow for each interval for each station to give an overall mean flow rate per 5-min interval for each ICA inlet over the project time period.

The water quality data used for this analysis were from a joint NOAA-Florida Department of Environmental Protection (FDEP) assessment program (Whitall et al 2019). The period of record used for this analysis was September 1st 2018 to September 1st 2021. To analyze water quality data at the reefs themselves, only water collected using Niskin bottles at the depth of the reef (not surface waters) were included in this analysis. The sampling protocol involved starting sample collection as far into the ebb tide as possible and at a minimum of two to three hours after the peak high tide. Sampling equipment was rinsed with deionized water three times between sites and then three times with site water once on site. Field clean equipment blanks were collected (at least one per day and at least one per 20 samples collected). Analytical chemistry was performed via standard methods. Post-processing was applied to address the relatively larger numbers of values below the method detection limits (Flynn 2010). A detailed description of the water quality data, including methods, temporal and spatial patterns, and data interpretation, can be found in Whitall et al. (2019) and Whitall and Bricker (2021). Using these water quality data, we calculated the estimated nutrient loads for each ICA so we could apportion how much was coming out of each inlet. We did this by using the data from the four centroid inlet sites (GOC002, BAK020, PEV040 and HIL050).

3.17. **Task 9c – Statistical oversight of the RRC research efforts and outputs (Williams and Maynard)**

Goals: Provide key statistical oversight and targeted assistance to help those researchers identify and execute appropriate statistical tests for their questions and hypotheses.

Significant findings: See previous corresponding tasks.

Methods:

Transcriptomics

The RRC transcriptomics data were filtered (by Dr Rodriguez) to focus on a set of 160 genes that significantly correlated to SCTLD susceptibility (across sample periods 2 and 3 only). The data had already had a variance stabilising transformation applied to them and, as such, they were not further transformed or filtered prior to analysis. As in 9a.3, a distance-based permutational multiple regression (McArdle and Anderson 2001) framework based on a Euclidean similarity matrix was used. Here, there was an *a priori* expectation that seawater temperature might correlate with the transcriptomics data. We therefore included all the derived temperature metrics (mean temperature, maximum temperature, temperature variation, number of HotSnaps) in the model-fitting process as an exploratory step, knowing that they were all highly correlated with each other and that their independent effects would therefore be hard to disentangle. We then incorporated the rainfall metrics into the model selection process (having normalized the variables to account for their differences in units and ranges), to test whether these offered better explanatory power than the temperature metrics. The resulting correlations were then visualized using canonical analysis of principal coordinates (to highlight the differences in transcriptomic data between the two sample periods), with the key predictors then overlaid as bubble plots.

Chemical Defenses

One of the major accomplishments was reanalyzing the disk diffusion assay data to ensure its accuracy for determining the antimicrobial activity of all the coral partitions over the three time periods of collections and working with Gareth Williams on the data analysis (Task 9c). We had determined that some of the zones of inhibition for the negative controls (solvent controls) increased during the 3rd sampling period (winter), which might explain why the zones of inhibition for the coral samples went up overall during that time period. We reentered all the data and recorded the test values of the coral partitions and controls from each assay plate. This required QA/QC because there was a lot of data, and we had to ensure there were no errors in reentering and copying the data to a new file. Two individuals worked on this to validate that all the data were entered correctly. During the antimicrobial testing, all test values in the disk diffusion assays on the EtOAc and BuOH coral partition data were run in triplicate (3 technical replicates), and the mean results of the 3 replicates were used for the treatment values. We then corrected all of the treatment data relative to control values by subtracting the control values from the treatment values (Treatment-Control (or T-C)) for each replicate. These data were then used for all of the statistical analyses (Task 9c).

In coordination with Task 9c, we tested for an effect of Sample Period (fixed factor, three levels: Fall 2021, Summer 2021, Winter 2022), Region (fixed factor, two levels: ECA and

Keys), and either SCTLD (history of SCTLD) (fixed factor, two levels: affected, unaffected), or Disease coring (disease present at coring) (fixed factor, two levels: present, absent) on the following response variables: EtOAc partition radius (T-C) in the disk diffusion assays and EtOAc partition mgs and BuOH partition radius (T-C) and BuOH partition mgs. As the response variables did not all conform to a normal distribution, we used a multivariate permutational analysis of variance (PERMANOVA) (Anderson 2001) on each of the univariate response variables in turn (creating a permutational ANOVA and negating the need for normality in the response data). These were run using a Euclidean distance matrix, 999 random permutations of the raw data, and Type III (partial) sums-of-squares using the PERMANOVA+ add-on for the PRIMER v7 software (Anderson et al. 2008). We investigated any significant main effects (including significant interactions) using PERMANOVA pairwise comparisons and quantified the directionality of the differences using summary statistics.

Metabolomics

Here, we treated the RRC corals as replicates and averaged the metabolome values across 15 *a priori* identified groups: all combinations of sample period (3 levels) and 'Location' (5 levels). This reduced the number of samples in the original metabolomics multivariate response matrix from 252 (having removed 9 samples due to missing predictor variable data) to 15, but it preserved the number of metabolome variables (n=2813). A distance-based permutational multiple regression (McArdle and Anderson 2001) framework was then used (as in 9a.3) to test whether variations in 'Bioactivity' (two predictors: EtOAc and BuOH radius mean, correlating at r=0.27) explained any of the underlying variation in the metabolome matrix. Here though, models were constructed from Bray-Curtis similarity matrices (not Euclidean matrices as before) to better account for the zero-inflated nature of the data. The resulting models were then visualized using distance-based redundancy analysis plots. Three different models were built: 1) untransformed, 2) 4^{th}-root transformed, and 3) presence/absence transformed metabolomics data. Analyses were completed using the DisTLM and db-RDA functions in the PERMANOVA+ add-on (Anderson et al. 2008) for PRIMER v7 (Clarke & Gorley 2015).

3.18. **Task 11: Proteomics (Woodley) – Not funded under this Scope of Work**

Goals: 1) rigorously analyze the protein profiles derived from the original RRC samples to identify differentials between profiles using multivariate statistics and 2) collaborate with other RRC PIs to help identify proteins indicative of functions identified in other components (e.g., transcriptomics, metabolomics, histology).

Significant findings: Determining proteins changes indicative of active disease required restructuring the colony groupings based on a more detailed disease history. We identified 35 proteins that suggest that during active SCTLD, protein processing in the coral host is disrupted, likely contributing to lesion formation due to cytoskeletal protein dysregulation.

Results and Discussion: The *Orbicella faveolata* proteomics data for Period 1 (May-June 2021) and Period 3 (Feb-March 2022) was initially evaluated based on their original resistance classification – High, Medium or Low Resistance – which was determined by the number of visits in which SCTLD was present on the colony prior to sampling Period 1. The results revealed **no consistent differences in protein abundancies** when comparing the High and Low Resistance groups in either Period 1 and Period 3. This result remained true regardless of whether the three regions (ECA, Looe Key, Sand Key) were grouped together or evaluated separately. However, regional differences in protein abundances were observed in both Period 1 and Period 3, with ECA colonies generally showing fewer changes compared to the Lower Keys (Looe and Sand Key) colonies. Additionally, more changes in protein abundancies were detected in Period 1 than in Period 3, suggesting possible seasonal variations that could be masking disease-related proteomic changes. These findings prompted further analyses to address the **regional** and **seasonal variations** in response to SCTLD, aiming to isolate the changes specifically associated with the disease itself.

After reviewing the individual colonies' disease history, we determined that to **accurately identify protein changes indicative** of **active disease**, would require restructuring the colony groupings (Figure 59). The colonies were reclassified based on the presence of disease relative to the sampling time, creating six new groups: **Never** (disease was never seen on these colonies), **Past Diseased** (disease was seen greater than 6 months prior to sampling), **Recently Diseased** (disease was seen less than 6 months prior to sampling), **Active** (disease was seen during the sampling), **Soon Diseased** (disease developed less than 6 months after sampling), and **Later Diseased** (disease developed more than 6 months after the sampling). It's important to note that the colony assigned to each group during sample Period 1 was not necessarily in the same group during sample Period 3, as disease progression is dynamic. Additionally, the two time periods were analyzed separately to minimize seasonal effects on the changes observed.

Comparing the Active and Never groups, we **identified 35 proteins** that were altered in abundance in both Period 1 and Period 3. These proteins were primarily involved in membrane trafficking, exosomes, chaperones and other folding catalysts, cytoskeletal proteins, and enzymes. Likewise, they played roles in signaling pathways related to protein processing in the endoplasmic reticulum, endocytosis, and cytoskeleton. This suggests that during **active** SCTLD, protein processing in the coral host is disrupted, likely contributing to lesion formation due to cytoskeletal protein dysregulation. The next step of our analyses

will be to examine disease-related changes across the other four disease states (past, recently, soon, later) to better understand how SCTLD affects coral proteomics over time.

This information will help us identify protein changes that contribute to disease susceptibility, those that occur early (prior to lesion formation), and those that persist after disease, potentially contributing to a corals' decreased health state, allowing for reinfection or other coral issues.

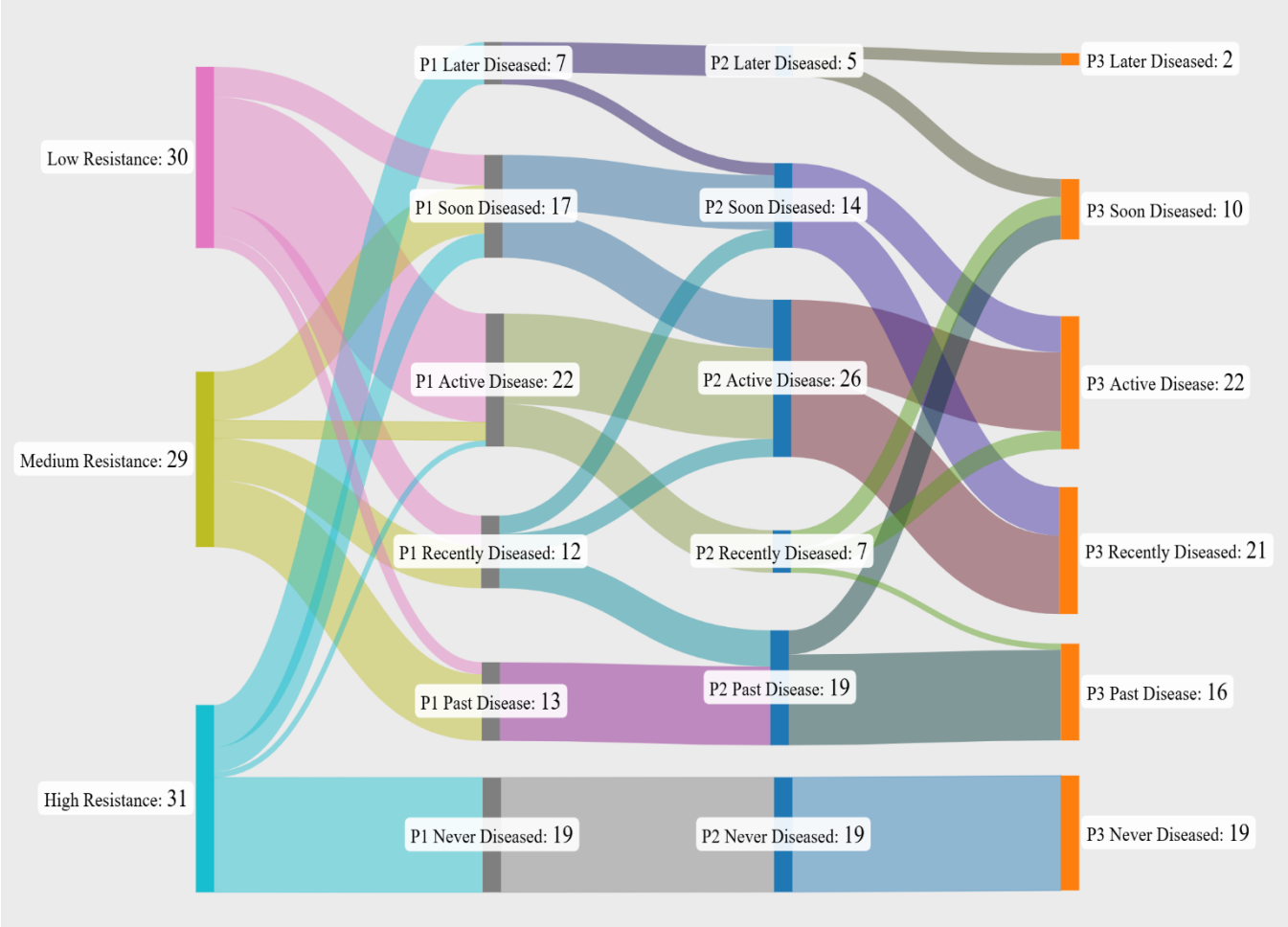

Figure 59. This diagram shows how the disease state of the colonies changed over time. The initial classifications based on susceptibility of SCTLD (High, Medium, Low Resistance) are shown on the far left, and then Sample Periods 1, 2, and 3 follow (left to right) showing how disease states changed over time.

4. CONCLUSIONS AND NEXT STEPS

In conclusion, the analyses of the many various components in this investigation, genomics, transcriptomics, metabolomics, proteomics, lipidomics, histopathology, microbiomes, endosymbionts, tissue regeneration, and fecundity, have elicited many future research leads to gain a wholistic understanding of the coral's condition. This project was successful in obtaining the data to realize the goal of understanding and determining SCTLD resistance and susceptibility factors in *Orbicella faveolata* on Florida's Coral Reef. There is much work remaining to uncover the many statistical associations and pathways across the various components.

The SCTLD Resistance Research Consortium's (RRC) integrated approach to understanding the underpinnings for SCTLD resistance and susceptibility among Florida *O. faveolata* populations has been a success. The synchronized core sampling across time of year, regions, and disease resistance classes of a statistically robust number of corals has given many insights into the genetic, biochemical, and physiological underpinnings in the holobiont of individuals.

Genetic analyses identified three colonies of a separate species, several clones, and a distinct lineage in the KJCAP. It discovered a highly connected population throughout the reef tract with no evidence of regionality or associations to disease resistance. Using size as a proxy for age, the genetics of these large colonies indicates that the *Orbicella* populations were once successfully recruiting throughout the reef system. Something that happens very rarely if at all today.

Disease was evident in all coral samples at varying levels. Histopathology scoring supported the resistance categories by showing increased lytic necrosis and degenerative Symbiodiniaceae in the low resistance colonies, but only over certain times of year. Histopathology scores were highest at the end of summer before and after releasing gametes and were lowest in March.

Coral disease was dynamic during the study with some corals getting more disease, some for the first time, and others contracting it less often. While all corals were sampled in healthy-looking tissue away from any disease, tracking these disease states facilitated identifying specific corals with recent disease to investigate resistance and possible disease markers. More research is needed to understand what specific aspects of these corals differed.

Metabolite, lipid, and protein data all provided evidence that a coral's state is dynamic over time and varied by region. Differences in resistance were found only in specific regions at certain times of the year. In the Lower Keys, resistance classes differed by metabolite species in June and September, by lipid species in June and March, and by protein species in June. In the KJCAP, no significant differences were found in all metabolite, lipid, or protein species between resistance classes. Although as a whole, certain patterns were seen, there were differences in specific metabolites, lipids, and proteins that warrant further investigation. Research is needed into the specific compounds causing these differences and their functions inside the cell to determine if they are related to gametogenesis, environmental stress, or disease resistance/susceptibility.

Orbicella favelota colonies with previous SCTLD lesions had a distinct transcriptomic signature during winter compared to colonies that had never been visually affected by the disease. Most genes were down-regulated in colonies SCTLD unaffected colonies during winter in both regions: 33 genes differentially expressed between SCTLD affected and unaffected colonies from the Lower Key during winter and 169 genes differentially expressed between SCTLD affected and unaffected colonies from the KJCAP. A network analysis used to find the correlation between gene expression and symbiont density collected per symbiont genus showed that *Breviolum* and *Cladocopium* were significantly correlated with some gene modules, and one module was significantly correlated with SCTLD susceptibilities and the symbiont density. Lyctic necrosis and antibiotic inhibition also significantly correlated with the module that also showed correlation with SCTLD susceptibility state.

Microbial communities vary through time, space, and lineage. Shifts in the corals' microbiomes may serve as early indicators of disease susceptibility or resilience in *O. faveolata*. Bacterial functions varied by region, Symbiodiniaceae composition, and by disease history. Corals with active disease had more variable bacterial functions, indicating a disruption of the function of the microbiome in the whole colony as disease lesions were not sampled. In the Lower Keys where SCTLD was more active, unaffected colonies harbored bacteria with more abundant genes for the production of antibiotics, which may play a protective role for the coral. These results suggest that while SCTLD disrupts bacterial functions in apparently healthy tissue on actively diseased colonies, this effect is temporary and is outweighed by the influence of the Symbiodiniaceae composition or local environmental conditions.

Environmental conditions (seawater temperature, inlet outflow, rainfall, wind) varied significantly during the three sampling periods. Sample period 1 occurred during moderate inlet outflow in the KJCAP, high rainfall, and moderate winds. Sample period 2 saw peak seawater temperatures, moderate rainfall, and low wind speeds. Sample period 3 experienced the lowest inlet outflow, lowest temperatures, minimal rainfall, and stronger seaward winds. Not surprisingly, all metrics of local human impacts were higher in the KJCAP than the Keys. Within the KJCAP, high intensity land use and population density appeared slightly higher in the North and Middle KJCAP than the South at the broadest scale, while septic tanks were slightly more abundant in the Middle KJCAP. These patterns highlight the spatial and temporal complexity of environmental stressors, such as seawater temperature, that influence coral health.

Although highly informative and successful, this incredibly valuable and unique project requires more time for data analyses and meetings to spin off additional research to gain the most understanding possible about the health and dynamics of one of Florida's Coral Reef's historically prominent reef-builders. More signs point to SCTLD being associated with the Symbiodiniaceae where environmental factors may be affecting their host to symbiont ratios which may increase susceptibility. More data analyses need to be completed that integrate the various RRC datasets in the lens of the Symbiodiniaceae to host dynamics in order to understand SCTLD and other extrinsic factors affecting coral health on Florida's Coral Reef.

5. REFERENCES

Aeby, G. S., & Santavy, D. L. (2006). Factors affecting susceptibility of the coral *Montastraea faveolata* to black-band disease. *Marine Ecology Progress Series*, *318*, 103–110. https://doi.org/10.3354/meps318103

Alvarez-Filip, L., Estrada-Saldívar, N., Pérez-Cervantes, E., Molina-Hernández, A., & González-Barrios, F. J. (2019). A rapid spread of the stony coral tissue loss disease outbreak in the Mexican Caribbean. *PeerJ*, *7*, e8069. https://doi.org/10.7717/peerj.8069

Anderson MJ (2001) A new method for non-parametric multivariate analysis of variance. *Austral Ecol* 26: 32-46

Anderson MJ, Gorley RN, Clarke KR (2008) PERMANOVA+ for PRIMER: Guide to software and statistical methods. PRIMER-E: Plymouth, UK

Bythell, J. C., Brown, B. E., & Kirkwood, T. B. L. (2018). Do reef corals age? *Biological Reviews*, *93*(2), 1192–1202. https://doi.org/10.1111/brv.12391

Clarke KR, Gorley RN (2015) PRIMER v7: User manual/Tutorial. PRIMER-E: Plymouth, UK

Clements, C. S., & Hay, M. E. (2019). Biodiversity enhances coral growth, tissue survivorship and suppression of macroalgae. *Nature Ecology & Evolution*, *3*(2), 178–182. https://doi.org/10.1038/s41559-018-0752-7

Cróquer, A., Weil, E., & Rogers, C. S. (2021). Similarities and differences between two deadly caribbean coral diseases: white plague and stony coral tissue loss disease. *Frontiers in Marine Science*, *8*. https://www.frontiersin.org/articles/10.3389/fmars.2021.709544

Denis, V., Debreuil, J., Palmas, S. D., Richard, J., Guillaume, M. M. M., & Bruggemann, J. H. (2011). Lesion regeneration capacities in populations of the massive coral *Porites lutea* at Réunion Island: Environmental correlates. *Marine Ecology Progress Series*, *428*, 105–117. https://doi.org/10.3354/meps09060

Dobbelaere, T., Muller, E., Gramer, L., Holstein, D., & Hanert, E. (2020). *Report on the potential origin of the SCTLD in the Florida Reef Tract*. https://www.slim-ocean.be

Eddy, T. D., Lam, V. W. Y., Reygondeau, G., Cisneros-Montemayor, A. M., Greer, K., Palomares, M. L. D., Bruno, J. F., Ota, Y., & Cheung, W. W. L. (2021). Global decline in capacity of coral reefs to provide ecosystem services. *One Earth*, *4*(9), 1278–1285. https://doi.org/10.1016/j.oneear.2021.08.016

Edmunds, P. J., & Yarid, A. (2017). The effects of ocean acidification on wound repair in the coral *Porites spp*. *Journal of Experimental Marine Biology and Ecology*, *486*, 98–104. https://doi.org/10.1016/j.jembe.2016.10.001

Fine, M., Oren, U., & Loya, Y. (2002). Bleaching effect on regeneration and resource translocation in the coral *Oculina patagonica*. *Marine Ecology Progress Series*, *234*, 119–125. https://doi.org/10.3354/meps234119

Fisher, E. M. (2007). *Assessing the health of coral Reef ecosystems in the Florida Keys at community, individual, and cellular scales*. [Doctoral Dissertation, University of South Florida]

Florida Fish and Wildlife Commission. (n.d.). *Stony coral tissue loss disease FAQ*. Florida fish and wildlife conservation commission. Retrieved December 16, 2024, from https://myfwc.com/research/habitat/coral/disease/faq/

Foster, N. L., Box, S. J., & Mumby, P. J. (2008). Competitive effects of macroalgae on the fecundity of the reef-building coral *Montastraea annularis*. *Marine Ecology Progress Series*, *367*, 143–152. https://doi.org/10.3354/meps07594

Grinblat, M., Eyal-Shaham, L., Eyal, G., Ben-Zvi, O., Harii, S., Morita, M., Sakai, K., Hirose, M., Miller, D. J., & Loya, Y. (2023). Energy allocation trade-offs as a function of age in fungiid corals. *Frontiers in Marine Science*, *10*, 1113987. https://doi.org/10.3389/fmars.2023.1113987

Hawthorn, A. C., Dennis, M., Kiryu, Y., Landsberg, J., Peters, E., & Work, T. M. (2024). *Stony coral tissue loss disease (SCTLD) case definition for wildlife* (19-I1). U.S. Geological Survey. https://doi.org/10.3133/tm19I1

Henry, L.-A., & Hart, M. (2005). Regeneration from injury and resource allocation in sponges and corals – a review. *International Review of Hydrobiology*, *90*(2), 125–158. https://doi.org/10.1002/iroh.200410759

Horricks, R. (2017). *Regeneration of artificially induced lesions in the Caribbean great star coral (*Montastraea cavernosa*) in the nearshore waters of Grenada.* [Doctoral Dissertation, University of Guelph].

Jones, N. P., Ruzicka, R. R., Colella, M. A., Pratchett, M. S., & Gilliam, D. S. (2022). Frequent disturbances and chronic pressures constrain stony coral recovery on Florida's Coral Reef. *Coral Reefs*, *41*(6), 1665–1679. https://doi.org/10.1007/s00338-022-02313-z

Koval, G., Rivas, N., D'Alessandro, M., Hesley, D., Santos, R., & Lirman, D. (2020). Fish predation hinders the success of coral restoration efforts using fragmented massive corals. *PeerJ*, *8*, e9978. https://doi.org/10.7717/peerj.9978

Kramarsky-Winter, E., & Loya, Y. (2000). Tissue regeneration in the coral Fungia granulosa: The effect of extrinsic and intrinsic factors. *Marine Biology*, *137*(5), 867–873. https://doi.org/10.1007/s002270000416

May, L. A., Miller, C. V., Moffitt, Z. J., Balthis, L., Karazsia, J., Wilber, P., & Woodley, C. M. (2023). Acute turbidity exposures with Port of Miami sediments impact *Orbicella faveolata* tissue regeneration. *Marine Pollution Bulletin*, *193*, 115217. https://doi.org/10.1016/j.marpolbul.2023.115217

McArdle BH, Anderson MJ (2001) Fitting multivariate models to community data: A comment on distance-based redundancy analysis. Ecology 82: 290-297

Meesters, E. H., Wesseling, I., & Bak, R. P. M. (1996). Partial mortality in three species of reef-building corals and the relation with colony morphology. *Bulletin of Marine Science*, *58*(3), 838–852.

Meesters, E. H., Wesseling, I., & Bak, R. P. M. (1997). Coral colony tissue damage in six species of reef-building corals: Partial mortality in relation with depth and surface area. *Journal of Sea Research*, *37*(1), 131–144. https://doi.org/10.1016/S1385-1101(96)00004-4

Meesters, E., Noordeloos, M., & Bak, R. (1994). Damage and regeneration: Links to growth in the reef-building coral *Montastrea annularis*. *Marine Ecology Progress Series*, *112*, 119–128. https://doi.org/10.3354/meps112119

Mendes, J. M., & Woodley, J. D. (2002). Effect of the 1995-1996 bleaching event on polyp tissue depth, growth, reproduction and skeletal band formation in *Montastraea annularis*. *Marine Ecology Progress Series*, *235*, 93–102. https://doi.org/10.3354/meps235093

Moberg, F., & Folke, C. (1999). Ecological goods and services of coral reef ecosystems. *Ecological Economics*, *29*(2), 215–233. https://doi.org/10.1016/S0921-8009(99)00009-9

NOAA. (2024, April 30). *Stony coral tissue loss disease (SCTLD)*. Coral Disease & Health Consortium. https://cdhc.noaa.gov/coral-disease/characterized-diseases/stony-coral-tissue-loss-disease-sctld/

NOAA Coral Reef Watch Daily 5km Regional Virtual Stations. (n.d.). Retrieved January 6, 2025, from https://coralreefwatch.noaa.gov/product/vs/map.php

Oren, U., Benayahu, Y., Lubinevsky, H., & Loya, Y. (2001). Colony integration during regeneration in the stony coral *favia favus*. *Ecology*, *82*(3), 802–813. https://doi.org/10.1890/0012-9658(2001)082[0802:CIDRIT]2.0.CO;2

Paddack, M. J., Sponaugle, S., & Cowen, R. K. (2009). Small-scale demographic variation in the stoplight parrotfish *Sparisoma viride*. *Journal of Fish Biology*, *75*(10), 2509–2526. https://doi.org/10.1111/j.1095-8649.2009.02451.x

Page, C. A., Muller, E. M., & Vaughan, D. E. (2018). Microfragmenting for the successful restoration of slow growing massive corals. *Ecological Engineering*, *123*, 86–94. https://doi.org/10.1016/j.ecoleng.2018.08.017

Page, C., & Willis, B. (2006). Distribution, host range and large-scale spatial variability in black band disease prevalence on the Great Barrier Reef, Australia. *Diseases of Aquatic Organisms*, *69*(1), 41–51. https://doi.org/10.3354/dao069041

Palmer, C. V., Traylor-Knowles, N. G., Willis, B. L., & Bythell, J. C. (2011). Corals use similar immune cells and wound-healing processes as those of higher organisms. *PLoS ONE*, *6*(8), 23992. https://doi.org/10.1371/journal.pone.0023992

Papke, E., Carreiro, A., Dennison, C., Deutsch, J. M., Isma, L. M., Meiling, S. S., Rossin, A. M., Baker, A. C., Brandt, M. E., Garg, N., Holstein, D. M., Traylor-Knowles, N., Voss, J. D., & Ushijima, B. (2024). Stony coral tissue loss disease: A review of emergence, impacts, etiology, diagnostics, and intervention. *Frontiers in Marine Science*, *10*. https://doi.org/10.3389/fmars.2023.1321271

Renegar, D.-E. A., Blackwelder, P., Moulding, A. L. (2008). Coral ultrastructural response to elevated pCO2 and nutrients during tissue repair and regeneration. *Proceedings of the 11th International Coral Reef Symposium*, 1314-1318.

Rinkevich, B. (1996). Do reproduction and regeneration in damaged corals compete for energy allocation? *Marine Ecology Progress Series*, *143*, 297–302. https://doi.org/10.3354/meps143297

Rivas, N., Hesley, D., Kaufman, M., Unsworth, J., D'Alessandro, M., & Lirman, D. (2021). Developing best practices for the restoration of massive corals and the mitigation of predation impacts: Influences of physical protection, colony size, and genotype on outplant mortality. *Coral Reefs*, *40*. https://doi.org/10.1007/s00338-021-02127-5

Rodríguez-Martínez, R. E., Jordán-Garza, A. G., & Jordán-Dahlgren, E. (2016). Low regeneration of lesions produced by coring in *Orbicella faveolata*. *PeerJ*, *4*, e1596. https://doi.org/10.7717/peerj.1596

Rosenau, N. A., Gignoux-Wolfsohn, S., Everett, R. A., Miller, A. W., Minton, M. S., & Ruiz, G. M. (2021). Considering commercial vessels as potential vectors of stony coral tissue

Loss Disease. *Frontiers in Marine Science*, *8*. https://www.frontiersin.org/articles/10.3389/fmars.2021.709764

Rotjan, R. D., & Lewis, S. M. (2005). Selective predation by parrotfishes on the reef coral Porites astreoides. *Marine Ecology Progress Series*, *305*, 193–201. https://doi.org/10.3354/meps305193

Ruiz-Diaz, C. P., Toledo-Hernandez, C., Mercado-Molina, A. E., Pérez, M.-E., & Sabat, A. M. (2016). The role of coral colony health state in the recovery of lesions. *PeerJ*, *4*, e1531. https://doi.org/10.7717/peerj.1531

Sharkey, R. (2024, December 10). Regional differences in the effects of stony coral tissue loss disease and antibiotic treatments on the fecundity of *Orbicella faveolata* in florida [Conference Presentation]. Reef Futures 2024, Cancun, Mexico.

Schlecker, L., Page, C., Matz, M., & Wright, R. M. (2022). Mechanisms and potential immune tradeoffs of accelerated coral growth induced by microfragmentation. *PeerJ*, *10*, e13158. https://doi.org/10.7717/peerj.13158

Schmid-Hempel, P. (2003). Variation in immune defence as a question of evolutionary ecology. *Proceedings of the Royal Society of London. Series B: Biological Sciences*, *270*(1513), 357–366. https://doi.org/10.1098/rspb.2002.2265

Toller, W. W., Rowan, R., & Knowlton, N. (2001). Repopulation of zooxanthellae in the caribbean corals *Montastraea annularis* and *Montastraea faveolata* following experimental and disease-associated bleaching. *The Biological Bulletin*, *201*(3), 360–373. https://doi.org/10.2307/1543614

Traylor-Knowles, N. (2016). Distinctive wound-healing characteristics in the corals *Pocillopora damicornis* and *Acropora hyacinthus* found in two different temperature regimes. *Marine Biology*, *163*(11), 231. https://doi.org/10.1007/s00227-016-3011-y

Walker, B. (2022). The SCTLD Resistance Research Consortium. *HCAS Ocean Science Research Symposium*. https://nsuworks.nova.edu/cnso_osj/february-2022/day2/8

Walker, B. K., Aeby, G. S., Baker, A. C., Buckley, S., Hawthorne, A., Meyer, J. L., Neely, K., Noren, H., Paul, J., Sharkey, R., Traylor-Knowles, N., Voss, J. D., Williams, G. J., Woodley, C. M., & Work, T. (2023). *SCTLD resistance research consortium summary report through may 2023*.

Weil, E. (2004). Coral reef diseases in the wider caribbean. In E. Rosenberg & Y. Loya (Eds.), *Coral Health and Disease* (pp. 35–68). Springer. https://doi.org/10.1007/978-3-662-06414-6_2

Woodhead, A. J., Hicks, C. C., Norström, A. V., Williams, G. J., & Graham, N. A. J. (2019). Coral reef ecosystem services in the Anthropocene. *Functional Ecology*, *33*(6), 1023–1034. https://doi.org/10.1111/1365-2435.13331

Dennison, C. E., Karp, R. F., Weiler, B. A., & Goncalves, A. (2021). The role of algal symbionts (genus Breviolum) in the susceptibility of corals to Stony Coral Tissue Loss Disease in South Florida.

Kemp, D. W., Hernandez-Pech, X., Iglesias-Prieto, R., Fitt, W. K., & Schmidt, G. W. (2014). Community dynamics and physiology of Symbiodinium spp. Before, during, and after a coral bleaching event. Limnology and Oceanography, 59(3), 788–797. https://doi.org/10.4319/lo.2014.59.3.0788

Kemp, D. W., Thornhill, D. J., Rotjan, R. D., Iglesias-Prieto, R., Fitt, W. K., & Schmidt, G. W. (2015). Spatially distinct and regionally endemic Symbiodinium assemblages in the threatened Caribbean reef-building coral Orbicella faveolata. Coral Reefs, 34(2), 535–547. https://doi.org/10.1007/s00338-015-1277-z

Rowan, R., Knowlton, N., Baker, A., & Jara, J. (1997). Landscape ecology of algal symbionts creates variation in episodes of coral bleaching. Nature, 388(6639), 265–269. https://doi.org/10.1038/40843

Rubin, E. T., Enochs, I. C., Foord, C., Mayfield, A. B., Kolodziej, G., Basden, I., & Manzello, D. P. (2021). Molecular Mechanisms of Coral Persistence Within Highly Urbanized Locations in the Port of Miami, Florida. Frontiers in Marine Science, 8. https://www.frontiersin.org/articles/10.3389/fmars.2021.695236